Optimization of Interfacial Zone Characteristics of Fiber-Cement Matrix

by

Gouri Sridevi

A Thesis Presented in Partial Fulfillment
of the Requirements for the Degree
Master of Science

ARIZONA STATE UNIVERSITY

May 1999

Optimization of Interfacial Zone Characteristics of Fiber-Cement Matrix

by

Gouri Sridevi

has been approved

May 1999

APPROVED:

_______________________________, Chair

____

____

Supervisory Committee

ACCEPTED:

____

Department Chair

____

Dean, Graduate College

ABSTRACT

A novel experimental method of conducting pullout tests on a single steel fiber embedded in a cementitious matrix is developed. Tests were conducted on series of specimens. The variable parameters are the embedded length and diameter of the fiber, and the age of the paste for the matrix. The pullout slip response was obtained and used to characterize the effect of the interface properties and age on pullout slip behavior.

In the second part of the thesis, a parameter modeling technique is developed. The motivation is to find the optimal parameters of an analytical model developed by Li [Li, 1995]. The problem of fitting the experimental data with this model is formulated as an optimization problem. The Genetic Algorithm (GA), a non-linear, non-gradient-based optimization technique, is used to obtain the solution. The design variables are the governing interfacial zone parameters in the model while the objective function is a compound least-squares function.

To

My Parents

ACKNOWLEDGEMENTS

I would like to thank my advisor and committee chair, Professor S.D. Rajan, for his guidance, support and tremendous help. I would also like to thank Dr. Mobasher for introducing me to the field of experimental solid mechanics, and for his help and guidance with the experimental and analytical part of the research. I would also like to thank Dr. Han Zhu for serving on my committee. Thanks to Dallas Kingsbury, for his assistance with the experimental work. Finally, I would like to express my gratitude to my family and friends for their encouragement without which it would have been difficult to achieve my goals.

TABLE OF CONTENTS

Page

CHAPTER

APPENDIX

LIST OF TABLES

Table Page

LIST OF FIGURES

Figure Page

Figure Page

Figure Page

CHAPTER 1

INTRODUCTION

1.1 OVERVIEW

Fiber reinforced concrete is extensively used as a construction material because it helps improve the desirable behavior of concrete. By adding fibers, tensile strength, resistance to crack growth and toughness properties of concrete are significantly increased. This action is achieved by means of a bridging action affecting the cracks [Alberto and Roberta, 1996]. When a fiber reinforced cement composite is subjected to a tensile force, cracks develop and the discontinuous fibers bridging the cracks are in the process of debonding, sliding and frictional pullout. The failure of steel fiber-reinforced cement composites is generally attributed to the failure of the bond between fibers and cement matrix [Naaman and Shah, 1976]. The interface between fiber and matrix plays a great role in determining stiffness, strength, toughness and overall behavior of the composite. Hence, the need to know pullout behavior of fibers is an important research topic.

The load applied to a matrix is partly transferred to the fiber along its surface. Because of the difference in stiffness between the fiber and the cement matrix, shear stresses develop along the surface of the fiber resulting in the development of cylindrical shear microcracks [Li, Mobasher et al., 1991]. The cracks tend to grow along the interface since the bonding strength of the interface is weaker than the homogeneous material. Therefore, the stiffness and frictional resistance (sliding) of the fiber-matrix interface are related to the strength of fiber reinforced composite.

Similarly, the post peak region of the load-deformation response is related to the energy absorption and toughness [Mobasher and Shah, 1989]. The mechanisms of fiber pullout increase the energy demand for the crack propagation. Consequently the fracture toughness (total energy consumption during the cracking process) can increase significantly. Hence, it becomes very important to have a correct description of the fiber pull out process, identifying the correct material parameters [Li et al., 1990].

The characterization of the strength or integrity of the interface is important in determining the bond parameters of fiber-matrix interface [Nahta and Moran, 1996]. Two different approaches have been used in the past to characterize the strength of the interface: shear lag or stress criterion and fracture mechanics approach. [Li et al., 1990]. Research and applications of the above two approaches are contained in several publications [Jenq and Shah, 1986; Naaman et al., 1991; Hutchinson et al., 1990; Mobasher et al., 1990].

In the stress-based approach, when the shear stress at the interface reaches a critical value, it is assumed that debonding takes place. The stress criterion can be expressed in terms of shear force per unit length [Li and Shah, 1990]. The cement matrix can be modeled as a shear lag with stiffness of k. When the shear force per unit length q on the interface reaches a critical value q_y, the fiber-matrix bond starts failing. The peak interfacial shear stress q_y differs from model to model.

Recent treatment of the interface fracture based on the shear lag or stress based criterion include works of [Lawrence, 1972; Marshall, Cox and Evans, 1985; Gopalratnam and Shah, 1987; Stang et al., 1990; Naaman et al., 1991] among others. Recently [Dubey and Banthia, 1999] have proposed a model that suggests ideas on overcoming some of the major limitations of the earlier models.

Fracture mechanics approach is based on the energy balance criterion. The debonding of the matrix-interface is treated as propagation of interface cracks. This method states that the debonding propagates with the consumption of energy. The energy required is characteristic for the bond between fiber and the matrix. In other words, it depends on the interface properties. Hence, the energy required is proportional to the increase in the debonded zone. Releasing the strain energy stored in the system provides the energy consumed during debonding. The fracture mechanics approach taken here is based on the energy release rate (strain energy released during unit extension of debonding zone). Fracture mechanics based theoretical models representing the crack propagation in fiber reinforced cement composites have been developed and studied in the past. A two-parameter fracture model was recently proposed [Jenq and Shah, 1986]. The two material parameters that characterize the interfacial strength are frictional stress of the interface and the critical debonding energy release rate. In another model, the concept of energy release rate was used [Li, Shah et al., 1990]. The R-curve approach for the fracture of quasi-brittle cementitious materials was proposed by several researchers [Quyang, Mobasher and Shah, 1990; Mobasher and Li, 1996].

1.2 THESIS OBJECTIVES

In this research the focus is on the following areas. An experimental test setup for determining the fiber-pullout response is developed and the interfacial zone characteristics of the fiber-cement matrix are thereby obtained. The experimental results are compared with a previously developed theoretical model. A parameter modeling technique is developed and then solved using a specially developed GA. Using the above technique the theoretical model is fitted with the experimental data and interfacial zone parameters are thereby obtained from the model.

CHAPTER 2

EXPERIMENTAL SETUP FOR FIBER PULLOUT TESTS

2.1 INTRODUCTION

Diverse sets of experiments to determine the interfacial zone characteristics have been used in the past. Examples include push out tests or tensile (pullout) tests on composite specimens. Tests on specimens with unidirectional fibers, multiple fibers with inclined orientations or a single fiber embedded in cement matrix have also been performed. In this research, a simple test setup for fiber pullout experiments was devised.

Straight and smooth steel fibers of constant circular cross-sectional area and predefined embedded lengths were used. Fibers of embedded lengths of 10 mm, 12.7 mm (0.5 in), 15 mm, 20 mm, 25.4 mm (1 in) and diameters of 0.5 mm and 1 mm were tested. The specimens were cured for 7, 14, 18 and 28 days respectively and tested in different batches. A typical specimen consisted of a steel fiber having a diameter d and length l embedded in the cement paste. The details of the specimen preparation are discussed in the following sections. The schematic diagram of a typical specimen is as shown in the Figure 2.1a and Figure 2.1b.

Figure 2.1a A typical specimen

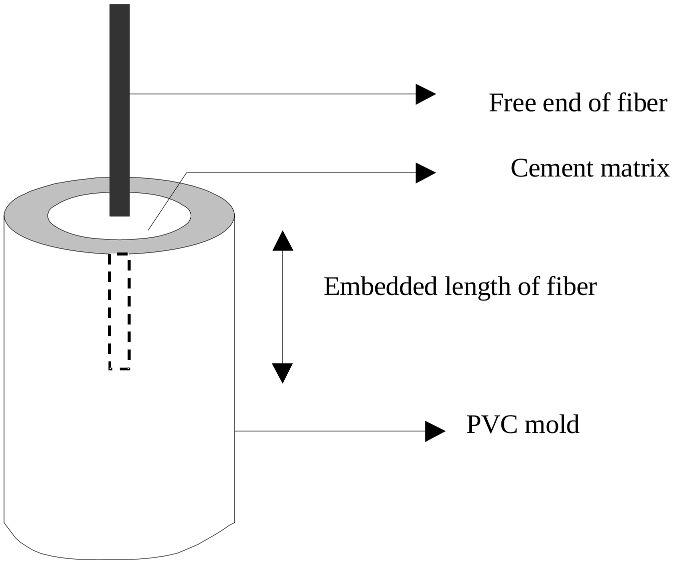

Figure 2.1b Schematic diagram of a specimen

2.2 SPECIMEN PREPARATION

The specimen consists of a hollow plastic mold open on both ends. It is filled with cement paste and contains a straight steel fiber of uniform cross-section embedded in the cement paste. Care was taken while casting the specimen so that the fiber was oriented exactly along the centroidal axis of the mold. The mold was a PVC pipe of 1-inch diameter and 2 inches length. The steel fiber was held in place at the center of the mold by cylindrical wooden holders, which had a central hole drilled into them. A picture of the sample is shown in Figure 2.1. The fiber was placed in between the wooden dividers and tied with tape so that it was secured in place. The wooden pieces also helped to orient the fiber. The required embedded length of the fiber was exposed. The wooden holders were then secured to the PVC mold with a tape such that the free end of the fiber stayed at the center of the mold. This arrangement plugged one end of the mold, and allowed the cement mixture to be poured into the pipe from the other end. The mold was thoroughly vibrated and left in place for 24 hours before it was cured in saturated lime-water solution.

2.3 EXPERIMENTAL PLAN

The entire process of specimen preparation, curing, testing was divided into a series of four trials or batches. Each series was cured for a different amount of time before being tested. The details of the specimen preparation and the contents of the mix for each batch are given below. The mix design in each of the 4 batches was kept constant. The general mix design of the cement paste was as follows.

$$\frac{Silica\,Fume}{Cement} = 15\%$$

$$\frac{Water}{Cement + Silica\,Fume} = 0.4$$

Superplasticizer (WRDA-19) was used to obtain a consistent mix. All the ingredients of the cement paste were thoroughly blended in a blender and the mix was then vacuumed to remove air pockets. The specimens were cast and vibrated to compact the cement matrix. This was performed to ensure that the cement matrix (and the interface) was continuous. The samples were left overnight in the laboratory before they were cured in lime water solution for a certain time period. Period of curing was varied between 7 to 28 days depending on the batch. At the end of the curing period, the specimens were removed from water and tested.

2.3.1 Series 1

The mix design used in Batch 1 was as specified in the above section. About 20 specimens were cast in this batch. The details of the samples are listed in Table 2.1. All the specimens were cured for a period of 28 days prior to testing. The peak load attained was very high because of a strong interface resulting from a longer duration of curing. It should be noted that complete pullout could not be achieved for most of the specimens. For most of the samples with fiber diameter of 1 mm, the fiber and the cement matrix slid out of the plastic mold. In some cases, partial pullout and partial sliding of the cement matrix took place. From the results obtained in this case it could be concluded that the force required to pullout the fiber was much higher than the peak load observed. In the case of the fibers with 0.5 mm diameter, the fiber fractured before complete pullout took place - the yield strength of the 0.5 mm fibers was much lower than the force required for pullout. The clamping forces on the fiber (due to tightening of the screws in the support fixture) made the fiber more vulnerable to fracture. From the results obtained, an estimate of yield strength of the fiber was made and the stiffness of interface was calculated.

Complete pullout-slip response was not obtained for most of the specimens cured for 28 days. Since the primary objective of the research was to understand how the fibers contribute to the early age properties of cement composites, the curing was limited to lower time periods in the subsequent trials.

2.3.2 Series 2

In this series about 24 specimens were cast using the general mix design, the details being shown in Table 2.2. All the specimens were cured for 7 days and taken out of the curing solution. The peak load of the specimens was relatively low. Some of the samples failed during handling and clamping. This is possibly due to the weak bond between fiber-interface brought about by a short curing period. In the subsequent batches the curing period was increased. However, complete pullout-slip data was obtained for most of the samples. Failure due to fracture was not seen in any of the specimens in this batch.

2.3.3 Series 3

Details of the specimens are shown in Table 2.3. In this batch 14 specimens were cast according to the general mix design discussed earlier. The specimens were tested after 14 days of curing in lime water solution. Most of the fibers pulled out completely from the cement matrix, although some failed during handling. Complete pullout response was obtained for most of the specimens.

2.3.4 Series 4

This was the last series of the fiber pullout experiments. 12 specimens with details shown in Table 2.4 were tested. All the specimens had a diameter of 1 mm and were cured for 18 days. Good results were obtained for most of the specimens. The stiffness of the interface (given by the slope of the initial linear portion of the graph) was very high.

Table 2.1 Series 1 (Curing Period: 28 days)

Diameter	**Length**	**Number of Specimens**
0.5 mm	0.5 in	5
0.5 mm	1.0 in	5
1.0 mm	0.5 in	5
1.0 mm	1.0 in	5

Table 2.2 Series 2 (Curing Period: 7 days)

Diameter	**Length**	**Number of Specimens**
0.5 mm	0.5 cm	3
0.5 mm	1 cm	3
0.5 mm	0.5 cm	3
1 mm	1 cm	3
1 mm	0.5 in	3
1 mm	1.5 cm	3
1 mm	2 cm	3
1 mm	1 in	3

Table 2.3 Series 3 (Curing Period: 14 days)

Diameter	**Length**	**Number of specimens**
0.5 mm	5 mm	4
0.5 mm	10 mm	5
0.5 mm	0.5 in	5

Table 2.4 Series 4 (Curing Period: 18 days)

Diameter	**Length**	**Number of Specimens**
1 mm	10 mm	4
1 mm	1 in	4
1 mm	15 mm	2
1 mm	20 mm	2

2.4 TEST SETUP

A uniaxial tension testing machine, MTS –SINTECH I/S, Model IIXX, was used for the pullout tests. The test setup is shown in Figure 2.3. A special set of grips was designed for this test. The mold was held at the bottom by a fixture, which was anchored, to the testing machine (Figure 2.2b). The crosshead was lowered and the free end of the fiber was tightened by means of screws to a grip attached to the crosshead (Figure 2.2a). As the crosshead moves a tensile load is applied to the fiber. The test was conducted under constant displacement control. An extensometer was mounted on the specimen to measure the slip. Test software, TESTWORKS, (Appendix A) was used to run the test and record the response.

This test setup has various advantages. Some of them are listed below.

Simple: It is relatively simple to mount the specimen and operate the test setup.

Reliable: The results from the pullout test can be reproduced. Hence the test setup is accurate.

Non-Invasive: The interface being a weak zone, any mishandling of the specimen or stresses on the fiber could damage the interface. This test setup doesn’t cause major distress to the specimen.

Accurate: The results from the pullout slip experiments obtained from this setup can be termed accurate because the interface is monitored as closely as possible, without disturbing it. A local clip gage mounted on the specimen measures the slip of the fiber from the cement matrix, and is much more accurate than the crosshead reading usually recorded.

Fast: The process of running the experiment is fast and efficient. Hence many specimens can be tested in a small duration.

Flexible: The test setup is highly flexible, because with little changes in the adjustments and fixtures, various pullout tests could be accommodated. Moreover, the rate of obtaining the data points, the crosshead movement etc. can be totally controlled.

Figure 2.2 a) Fixture that grips the fiber, pinned to the load cell.
b) Fixture that holds the mold at the bottom, anchored to the testing machine.

Figure 2.3 Test Setup for the fiber pullout experiments.

2.5 DISCUSSION OF THE EXPERIMENTAL RESULTS

The pullout tests carried out on different specimens are discussed in the following sections. The results of experiments are tabulated in Table 2.5. The load-slip curves generated for all the specimens can be found in Appendix A.

2.5.1 Load-Slip Response

The pullout force versus slip response of the fiber was plotted for different specimens. A typical pullout force-slip curve is shown in Figure 2.4. The first portion of the graph is linear with a steep slope - the load increases rapidly. The increase in the slip initially is small compared to the rate of increase of the load. As the load increases beyond the linear region a certain degree of nonlinearity is observed. The peak response is reached. The peak also corresponds to the maximum load. Beyond the peak, the load suddenly drops. At this stage the slip of the fiber takes place at a constant load and drops down to zero as the fiber pulls out completely. The graph in general could be categorized into the following regions.

1. Linear
2. Nonlinear
3. Peak
4. Post-Peak

These four regions can be clearly seen in Figure 2.4.

Table 2.5 Results from the fiber-pullout experiments

ID	Name	Length (mm)	Dia (mm)	Curing (days)	P_{max} (lb)	Slip at peak (in)	Stiffness (lb/in)	Energy (lb-in)	Mode of failure
1	05D05LS6	12.7	0.5	28	12.6768	0.01478	994.4	0.26096	*
2	05D05LS7	12.7	0.5	28	12.6	0.41035	4347	0.2178	*
3	05DiLS12	25.4	0.5	28	13.635	0.031175	438	0.349	*
4	05D1LS13	25.4	0.5	28	11.8	0.016542	461	0.1717	*
5	05D1LS14	25.4	0.5	28	12.92	0.017639	545	0.028	*
7	05D1cLS17	10	0.5	7	13.9	0.014628	2470.83	0.73081	**
8	1D05iLS28	12.7	0.5	7	14.03	0.018327	4203.36	0.3183	*
9	1D05iLS29	12.7	0.5	7	14.05	0.03989	913	1.0549	**
10	1D05iLS30	12.7	0.5	7	8.4	0.018415	386.5	0.45374	**
11	4B05D1cL	10	0.5	14	9.1	0.0165	530	0.22055	**
13	4B05D1cL3	10	0.5	14	8.73	0.00535	1691.97	0.4564	**
14	4B05D05iLS4	12.7	0.5	14	13.51	0.035028	1259.44	0.09543	**
15	4B05D1cLS5	10	0.5	14	4.06	4.79E-04	100957	0.07776	**
16	4B05D05iLS6	12.7	0.5	14	13.02	0.038389	1504	0.838	**
17	4B05D05iLS7	12.7	0.5	14	14.04	0.05796	1299.5	0.9567	*
18	1D05LS3	12.7	1	28	57.5	1.839E-3	1.66E+04	9.8984	**
19	1D05LS5	12.7	1	28	73.6	N/A	N/A	N/A	Partial
20	1D05iLS24	12.7	1	7	19.4	2.05E-03	1.60E+04	2.2883	**
21	1D05iLS25	12.7	1	7	26.9	9.65E-04	7.79E+04	4.8195	**
23	1D1iLS27b	25.4	1	7	81.1	0.06136	3.26E+04	4.8942	*
24	4B1D1iLS12	25.4	1	18	29.63	1.90E-03	2.35E+04	3.5872	**
25	4B1D1iLS13a	25.4	1	18	52.6	2.87E-03	4.12E+04	7.8653	**
26	4B1D1iLS14	25.4	1	18	75.07404	0.023563	1.99E+04	13.72	**
28	1D1cLS23	10	1	7	36.8	5.94E-04	1.42E+05	5.274	**
29	4B1D1cLS8	10	1	18	16.14	N/A	N/A	N/A	**
30	4B1D1cLS9	10	1	18	11.375	N/A	N/A	N/A	**
31	4B1D1cLS10	10	1	18	27.063	6.27E-04	8.36E+04	2.4986	**
34	1D15cLS19	15	1	7	12.5	N/A	N/A	N/A	**
35	1D15cLS20	15	1	7	34.13	4.30E-03	2.98E+04	1.6896	**
37	4B1D15cLS16	15	1	18	34.53	2.68E-03	1.44E+04	2.67202	**
38	4B1D2cLS17	15	1	18	62.14	7.05E-03	1.66E+04	9.4343	**
39	4B1D2cLS18	20	1	18	45.69	7.76E-03	8745.38	7.8653	**
40	1D2cLS26	20	1	7	46.3	2.68E-03	2.26E+04	7.46765	**

*	Failure due to fracture of fiber
**	Complete pullout of fiber

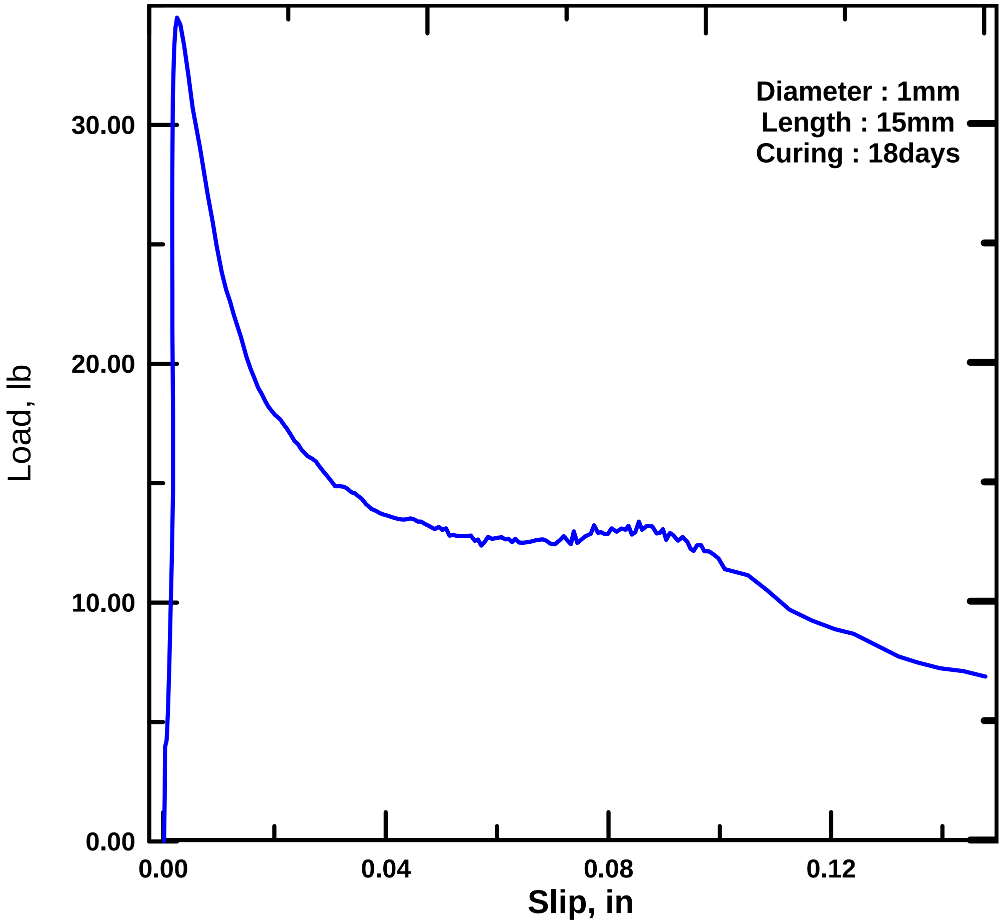

Figure 2.4 A typical pullout-slip response curve

2.5.1.1 Linear region

This region constitutes the initial response of the pullout process. It is characterized by a steep increase in load with a very low increase in slip. The slope of this region is a measure of the stiffness of the interface (Figure 2.5). The stiffer the interface, the higher the slope. It is observed that the stiffness increases with increase in the curing period.

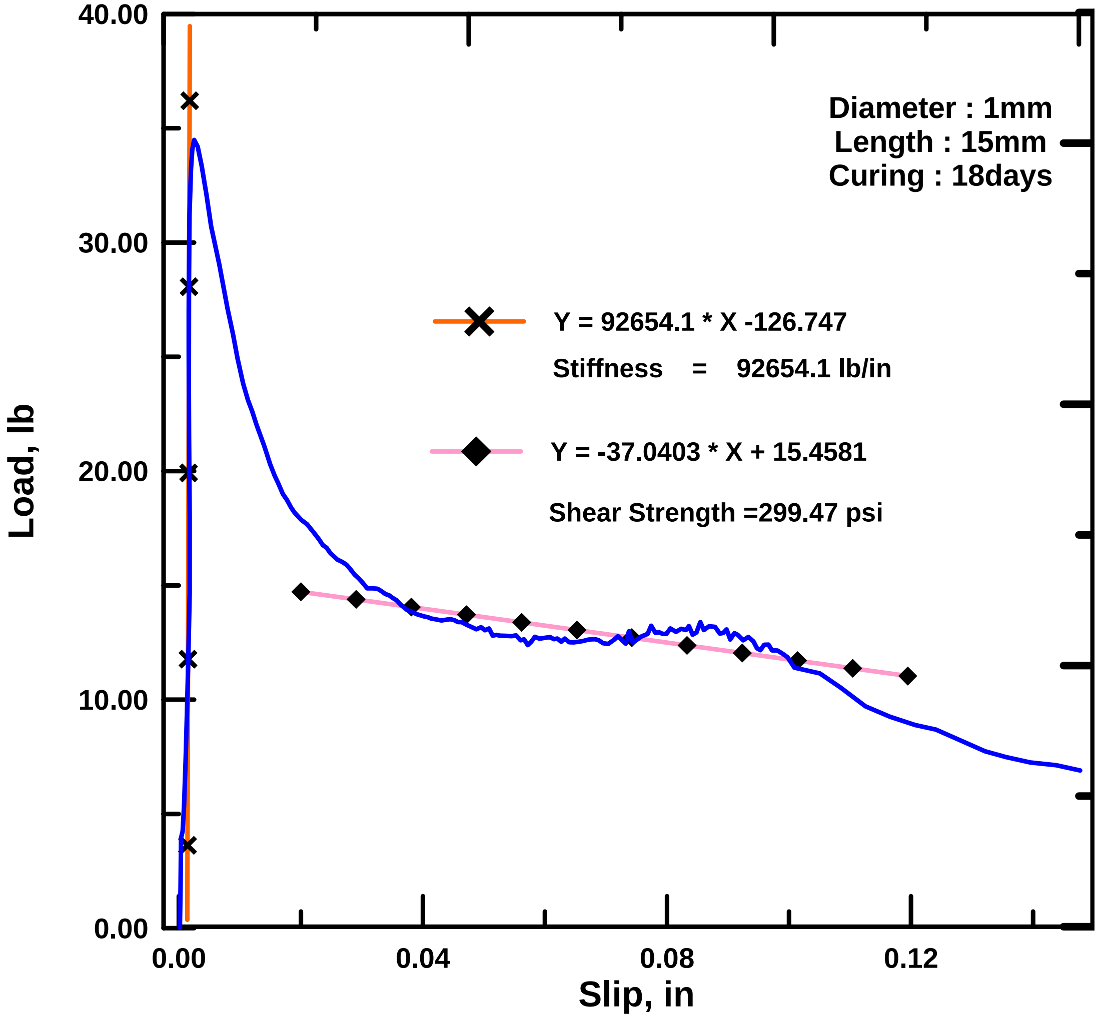

Figure 2.5 Pullout-slip response, showing slope of the pre-peak linear region (stiffness) and that of the post-peak response (frictional shear strength).

2.5.1.2 Non-linear region

This is the pre-peak response beyond the linear region. The rate of increase of the load decreases in this region until the peak load is reached. Theoretically this region marks the onset of debonding of the fiber from the interface. The increase in slip in this zone is small as observed in the linear region.

2.5.1.3 Peak region

The peak is the region corresponds to the peak of the overall curve. The pullout force reaches a maximum (P_{max}) at the peak point. The slip of the fiber at this point is known as the slip at the peak and can be considered as the critical length of the debonded fiber (debonding continues without increase in the load). The peak pullout force depends on the embedded length, diameter of the fiber and the curing period, the mix design being constant. An increase in the value of the maximum load was observed with the increase in embedded length. Figures 2.6 and 2.7 show the comparison between peak pullout force and embedded length of the fibers. However, when the embedded length exceeded a certain value, the fibers fractured before complete pullout could take place. P_{max} increased if the specimen was cured for a longer duration. This is because the interface strengthens with curing and greater force is required for pullout. This is shown in Figure 2.8. An increase in the peak loads is seen, as the curing period varies from 7 days to 18 and 28 days.

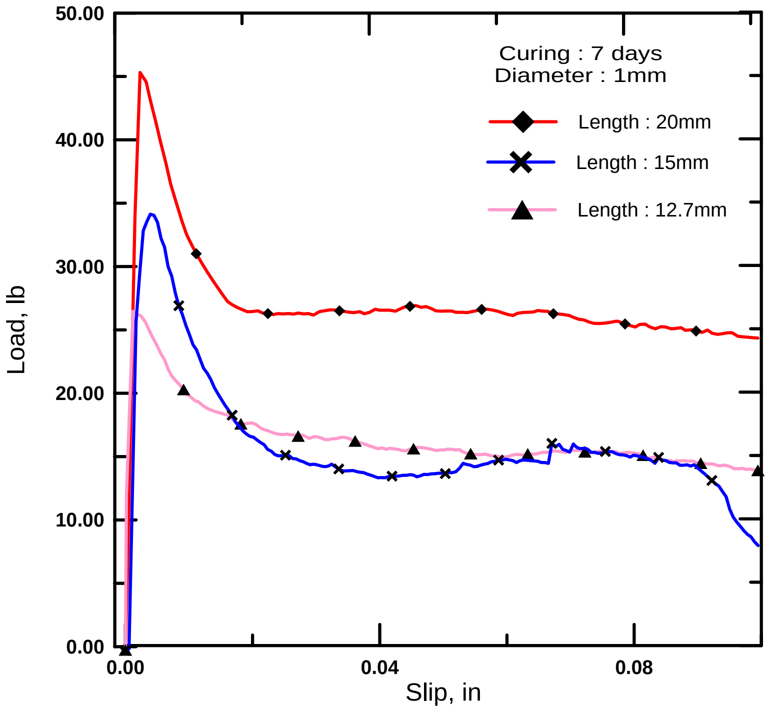

Figure 2.6 Pullout slip curves of specimens cured for 7 days with different lengths

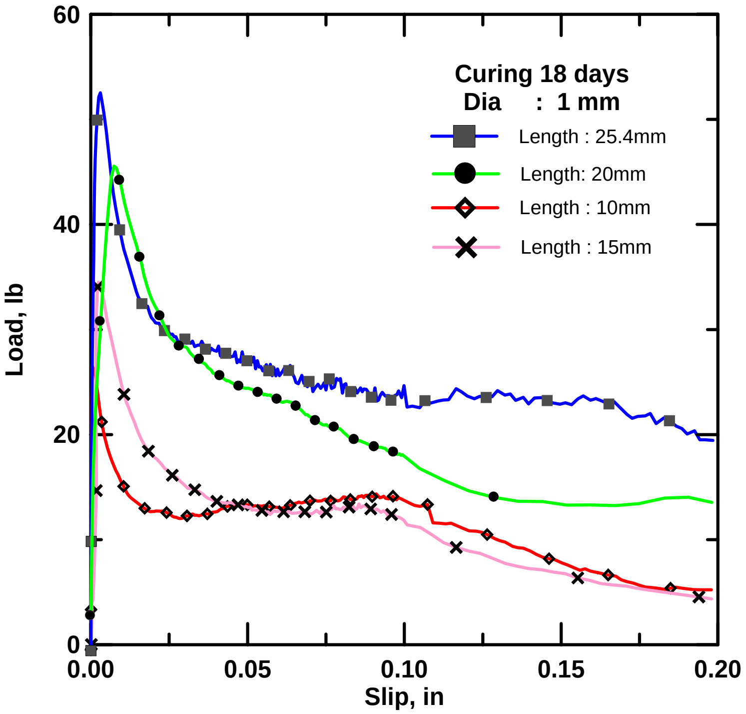

Figure 2.7 Pullout slip curves of specimens cured for 18 days with different lengths

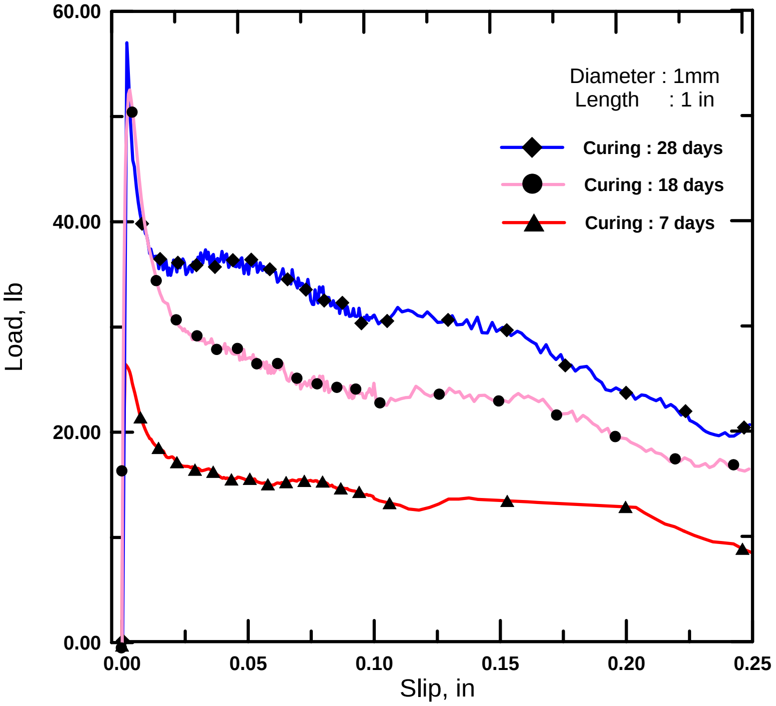

Figure 2.8 Pullout slip response of specimens cured for different periods.

2.5.1.4 Post-peak region

The pullout-slip response beyond the peak load is referred to as the post-peak region. In this region, the load drops rapidly to a fixed value after which it remains quite constant. The immediate post-peak region is governed by the shear strength of the fiber and continues till the fiber is completely debonded from the interface. The slope of this portion of the curve (Figure 2.5) gives the value of frictional shear strength of the interface ($\tau_f\ 2\pi r$) acting on the fiber surface (Figure 2.9).

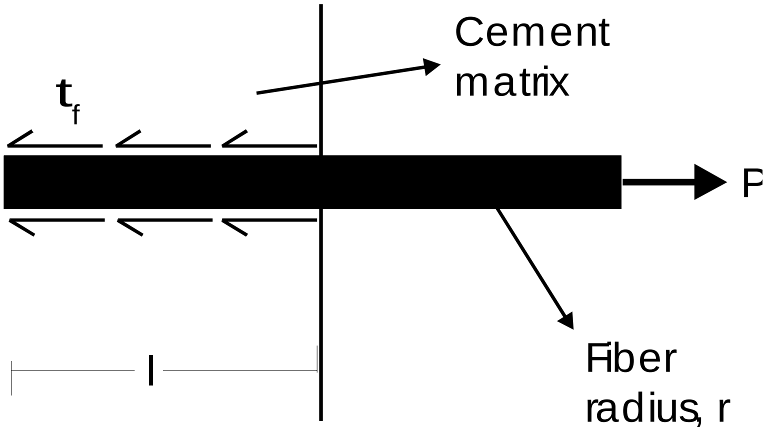

Figure 2.9 Frictional force acting on the interface

The frictional force, F, acting on the interface is

$$F = 2\pi r l \tau_f \tag{2.1}$$

where

r = radius of the fiber

l = length of the fiber

τ_f = Shear strength of the interface

As the fiber slides out, if at any instant the slip is s, then the governing frictional force on the interface is given by

$$F = (l - s)\left(2\pi r \tau_f\right) \tag{2.2}$$

The pullout force attains a constant value after complete debonding of the fiber. At this stage frictional sliding of the fiber from the matrix begins and continues until complete pullout takes place. The pullout force slowly reduces to zero as the fiber pulls out completely.

2.5.2 Failure due to Fracture

As discussed earlier, the peak load increases with the embedded length. However, if the embedded length exceeds a certain value, the fibers fracture before complete pullout takes place. Figures 2.10 shows the failure of a specimen due to fracture. As can be observed, the pullout force increases to a certain value and the suddenly drops down to zero. The load drops when the fiber yields usually before P_{max} is reached. This condition was also observed when the specimens were cured for a longer duration (Figure 2.12). With a longer curing period (also increase in age), the strength of the interface and that of the bond between the fiber-interface increases tremendously. Therefore it requires a higher force to break the bonds and pull out the fiber completely. The fiber yields unable to withstand the large forces applied at the fiber end. Fracture of the fiber occurs before complete pullout when the yield or ultimate strength of the fiber is lower than the peak force required to pullout the fiber. In such cases the peak load is not attained and the pullout force drops suddenly as the fiber fractures.

Fibers with smaller diameters and longer lengths or longer curing period are susceptible to fracture before complete pullout due to their low strength. All the specimens of 0.5 mm diameter, with different embedded lengths, cured for 18/28 days, fractured before complete pullout. Figure 2.11 shows this phenomenon. The maximum pullout force attained gives a measure of the yield/ultimate strength of the fiber. From Figure 2.11, it can be seen that the fibers (diameter of 0.5 mm and 28 days curing) fractured at a load of 55 N approximately. The strength of the fiber can be calculated as shown below.

$$Ultimate\,Strength = \frac{Peak\,load}{Area} = \frac{55}{(\pi\,(0.25)^2)} = 280\,MPa \tag{2.3}$$

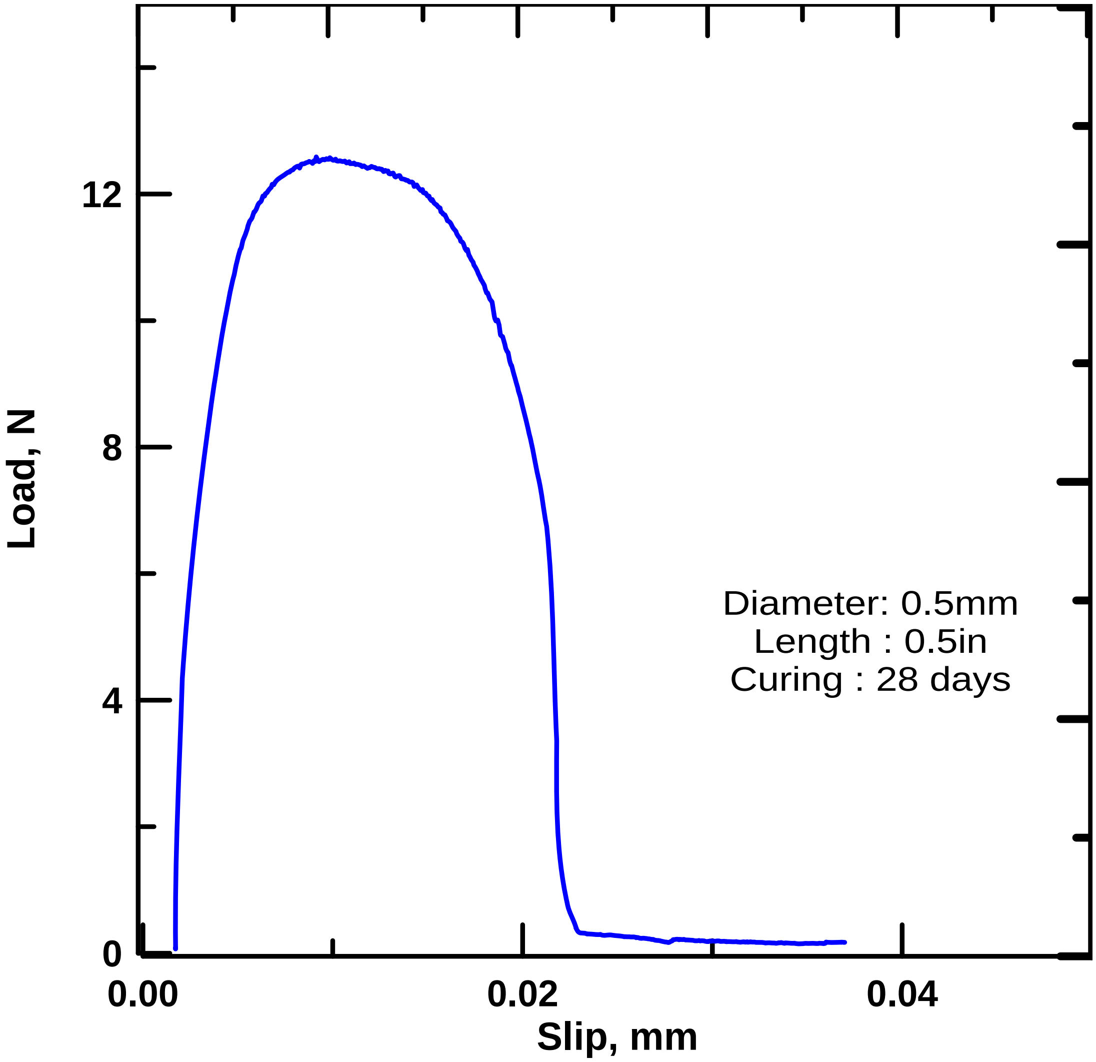

Figure 2.10 Failure due to fiber fracture before complete pullout took place

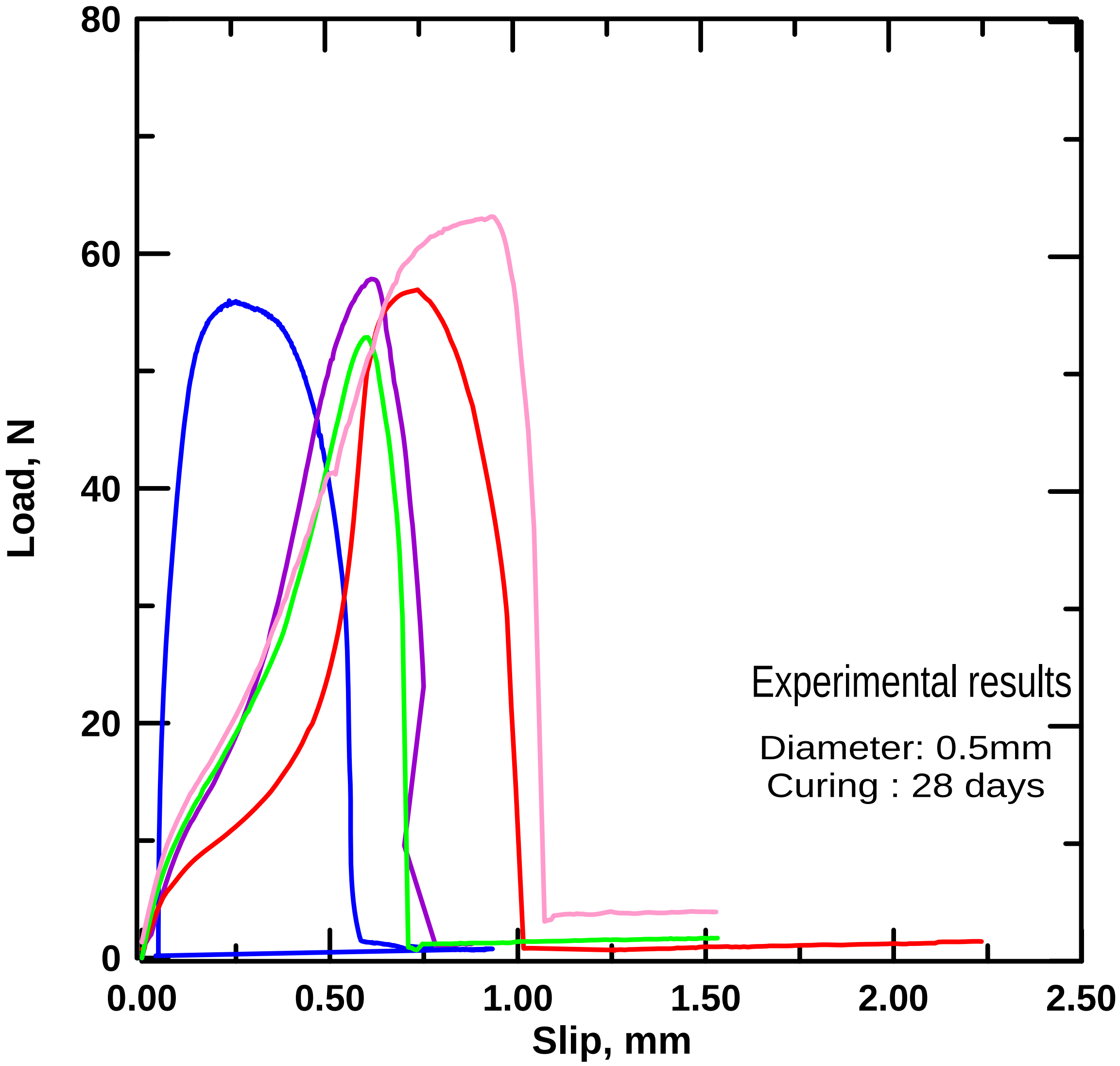

Figure 2.11 Load-slip curves for different fibers that fractured before complete pullout

2.5.3 Peak Load Vs Curing - General Trend

As seen earlier, the peak pullout force increases with an increase in the curing period. The peak pullout force for all the specimens with different lengths and diameters (Table 2.5) is plotted against the curing period in Figure 2.12. The general trend observed is a rise of P_{max} with the curing period. Though the higher values of P_{max} in the Figure 2.12 show an ascending trend, there is an inconsistency in the lower values. Very low values of peak load for a curing period of 28 days were observed. The ascending trend of P_{max} is seen in the 7 and 18 days curing specimens but the low values of P_{max} for 28 days curing period remained constant. This discrepancy resulted due to the fracture of the fibers before complete pullout.

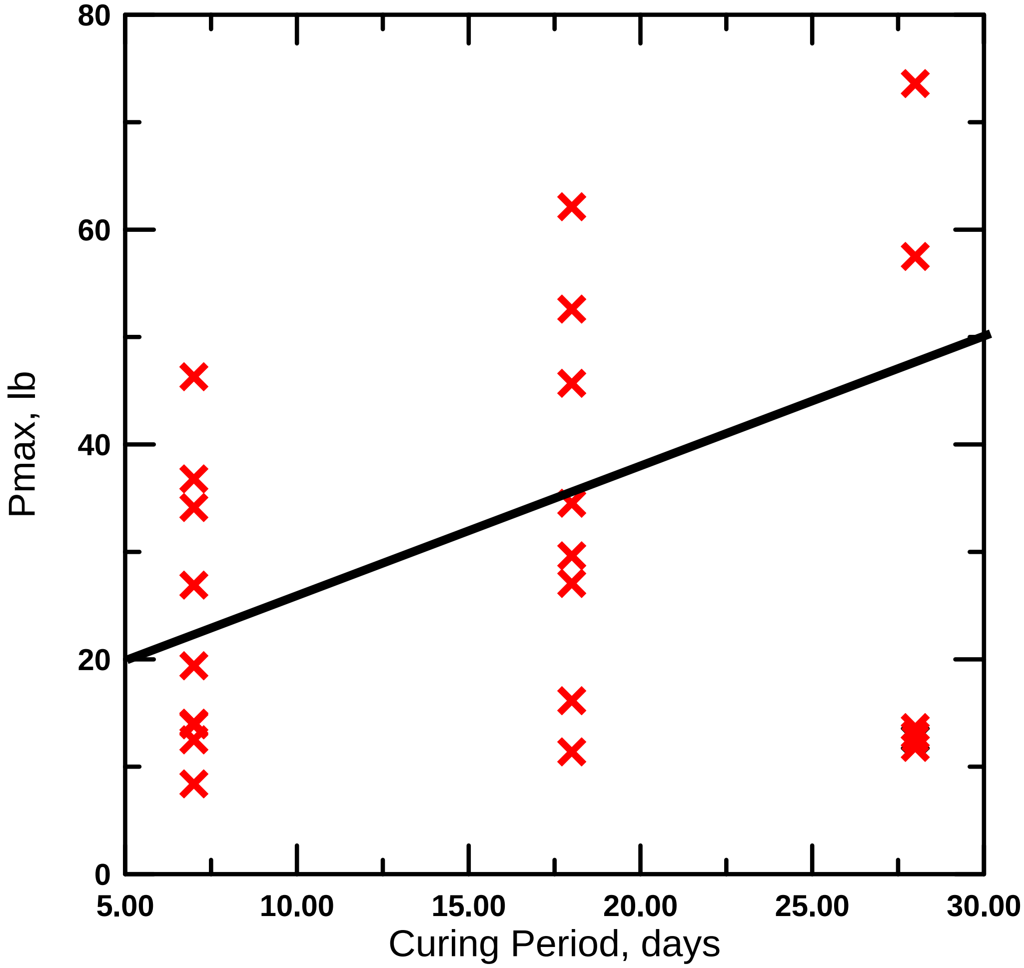

Figure 2.12 The effect of curing on the peak pullout force of fibers: a general trend

2.5.4 Total Energy Absorbed

It can be postulated that the total energy absorbed during the process of debonding and pullout is the area under the pullout-slip curve.

$$G_p = \int_0^l P(a)\ du \tag{2.4}$$

The energy absorbed increases as the embedded length of the fiber increases to a certain value (yield point of the fiber) after which the fibers start yielding and fail due to fracture. Figure 2.13 shows the graph of energy absorbed versus lengths, for specimens with 1 mm diameter cured for 18 days. An increase in energy is observed, with the increase in embedded length. When the fiber fails by fracture or yielding, the energy absorbed is much lower than when the fiber pulls out completely. The comparison of graphs, when the fiber (diameter 0.5 mm, embedded length 10 mm, 7 days curing) failed due to fracture and complete pullout is shown in Figure 2.14. The energy absorbed in the case of complete pullout is 0.731 lb-in whereas the energy in case of fiber fracture is just 0.318 lb-in. Apparently the energy absorbed is higher when the fiber pulls out completely than when the fiber fails due to fracture. The peak load in both the cases being quite the same, this difference in the energy absorbed is attributed to the post-peak fiber pullout mechanism. The post-peak frictional sliding contributes significantly to the energy absorbed, and thereby increases toughness. This is because as the fibers start sliding out of the cement composite, lot of energy is consumed. Thus, the total energy consumption depends on the complete pullout process than just the peak load.

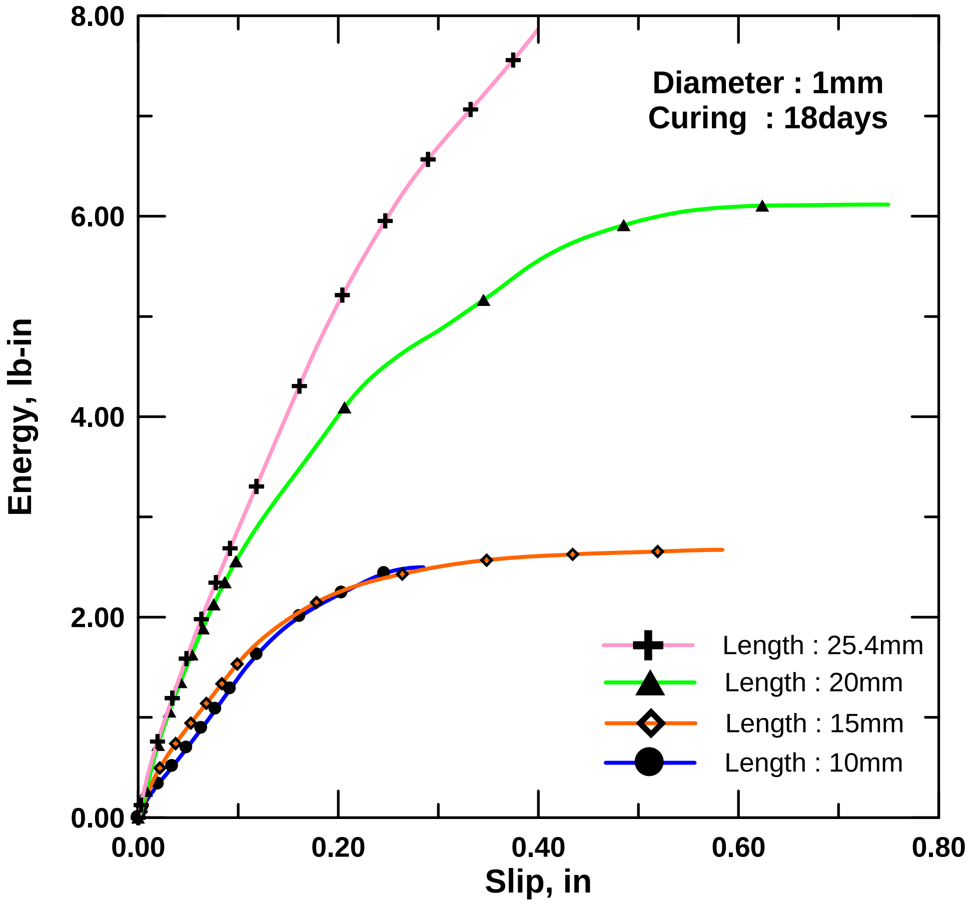

Figure 2.13 The total energy absorbed during pullout of fibers with different lengths

The energy absorption capability of the composite is increased tremendously if the failure takes place by pullout of fibers. To ensure this mode of failure the fiber lengths should not be large enough to cause failure due to fracture. But if the fiber lengths are smaller, the energy absorption capability of the composite is low. Hence it is advantageous to estimate an optimum length of the fibers to maximize the toughness. When the fiber lengths are smaller, although complete pullout takes place, the energy absorbed is lower and can be improved.

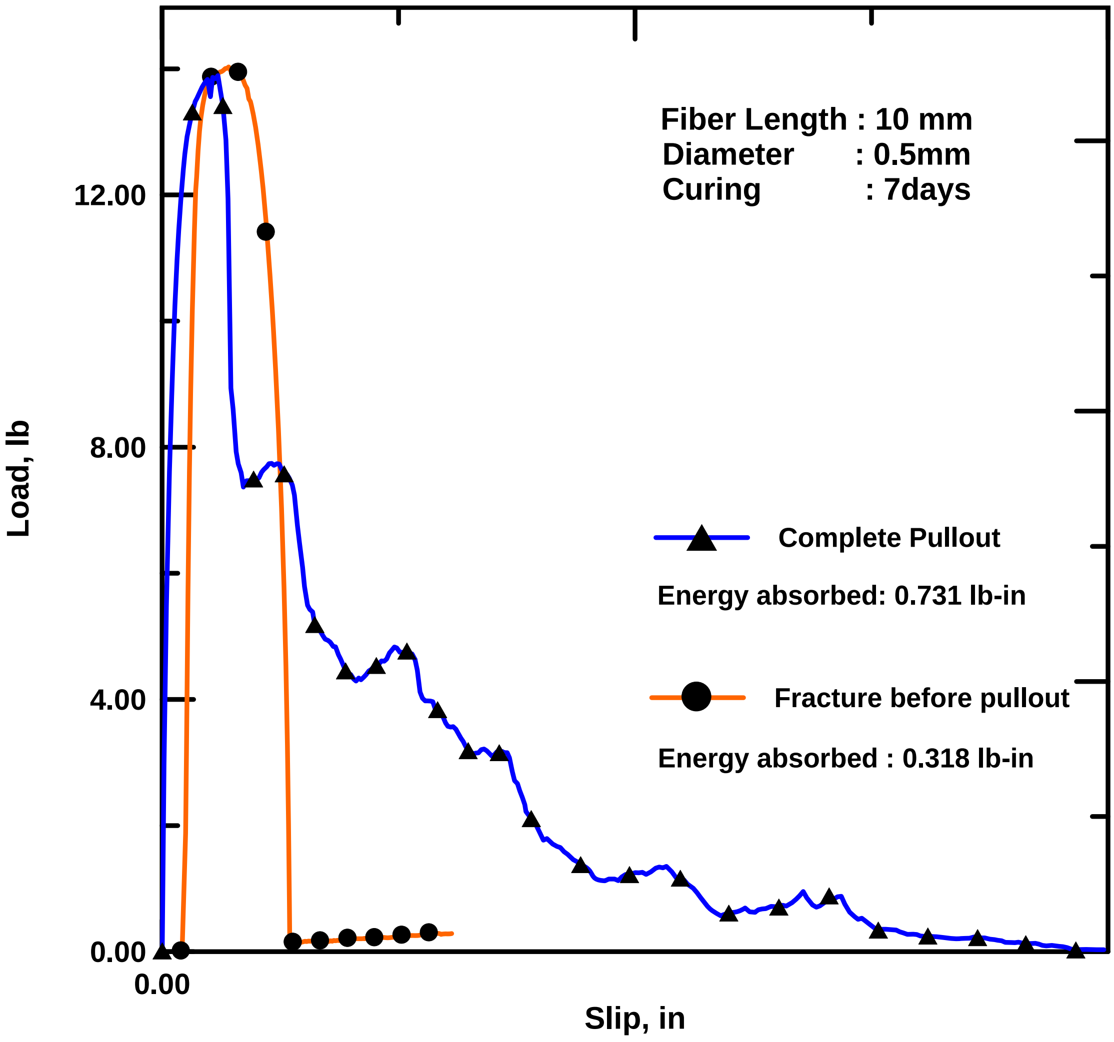

Figure 2.14 Comparison of pullout slip response when the fiber failed by fracture and completely pulled out

2.5.5 Interfacial Zone Parameters

The interfacial zone parameters that characterize the force-slip response of a fiber in a tension test, are the interfacial zone stiffness and the shear strength. The pre-peak region is governed by the stiffness of the interface. The post-peak region is a measure of the shear strength of the interface. The constitutive shear strength of the interface for a given curing period can be obtained from the pullout-slip curves. For example, from the plots shown in Figures 2.7 and 2.8, the force corresponding to the frictional sliding of the fiber is measured. The frictional force for each specimen is plotted against the length of the fiber (Figure 2.15).

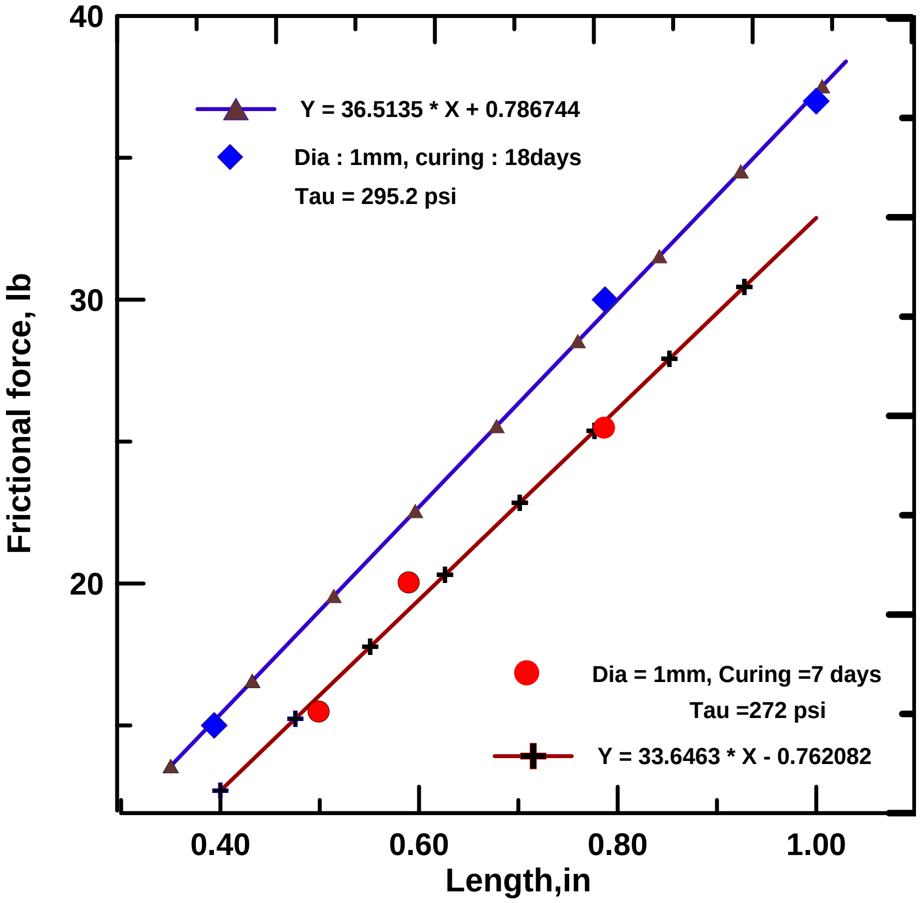

Figure 2.15 Frictional force of different specimens vs. length

A linear fit is obtained from the above set of points. The slope of the new plot gives the shear stress per unit length of the fiber. The shear strength, τ_f, acting on the interface from Eqn. (2.1) is given by

$$\tau_f = \frac{F}{2\pi r l} = \frac{slope}{2\pi r} \tag{2.5}$$

From the above equation, the constitutive shear strength of the interface is obtained for a given curing period.

Curing: 7 days

The fit of the frictional forces is as follows.

$$F = 33.6\, l - 0.76 \tag{2.6a}$$

$$Slope = 33.6,\ radius = 0.5\ mm\ (0.0197\ in) \tag{2.6b}$$

$$\tau_f = \frac{slope}{2\pi r} = \frac{33.6}{0.12} = 272\ psi \tag{2.6c}$$

Curing: 7 days

The fit of the frictional forces is as follows.

$$F = 36.5\, l + 0.78 \tag{2.7a}$$

$$Slope = 36.5,\ radius = 0.5\ mm\ (0.0197\ in) \tag{2.7b}$$

$$\tau_f = \frac{slope}{2\pi r} = \frac{36.5}{0.12} = 295\ psi \tag{2.7c}$$

The strength of the specimen increases with the increase in shear strength. But a high increase in the shear strength of the interface doesn’t allow complete debonding of the fiber resulting in fracture. This leads to a significant decrease in the toughness of the composite although there is an increase in the strength. However toughness is a desirable property in controlling cracking. Therefore, to increase toughness, lower shear strength resulting in a weaker bond is desirable. This will enable the fibers to slip out during pullout preventing a catastrophic failure.

2.6. SUMMARY OF RESULTS

The experimental results indicate that a typical force-slip curve is predominantly linear prior to the peak (P_{max}) with a steep rise. When the peak load is reached, the pullout force drops down till it reaches a constant value. Slip of the fiber continues at this constant force, until the force down steadily, to zero, indicating that the fiber pulled out completely. The interfacial zone parameters could be obtained from the pullout-slip response of the fiber from the matrix. However, the diameter of the fibers, the embedded length and the curing period effect these parameters tremendously. If the length of the fibers exceeds a certain value, the fiber starts yielding before complete pullout takes place. The total energy absorbed during the pullout process can also be determined from the area under the pullout-slip curve. The energy is dependent on the length of the fiber and its geometry. The total energy absorbed gives a measure of the toughness of fiber reinforced composites.

CHAPTER 3

MODELING OF FIBER PULLOUT FROM CEMENTITIOUS MATRICES

3.1 INTRODUCTION

Theoretical models for the analysis of fiber pullout problems have been developed based on mainly two approaches. The two different approaches that characterize the strength of the interface are based on shear lag or stress criterion, and fracture mechanics or energy based approach. A theoretical model (Li et al., 1990) based on friction-fracture criterion is discussed below.

3.2 THEORETICAL MODEL

A two-dimensional model with geometry as shown in Figure 3.1a is considered. A single elastic fiber is embedded over a length l in cement matrix. The fiber has a uniform geometry and a Young's modulus of E_f. The fiber is also assumed to be straight and smooth. A tensile force P is applied at the free end of the fiber, which is increased monotonically. The displacement at the end of the fiber $U(l)$ is assumed to be uniform over the cross-section. The bonded interface is modeled as an elastic-perfectly-plastic interface (Figure 3.1b) with stiffness k and ultimate adhesional bond strength of q_y which is the shear force per unit length of the fiber. Assuming that the fiber has debonded over a length a, the frictional shear force per unit length acting in this region is q_f. The effect of Poisson's ratio of the fiber and the matrix is ignored in the model formulation. Considering a unit length of the interface, its constitutive response is expressed as

$$q = kU(x) \qquad 0 < x < l\text{-}a \tag{3.1}$$

$$q = q_f \qquad l\text{-}a < x < l \tag{3.2}$$

The shear force per unit length, q, acting along the interface is equal to the derivative of the fiber force, *P*, with respect to *x*. The equilibrium relationships can be written as follows.

$$\frac{dP}{dx} = q \tag{3.3}$$

$$P = E_f A \frac{dU}{dx} \tag{3.4}$$

$$q = kU \tag{3.5}$$

The slip at the fiber end obtained by imposing boundary conditions (displacement and stress continuity across the bonded and debonded zone) is

$$U(l) = \frac{(P - q_f a)\chi}{E_f A\omega} + \frac{Pa - \frac{1}{2} q_f a^2}{E_f A} \tag{3.6a}$$

where

$$\omega = \sqrt{\frac{k}{E_f A}} \quad , \quad \chi = \coth(\omega(l - a)) \tag{3.6b}$$

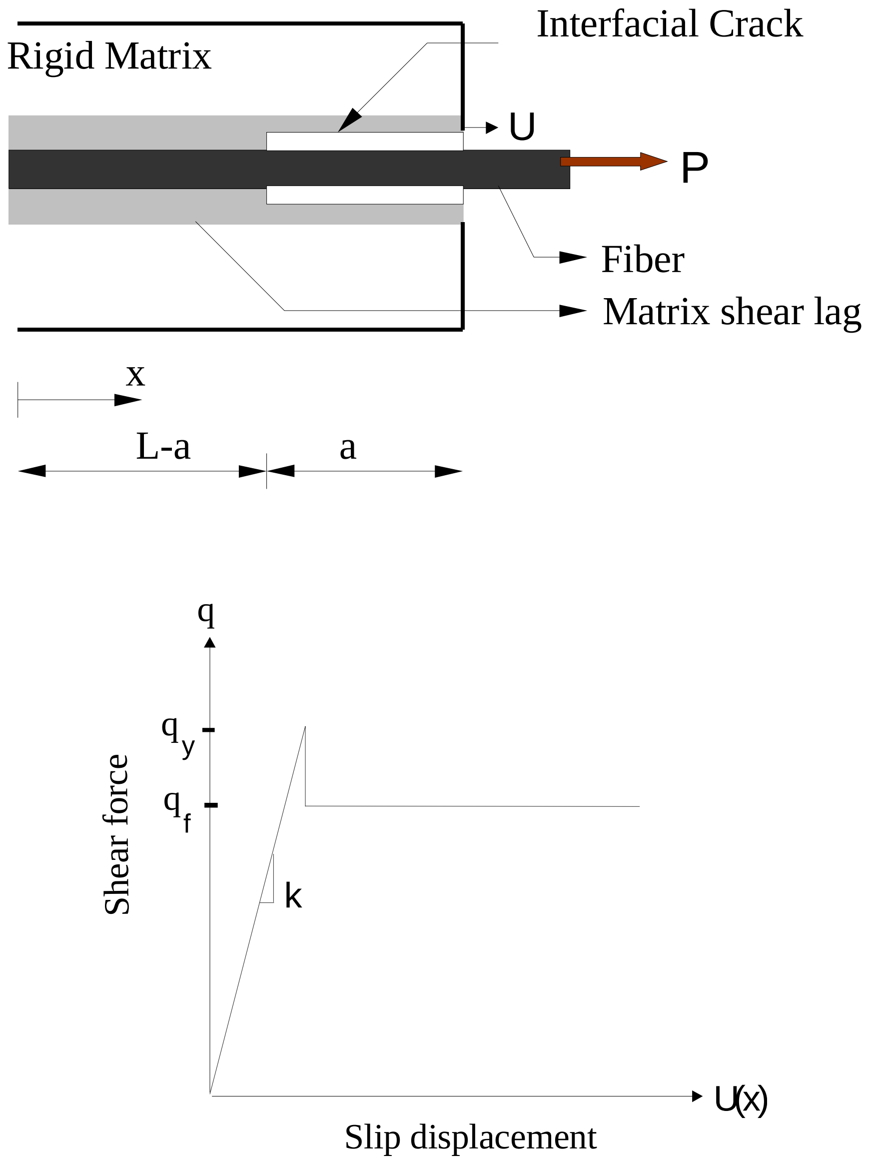

Figure 3.1 a) Geometry of the fiber pullout model, with interface modeled as shear lag
b) Constitutive response of the elastic-perfectly plastic interface with stiffness k, adhesional bond strength q_y, frictional shear strength q_f

3.2.1 Energy Based Approach

In this approach, it is assumed that the debonding of the fiber requires certain energy and this energy is characteristic of the bond between the fiber and the interface. The growth of the debonded zone is considered analogous to the propagation of a mode II crack tip. It is postulated that when a load is applied at the fiber end, the fiber starts debonding by releasing energy into the interface.

Initially the crack (debonded zone) propagation is stable until it reaches a certain value, after which it requires little or no load to grow further. That value is called the critical crack length (a_c) and the corresponding load is the ultimate pullout force. When the ultimate pullout force is reached, the debonding propagates by itself, with little or no force. This is called steady state crack growth. The steady state crack growth continues until the fiber is debonded completely. Any load applied at this stage is utilized in opposing the frictional resistance offered by the interface to the sliding fiber. This phenomenon is shown in Figure 3.2.

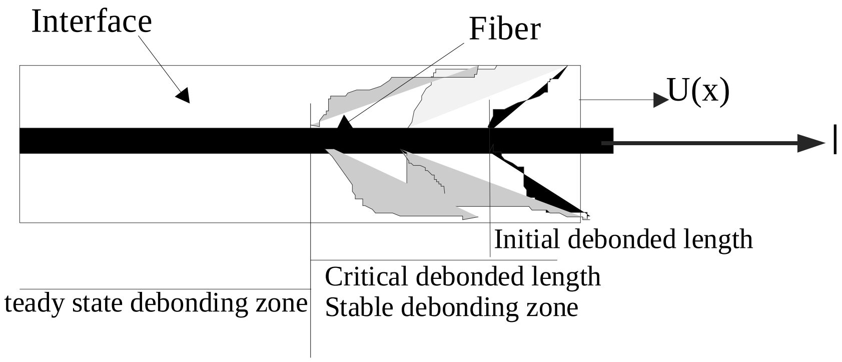

Figure 3.2 Debonding along the interface, in a friction-fracture model

3.2.2 Model Formulation using R-curves

Strain energy release rate curves and R-curves were used to formulate the model in the three zones, depending on the length of the crack. The total strain energy is defined as the algebraic sum of the work done by external forces, strain energy stored in the bonded and the debonded system and the inelastic work done by friction as shown below.

$$S.E = W_{ex} - W_{\varepsilon} - W_{f} \tag{3.7}$$

Strain energy release rate, G, is given by

$$G = \frac{\partial W_{ex}}{\partial a} - \frac{\partial W_{\varepsilon}}{\partial a} - \frac{\partial W_{f}}{\partial a} \tag{3.8a}$$

or,
$$G = \frac{1}{2E_f A\omega\Omega}\left[\frac{dP}{da} q_f a\chi - \left(P\chi^2 - q_f a\right)\left(P - q_f a\right)\omega - Pq_f \chi\right] \tag{3.8b}$$

An R-curve could be defined as the locus of the fracture energy release rates for different size specimens, initial crack length being the same. This model [Mobasher and Li, 1995] computes the slip at every increment of the interface debonding, using the updated load. This is achieved using an iterative approach. Three different conditions are used to generate the load slip response.

The stable crack growth condition is modeled using R-curves such that the toughness increases with the increase in the debonded length, until the ultimate load value is reached, which also corresponds to the critical length of the crack a_c or the critical debonded length. It could be expressed in terms of initial debonded length a_0 as follows

$$a_c = a_0 + \Delta a_c = \alpha a_0 \tag{3.9}$$

$$R(a) = \beta \left[1 - \frac{d_2}{d_1} \left(\frac{\alpha a_0 - a_0}{a - a_0} \right)^{d_2 - d_1} \right] \left(a - a_0 \right)^{d_2} \tag{3.10}$$

$$d_{1,2} = 0.5 + \frac{\alpha - 1}{\alpha} \pm \left[0.25 + \frac{\alpha - 1}{\alpha} + \left(\frac{\alpha - 1}{\alpha} \right)^2 \right]^{\frac{1}{2}} \tag{3.11}$$

The stable crack growth was modeled using the following equations:

$$\begin{gathered} R(a_c) = G(a_c) = \Gamma \\ \frac{\partial R}{\partial a} > \frac{\partial G}{\partial a} > 0 \quad for\ a < a_c \end{gathered} \tag{3.12}$$

Steady state crack growth condition is used beyond the peak load. When the crack length reaches the critical value, the R-curve is tangent to the strain energy release rate and the following conditions apply.

$$R = G\,,\ \frac{\partial R}{\partial a} = \frac{\partial G}{\partial a} \tag{3.13}$$

The governing second order differential equations were obtained by substituting Eqns. (3.8), (3.9) and (3.10) in the above equation (3.13). The solutions to the differential equations and the calculation of the parameters α and β are dealt with extensively in Li’s thesis [1995]. When the fiber debonded, frictional pullout was used to model the response of the fiber at this stage till the fiber pulls out completely. This was formulated as two different cases, as a linear response in case 1, Eqn. (3.14a), and as a nonlinear response in case 2. In the case 1, it is assumed that the pullout force suddenly drops to a value from where on it is governed by friction, defined by a linear function given below.

$$P = x\left(q_{dynamic}\, 2\pi r\right) \tag{3.14a}$$

Where $q_{dynamic}$ is the dynamic frictional strength and x is the slip, r being the radius of the fiber. But in case 2, the force was assumed to decrease gradually beyond the peak, as opposed to a sudden drop, and resulted in a nonlinear function, Eqn. (3.14b).

$$P = P_{\max}\, e^{-\delta S} \tag{3.14b}$$

Where P is the pullout force, S is the slip and δ is a constant that governs the non-linearity of the curve. $P_{\max}$ is the peak pullout force of the curve.

The theoretical pullout-slip response is generated using a FORTRAN source code which implements the model discussed above. The program requires the following material properties and geometry of the fiber as input, the units being N and mm.

1. Total number of increments
2. Young's modulus of the fiber
3. Young's modulus of the matrix
4. Poisson’s ratio of the fiber
5. Poisson’s ratio of the matrix
6. Shear stiffness, ω
7. Fiber strength, σ_{fu}
8. Interface pullout shear coefficient, $d(q_y/q_f)$

9. Interface shear strength, q_y, N/mm
10. Initial debonded length, mm
11. Fiber length, mm
12. Fiber radius, mm
13. Bond fracture energy, γ, N-mm

Parametric study was carried out to determine the influence of each of the above parameters, on the load-slip curves generated by the model.

3.3 COMPARISON WITH EXPERIMENTAL RESULTS

Good agreement was seen between the experimental and the theoretical results. Figure 3.3 compares the two curves generated for a specimen of embedded length 15 mm, diameter 1 mm and a curing period of 7 days. The pre-peak region generated by the model matches closely with the experimental results, implying that the stiffness and the peak load are predicted accurately by the model. However, the post peak response predicted by the model is higher than that observed in the actual experiments. This is because certain losses are not accounted for in the model - a constant shear strength criterion was used as a dissipative mechanism in the model.

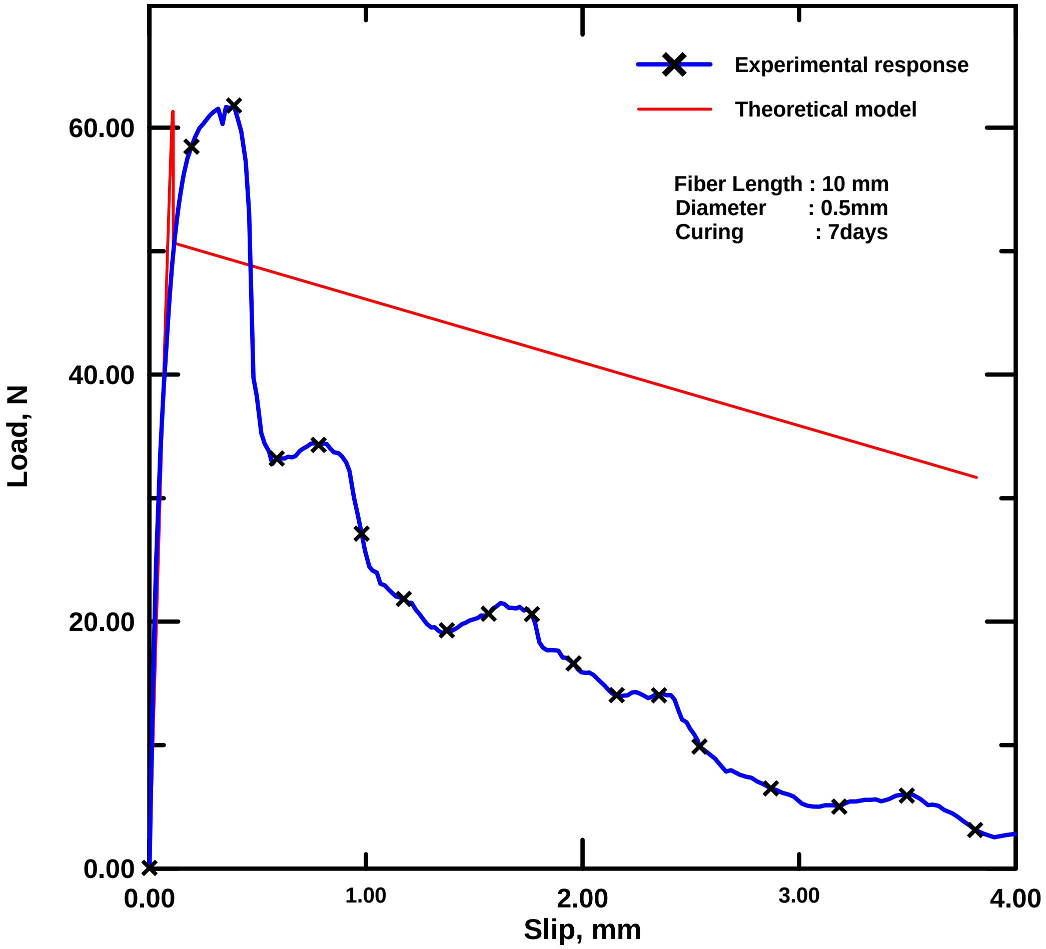

Figure 3.3 Comparison of the experimental fiber pullout-slip response and the theoretical curve generated by the model

CHAPTER 4

OPTIMIZATION OF INTERFACIAL ZONE PARAMETERS

4.1 OVERVIEW OF PARAMETER MODELING

The experimental pullout-slip results and the details of the theoretical model were discussed in earlier chapters. The objective here is to determine the parameters governing the interfacial zone characteristics viz. the shear strength, adhesional bond strength, energy absorption capacity, frictional strength and stiffness. Of particular interest is to achieve these values from the theoretical model by utilizing the available experimental results as well. To achieve this, the results from the theoretical model are matched with the experimental curve and the interfacial parameters are obtained from it. The results obtained from this kind of curve fitting are extremely useful. They could be used in studying the general characteristics of the theoretical model and adaptations that need to be made for close agreement with the experimental results. Moreover, the results obtained could be extended to predict the experimental response, given the geometry and the material properties of the fiber without actual experimentation.

Conventional techniques viz. least squares fit, regression, interpolation etc., have been used for curve fitting of experimental data (Noggle, 1993). The above methods involved mainly obtaining the constants of an equation or a model that is used to fit the data. Such a scheme is not possible when the model to be fitted is obtained from a computer simulation governed by nonlinear differential equations as in the present case. To overcome this limitation, the Genetic Algorithm, an optimization technique can be used. Recently Genetic Algorithm was used for curve fitting experimental data with a mathematical model using least squares error fit (Karr et al., 1991). In this paper the experimental results are fitted to a theoretical model rather than a mathematical model. Moreover, the form of the theoretical model is not governed by a single mathematical equation but is a computer simulation.

The theoretical model discussed in Chapter 3 is used here. The model is matched with the available experimental fiber pullout-slip response. The parameters in the model are then estimated. The process of matching the two curves is achieved using a least-squares objective function - minimize the error between the pullout-slip response predicted by the theoretical model and the experimental curves. Use of this methodology overcomes the problem of not knowing the theoretical model parameters a priori.

4.2 DESIGN PROBLEM FORMULATION

To formulate the mathematical model for optimization certain parameters that describe the design of the system, called the design variables, $\mathbf{x}$, are to be identified. The second step is to define an objective function, $f(\mathbf{x})$, that is dependent on the design variables. Finally, constraints that have to be satisfied by the design and appropriate bounds on the design variables are imposed as shown next.

4.2.1 Design Variables

These are problem parameters that can be varied during the design iterations and whose values are sought as the answer to the design problem. Different variables that determine the theoretical model were studied to zero in on the variables that control the design. Various parameters that were used in the governing equations, which predict the pullout-slip response, are listed below.

(a) Material properties of the fiber and cement matrix namely the Young's modulus, Poisson's ratio and the fiber strength, σ_{fu}.

(b) Geometry of the fiber defined by its length and radius.

(c) Interface parameters viz. the stiffness ω, shear coefficient, d, shear strength, q_y.

(d) Bond energy γ, and the initial debonded length.

(e) Dynamic interface shear strength, $q_{dynamic}$.

Of the above variables, the geometry and the material properties remain constant for each run; hence they could not be optimized. The initial debonded length of the flaw size is nominal and is required to initiate the debonding process. Hence, it doesn't control the design. Therefore, the interface parameters actively control the design and could be optimized to fit the experimental results. The following parameters were chosen as the design variables - the stiffness ω, shear coefficient, d, shear strength, q_y, bond energy γ, dynamic shear strength, $q_{dynamic}$.

4.2.2 Constraints and Bounds on Design Variables

These are problem parameters that need to be satisfied for the design to be acceptable. Bounds on the design variables were imposed to ensure that the range of values for the design variables was scientific. The selection of bounds was based on past results and parametric studies. For example, the shear coefficient d is the ratio of q_f and q_y, and cannot exceed 1. Sometimes it may be required to change the bounds on the design variables so as to obtain a better solution. This is characteristic of GA-driven solution procedures. The current problem has two constraints.

$$q_{dynamic} < q_y \tag{4.1a}$$

$$\frac{q_{dynamic}}{q_y} < D \tag{4.1b}$$

4.2.3 Objective Function

This is a function whose value is to be minimized or maximized during the design process. The objective here is to minimize the error between the theoretical and the experimental curves by modifying the parameters that affect the theoretical curve. Figure 4.1 shows typical experimental and theoretical curves.

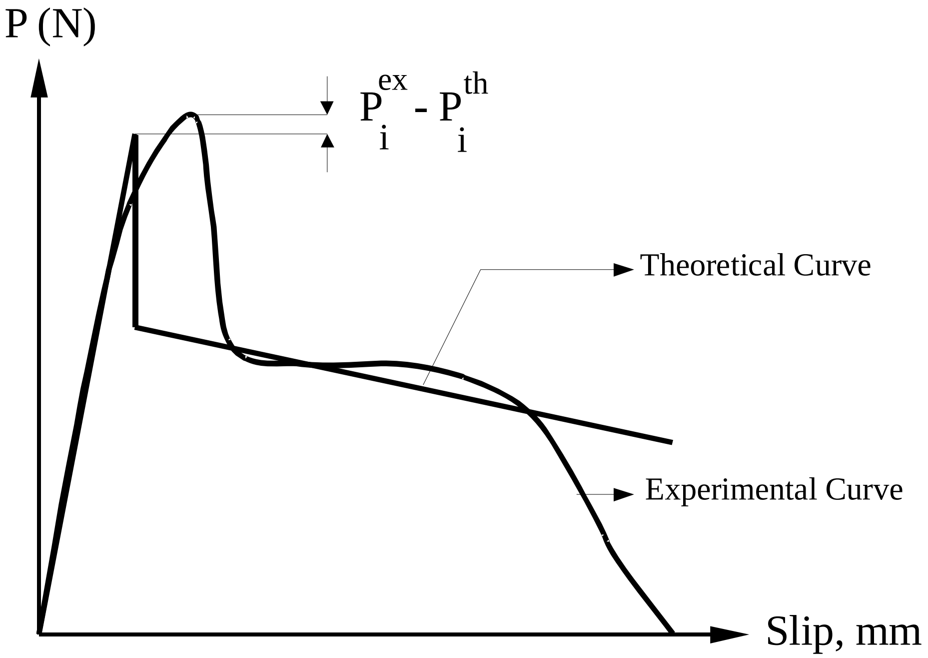

Figure 4.1 Typical experimental and theoretical pullout-slip curves for a specimen.

4.2.4 Problem Definition

The problem is formulated as a constrained optimization problem as follows. Find design variable vector, $\mathbf{x}$, to minimize

$$f(\mathbf{x}) = \sum_{i=1}^{n} w(P_i^{th} - P_i^{ex})^2 \tag{4.2}$$

Subject to

$$0.01 \le x_1 \le 1.5 \tag{4.3a}$$

$$0.01 \le x_2 \le 1 \tag{4.3b}$$

$$1 \le x_3 \le 5 \tag{4.3c}$$

$$0.001 \le x_4 \le 0.2 \tag{4.3d}$$

$$0.1 \le x_5 \le 1 \tag{4.3e}$$

where

$f(\mathbf{x})$	error between the experimental and theoretical curves
x_1	stiffness of the interface, ω
x_2	interface shear coefficient , d
x_3	interface strength, q_y
x_4	bond energy, γ
x_5	dynamic shear strength, $q_{dynamic}$
w	weight function
P_i^{th}	thoretical load at a particular value of slip
P_i^{ex}	experimental load at the corresponding slip

As discussed in Chapter 3, the theoretical model predicts the pre-peak region with a good accuracy. After the peak the model doesn’t predict the response as accurately because of the complicated behavior of the fiber-interface after the fiber is completely debonded such as frictional losses, rotations and other mechanisms that come into effect. Hence it is of interest to achieve higher accuracy in fitting the curve in the pre-peak region than in the post peak region. This strategy can be implemented using a weighted objective function. If w_i be the weight at every point i then the objective function could be re-written as

$$f(\mathbf{x}) = \sum_{i=1}^{n} w_i \, (P_i^{th} - P_i^{ex})^2 \tag{4.4}$$

As higher accuracy is needed in the pre-peak region than the post peak region, a weighting curve of the form shown in Figure 4.2 is of interest. For example, if the pre-peak region is considered to be twice as important as the post-peak region, a normalized weight varying between 1.0 and 0.5 can be used in the post-peak region. Figure 4.2 shows the plot of a sample weighting function governed by the following equation, in the post-peak region. The equation used in this case is given by

$$y = 0.01074x^2 - 0.10738x + 1.0011 \tag{4.5}$$

where y is the weight and x is the slip.

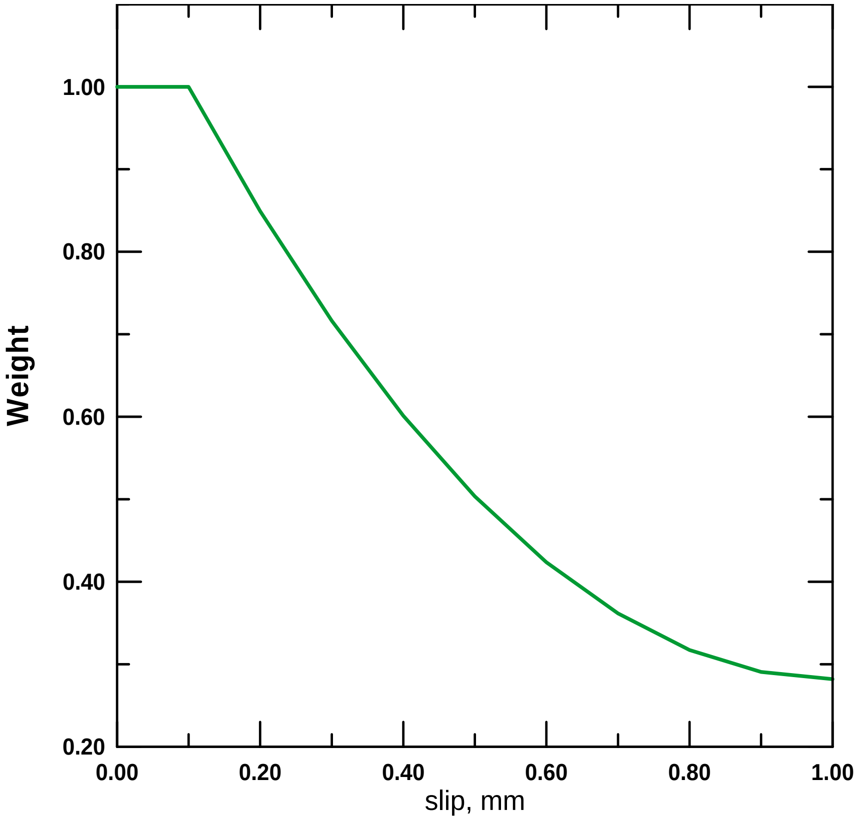

Figure 4.2 Typical weighting function

In this research, different approaches were studied. The above form of the objective function (Eqn. 4.4) did not yield satisfactory results - peak load and the slope could not be matched satisfactorily in spite of the use of weight functions. Hence different compound objective functions were formulated and tried.

Case 1

The theoretical model is governed by a linear variation in the post peak region.

$$f(\mathbf{x}) = w_1 (S^{th} - S^{\exp})^2 + w_2 (P_{\max}^{ex} - P_{\max}^{th})^2 + w_3 \sum_{i=1}^{n} (P_i^{ex} - P_i^{th})^2 \tag{4.6a}$$

The weights on the objective function are chosen based on the disparity of absolute values between the parameters. In this case, x_5 is the dynamic shear strength, $q_{dynamic}$**, and** $0.1 \le x_5 \le 2.5$. The results are discussed in Section 4.4.

Case 2

The theoretical model is governed by nonlinear equation in the post peak region.

$$f(\mathbf{x}) = w_1 (S^{th} - S^{\exp})^2 + w_2 (P_{\max}^{ex} - P_{\max}^{th})^2 + w_3 \sum_{i=1}^{n} (P_i^{ex} - P_i^{th})^2 \tag{4.6b}$$

In this case, x_5 is an exponential decay parameter, $0.1 \le x_5 \le 25.0$, which governs the expression for the nonlinear post peak region.

Case 3

In this case, the objective function is normalized, Eqn. (4.6c), and the theoretical model is governed by a nonlinear function in the post peak region. By normalizing the objective function, the disparity of values between its components is reduced and they are comparable. Hence a better fit is expected even before using the weights.

$$f(\mathbf{x}) = w_1 \left(\frac{S^{th} - S^{\exp}}{S_{\max}^{\exp}} \right)^2 + w_2 \left(\frac{P_{\max}^{ex} - P_{\max}^{th}}{P_{\max}^{ex}} \right)^2 + w_3 \sum_{i=1}^{n} \left[\frac{1}{n} \left(\frac{P_i^{ex} - P_i^{th}}{\max(P_{\max}^{ex}, P_{\max}^{th})} \right)^2 \right] \tag{4.6c}$$

where

S^{th}	Slip of theoretical model at the peak load
$S^{\exp}$	Slip of experimental curve at the peak load
P_i^{ex}	Experimental load
P_i^{th}	Theoretical load
n	Total number of data points in the post-peak region
w_1, w_2, w_3	Discrete weights

4.3 BRIEF OVERVIEW OF GENETIC ALGORITHM

Genetic Algorithm (GA) is a search strategy based on the rules of natural genetic evolution. GA's have been used to solve a variety of design problems. Because of their discrete nature, GA's lend themselves well to the process of automating the design. GA's do not require gradient or derivative information. For this reason alone, it has been applied by researchers to solve discrete, non-differentiable, combinatory and global optimization engineering problems, such as transient optimization of gas pipeline, topology design of general elastic mechanical system, time scheduling, circuit layout design, composite panel design, pipe network optimization, and several hundred others. GA's are recognized to be different than traditional gradient-based optimization techniques in the following four major ways [Goldberg, 1989].

1. GA's work with a coding of the design variables and parameters in the problem, rather than with the actual parameters themselves.

2. GA’s make use of population-type search. Many different design points are evaluated during each iteration instead of sequentially moving from one point to the next.

3. GA’s need only a fitness or objective function value. No derivatives or gradients are necessary.

4. GA’s use probabilistic transition rules to find new design points for exploration rather than using deterministic rules based on gradient information to find these new points.

The idea behind GA is to simulate the behavior of natural evolutionary selection. Although there exist many different variations of GA’s, the basic structure is the same as shown in Figure 4.3. The details are discussed below (Rajan, 1999).

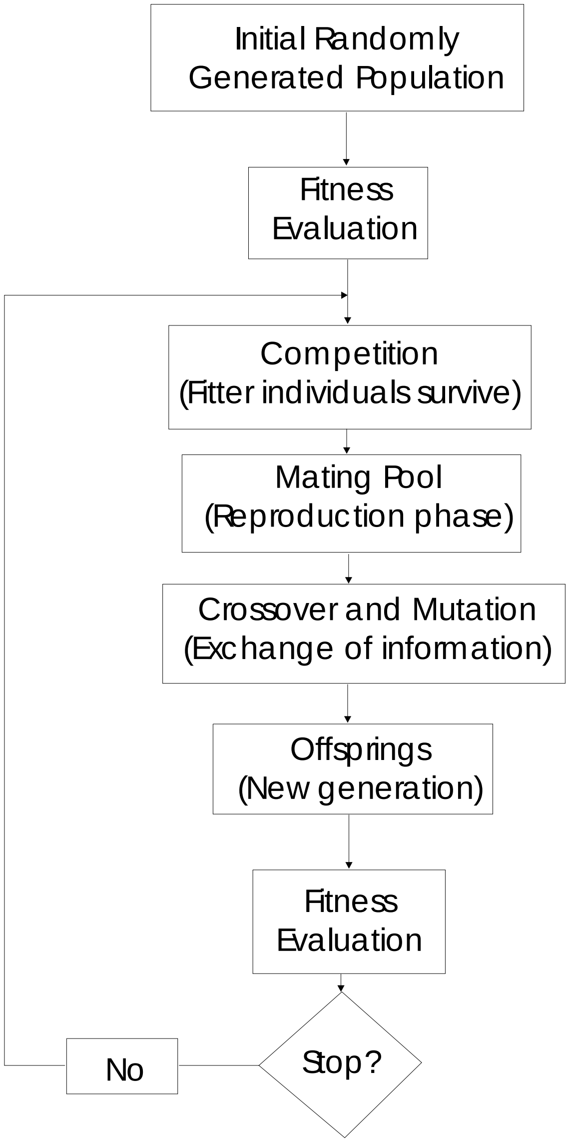

Figure 4.3 Flow in a Simple Genetic Algorithm (SGA)

4.3.1 The Basic Algorithm

The genetic algorithm is used to solve the following problem.

Minimize $\hat{f}(\mathbf{x})$ (4.7)

Subject to $x_k^L \le x_k \le x_k^U\,,\ k = 1,2,\ldots,n$

The problem is primarily an unconstrained minimization problem with lower and upper bounds on the design variables. The necessary background is presented first before detailing the algorithm. In the language of GA, $\hat{f}(\mathbf{x})$, the fitness function, is computed and not $f(\mathbf{x})$, the objective function.

4.3.2 Binary Encoding and Decoding of Design Variables

Binary encoding is the most popular way of encoding the design variables. A binary number is represented as $(b_m...b_1b_0)_2$ where b_i is either 0 or 1. The relationship between binary and decimal numbers is shown below.

$$(b_m...b_1b_0)_2 = (2^0 b_0 + 2^1 b_1 + ... + 2^n b_m)_{10} \tag{4.8}$$

The process of taking a decimal number and constructing its binary representation (not value) is called encoding. Decoding is the inverse process of taking the binary encoded value and constructing its decimal equivalent.

Continuous Design Variables: A design variable x_i is between x_i^L and x_i^U, where x_i is a decimal number. If m bits are available to represent x_i, then the precision p_i with which the number is represented is given by

$$p_i = \frac{x_i^U - x_i^L}{2^m - 1} \tag{4.9}$$

To understand the term in the denominator, an example with 3 bits is illustrated. The possible binary representations with 3 bits are 000, 001, 010, 011, 100, 101, 110 and 111. Or, 8 possible combinations. In other words, if there are m bits then there are 2^m combinations or

$2^m - 1$ intervals. The range of values between x_i^L and x_i^U is divided into $2^m - 1$ intervals. The following Table (4.1) shows the relationship between the binary representation and their decimal equivalents with this example.

Table 4.1 Binary representations and corresponding decimal equivalents

Binary Representation $(b_2b_1b_0)_2$	**Decimal Equivalent** $x = x^L + p(b_2b_1b_0)_2$
000	1.0
001	2.0
010	3.0
011	4.0
100	5.0
101	6.0
110	7.0
111	8.0

The decoding is achieved using

$$x = x^L + p(b_m ... b_1b_0)_2 \tag{4.10}$$

where decimal values are used.

Integer Design Variable: With integer design variables, one approach is to apply Eqn. (4.9) with the precision p being 1 and compute the least number of bits required to achieve the precision. The number of bits obviously is an integer. For example, let $x^L = 1$, $x^U = 10$ and $p = 1$. Using

$$2^m - 1 = \frac{x_i^U - x_i^L}{p} \Rightarrow m = \log\left(x_i^U - x_i^L + 1\right) / \log(2) \tag{4.11}$$

Discrete Design Variable: The representation is similar to integer design variables with $x^L = 1$ and $x^U = q$ where there are q possible discrete values. The discrete values are usually stored in a Table in some sorted manner and the integer value between 1 and q is used as an index to obtain the corresponding value(s) from the Table.

Zero-One (Binary) Design Variable: There is nothing special that needs to be done in this case because exactly one bit is needed to represent a zero-one design variable.

Chromosome: To represent all the design variables in a problem, a *chromosome* needs to be created for the problem. A chromosome is a concatenated binary string of all the binary representations of the design variables. If there are n design variables with $m = 3$ to represent each design variable, then the chromosome looks as shown in Figure 7.4.1-1 with x being 0 or 1.

xxx xxx xxx xxx
x_1 x_2 x_3 x_n

Figure 4.4 Possible chromosome

The number of bits do not have to be equal for all the design variables nor do the design variables have to ordered from 1 to n in the chromosome. The basic steps in the algorithm are discussed next.

4.3.3 Initial Population

The first step is to create the initial population. Unlike gradient-based methods where the search for the optimal solution takes place by moving from one point to the next, in a GA the traits of a population (of members) are used to move from one generation to the next. Figure 4.5 shows an initial population consisting of z members. The initial population is usually created randomly.

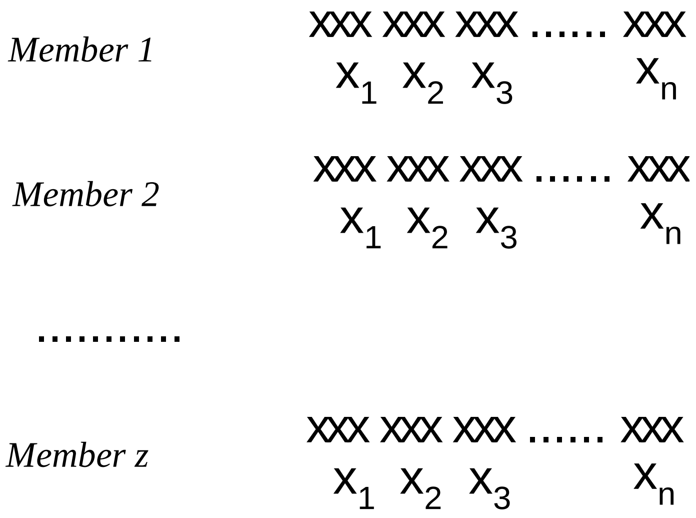

Figure 4.5 Initial population

With the example in Figure 4.5, the size of the chromosome is $3n$ bits. A random number generator can be used to generate a random number between 0.0 and 1.0. Invoking the random number generator $3n$ times, each member of the population can be generated as follows – if the random number is ≤ 0.5 then a 0 is assigned to that bit otherwise if the number is > 0.5 a 1 is assigned to that bit.

4.3.4 Fitness Evaluation

Once the initial population is generated, the actual search process starts. The chromosome is decoded to obtain the values of the design variables, $\mathbf{x}$ and the fitness function value is computed for each member of the population. In other words, there are z fitness values $\hat{f}(\mathbf{x})$ that are calculated.

4.3.5 Reproduction

To generate the members of the next generation, the reproduction phase has at least three distinct steps. First the mating pool is created. Typically, the weaker members (higher fitness values) are replaced with stronger members (lower fitness values). To produce offspring, two members from the mating pool are selected and a crossover operation is carried out to create the chromosome of the offspring. Finally, to bring diversity into the population, the mutation operation is carried out.

4.3.5.1 Mating Pool

The mating pool is constructed by selecting members from the population. Two commonly used methods are described. In the *roulette wheel selection*, the chance of being selected is based on the fitness value. The individual members of the population are mapped to segments of a line such that the length of the segment is related to its fitness value.

Table 4.2 Fitness and selection probabilities of individuals

Individual	**1**	**2**	**3**	**4**	**5**	**6**	**7**	**8**	**9**	**10**	**11**	**12**	**13**	Sum
Fitness	1.20	1.50	1.70	2.20	2.50	2.70	3.90	4.50	4.70	5.20	5.50	6.10	7.80	49.50
	41.25	33.00	29.12	22.50	19.80	18.33	12.69	11.00	10.53	9.52	9.00	8.11	6.35	231.21
Selection Probability	0.18	0.14	0.13	0.10	0.09	0.08	0.05	0.05	0.05	0.04	0.04	0.04	0.03	1.00
Cumulative Value	0.18	0.32	0.45	0.54	0.63	0.71	0.76	0.81	0.86	0.90	0.94	0.97	1.00	

The sum of the fitness values is $S = \sum_{i=1}^{13} \hat{f}_i = 49.5$. A scaled fitness value is created as $\hat{f}_{is} = \frac{S}{\hat{f}_i}$. Let $S_S = \sum_{i=1}^{13} \hat{f}_{is} = 231.21$. The selection probability, $p_i = \frac{\hat{f}_{is}}{S_S}$. As can be seen from Figure 4.6, the length of the segment is more for lower fitness values than for larger fitness values.

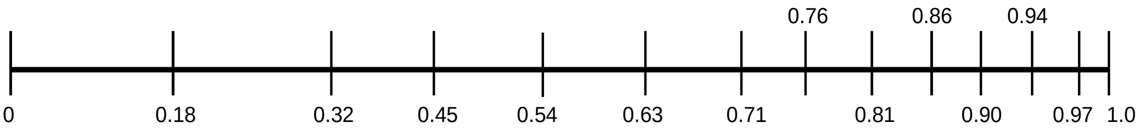

Figure 4.6 Scaled values of fitness

For selecting the individual into the mating pool, a random number between 0 and 1.0 is generated. In the *tournament selection method*, using a random number generator, two members of the population are selected. Their fitness values are compared head-to-head and the one with the lower fitness value is put into the mating pool. This is done z times to create the mating pool of size z. This method is used in the current research. In a "double elimination" tournament selection method, all the individuals in the population are placed in a bag. Two individuals are chosen at random. Their fitness values are compared head-to-head and the one with the lower fitness value is put into the mating pool. These two individuals are then eliminated from the bag and the process is repeated until the bag is empty. This will occur when the mating pool is half full. To complete the mating pool, the process is repeated once again. In a simple GA, once the mating pool is constructed, two parents are selected and the reproduction process is carried out using the crossover and mutation operators.

4.3.5.2 Crossover

Crossover is the exchange of information between parent chromosomes to form the child chromosomes. There are several types of crossover operators. Three most commonly used operators are discussed here.

One-point crossover: Consider two chromosomes selected randomly from the mating pool. They are labeled Parent 1 and Parent 2 in Figure 4.7.

Parent 1 10001001
Parent 2 00110111

Figure 4.7 Parents selected for the crossover operation

Based on a predetermined probability (0.9 in the current analysis) a single crossover point in chosen. If the length of the chromosome is n_c bits, then a random number is generated between 1 and n_c. This point or location is used as the crossover point. Two offspring are formed and they become the part of the next generation. The first offspring is formed by taking the front or left section of Parent 1 and the rear or right section of Parent 2. The second offspring is formed by taking the front or left section of Parent 2 and the rear or right section of Parent 1. The results are shown in Figure4.8.

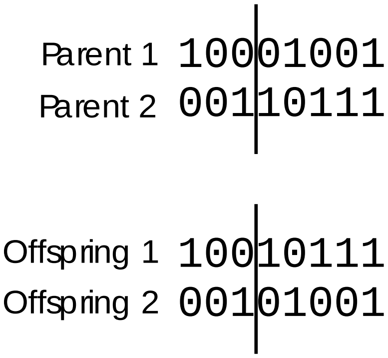

Figure 4.8 Offspring resulting from one-point crossover operation occurring at location 3

In the present analysis, one point crossover is used. Elitist approach, in which the best member of current population is carried over to the next generation, is used.

Two-point crossover: The idea of the single point crossover can be extended to include multi-point crossover locations. The section between the first variable and the first crossover point is not exchanged. However, the bits between every other successive crossover point are exchanged between the two parents. This process is illustrated with a two-point crossover example.

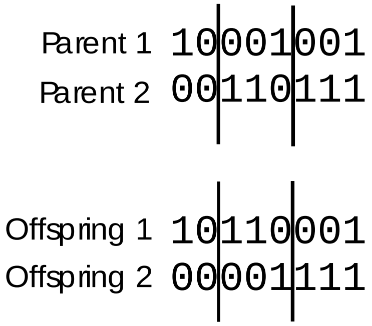

Figure 4.9 Offspring resulting from two-point crossover occurring at locations 2 and 5

***Uniform crossover*:** In uniform crossover, every location is a potential crossover point. First, a crossover mask is created randomly. This mask has the same length as the chromosome and the bit value (parity) is used to select which parent will supply the offspring with the bit. If the mask value is 0 then the bit is taken from the first parent, else the bit is taken from parent 2.

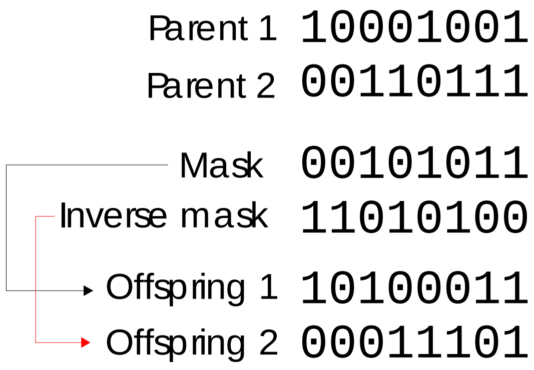

Figure 4.10 Example showing uniform crossover

If two offspring are needed, the mask is used with the parents to create the first offspring and the inverse of the mask is used to create the second offspring.

4.3.6 Mutation

This operator occurs much less frequently both in nature and in the GA. Offspring variables are mutated by the small random changes with a low probability. The basic idea is to introduce some diversity into the population. In other words, delay the situation where all the population becomes so homogenous that no further improvement is possible. If the length of the chromosome is n_c bits, then a random number is generated between 1 and n_c. The bit at that location is switched. An example is shown in Figure 4.11

Before	10010111
After	10000111

Figure 4.11 Example showing mutation taking place at location 4

Next Generation: The new generation is formed when sufficient offspring are generated in the reproduction phase. The whole process of fitness evaluation and reproduction starts all over again with this new population. The iterative process is stopped. Typically this is done if a predetermined number of iterations have been completed or if the fitness function does not change appreciably. Unlike most gradient-based techniques, there is no convergence criterion for the iterative process associated with the GA.

4.4 NUMERICAL EXAMPLES

Using the objective functions defined in equations 4.6a, 4.6b and 4.6c, the results obtained from curve fitting are summarized in Table 4.3.

Table 4.3(a) Summary of results from parameter modeling (Objective function 4.6a)

Specimen name	Weights (w_1, w_2, w_3)	Design Variables $(\omega, d, q_y, \gamma, decay)$	Number of Points, n	Objective function	Normalized Least Squares
1D15Cls20	10^5, 1, 1	N/A		N/A	N/A
1D2cLS26	10^5, 1, 1	[0.06, 0.5, 0.42, 0.051, 1.9]		116396	518.355
1D05Ils29	10^5, 50, 1	[0.02, 0.99, 4.7, 0.2, 1.2]		57853	259.197
4B1D15Cls16	10^5, 50, 1	[0.05, 0.85, 3.4, 0.051, 1.4]		102862	568.229
4B1D1iLS14	10^4, 50, 1	[0.14, 0.66, 4.9, 0.086, 2.3]		210098	2786.48
1D05iLS25	10^4, 50, 1	[0.08, 0.88, 2.9, 0.021, 2.1]		13968	49.903
4B05D1cL3	10^4, 50, 1	[0.02, 1, 3.3, 0.176, 0.9]		6575	25.644
1D05LS3	10^4, 50, 1	[0.13, 0.61, 4.1, 0.051, 2.1]		87135	366.662
1D1cS23	10^4, 50, 1	[0.04, 0.93, 4.7, 0.181, 2.5]		219918	676.77
4B1D1iLS13a	10^4, 50, 1	[0.03, 0.88, 4.5, 0.096, 1.5]		136032	3176.25
1D1cS23[1]	10^4, 50, 1	[0.15, 0.74, 1.6, 0.026, 0.3]		27965	61.7682

Table 4.3(b) Summary of results from parameter modeling (Objective function 4.6c)

Specimen name	Weights (w_1, w_2, w_3)	Design Variables $(\omega, d, q_y, \gamma, decay)$	Number of Points, n	Objective function	Normalized Least Squares
4B1D15Cls16	1, 1, 1	[0.04, 0.94, 3.7, 0.071, 0.2]		9.35463	937.518
4B1D2Cls18	1, 1, 1	[0.02, 0.24, 5, 0.146, 0.3]		0.237363	242.362
1D05iLS29	1, 1, 1	[0.01, 0.98, 2.9, 0.176, 0.5]		0.673303	241.589
1D05iLS25	1, 1, 1	[0.06, 0.55, 1.4, 0.081, 0.8]		0.4959	729.853
4B05D1cL3	1, 1, 1	[0.02, 0.35, 2, 0.166, 0.8]		0.1658	10.8155
1D2cLS26	1, 1, 1	[1.33, 0.18, 3.4, 0.011, 2.1]		0.2157	N/A
4B1D1iLS13a	1, 1, 1	[0.04, 0.9, 3.6, 0.181, 2.3]		0.6861	3207.34
1D1cS23	1, 1, 1	[0.05, 0.45, 2, 0.076, 0.1]		0.1779	149.083
1D15Cls20	1, 1, 1	[0.02, 0.32, 1.6, 0.131, 0.4]		0.24764	415.531

Normalized Least Squares: $\frac{1}{n}\sum_{i=1}^{n}(P_i^{th} - P_i^{ex})^2$

---

[1] Using Objective function (4.6b)

Table 4.4 Comparison of results using scheme (4.6a) vs scheme (4.6c)

Specimen Name	Scheme 4.6a		Scheme 4.6c	
	Obj*	NLSQ	Obj*	NLSQ
1D15Cls20	N/A	N/A	0.248	415.5
1D2cLS26	116396	518.36	0.216	N/A
1D05Ils29	57853	259.2	0.673	241.6
4B1D15cLS16	102862	568.2	9.35	937.5
1D05iLS25	13968	49.9	0.496	729.8
4B05D1cL3	6575	25.6	0.166	10.82
1D1cS23	219918	676.8	0.178	149.1
4B1D1iLS13a	136032	3176.25	0.686	3207.3

* Objective function

Cases 4.6a and 4.6b show similar response to optimization because the theoretical model has been changed and not the objective function. By making the post peak response nonlinear, the theoretical model agrees more closely with the experimental response. Hence only cases 4.6a and 4.6c have been analyzed to study the effect of normalization on the objective function as opposed to a direct function. Because of normalization a better overall fit is obtained even without using any weights. This trend is shown in figures 4.23 through 4.31. However, weights could be used if a higher accuracy of fit is desired in certain regions. For example weights could be used to match the peak load more accurately because it is highly desirable.

Table 4.4 shows the comparison of scheme 4.6a and scheme 4.6c. It is seen that the normalized values of least squares are lower in scheme 4.6c compared to 4.6a. But the results are superior in scheme 4.6a because higher weights are used hence higher accuracy is obtained in the interface parameters. However, by using weights in scheme 4.6c, better estimation of interface parameters can be obtained.

All the specimens were not used for curve fitting because some of them were fractured before complete pullout. The following figure shows that the stiffness and peak are predicted closely and the post peak response shows an averaged matching pattern.

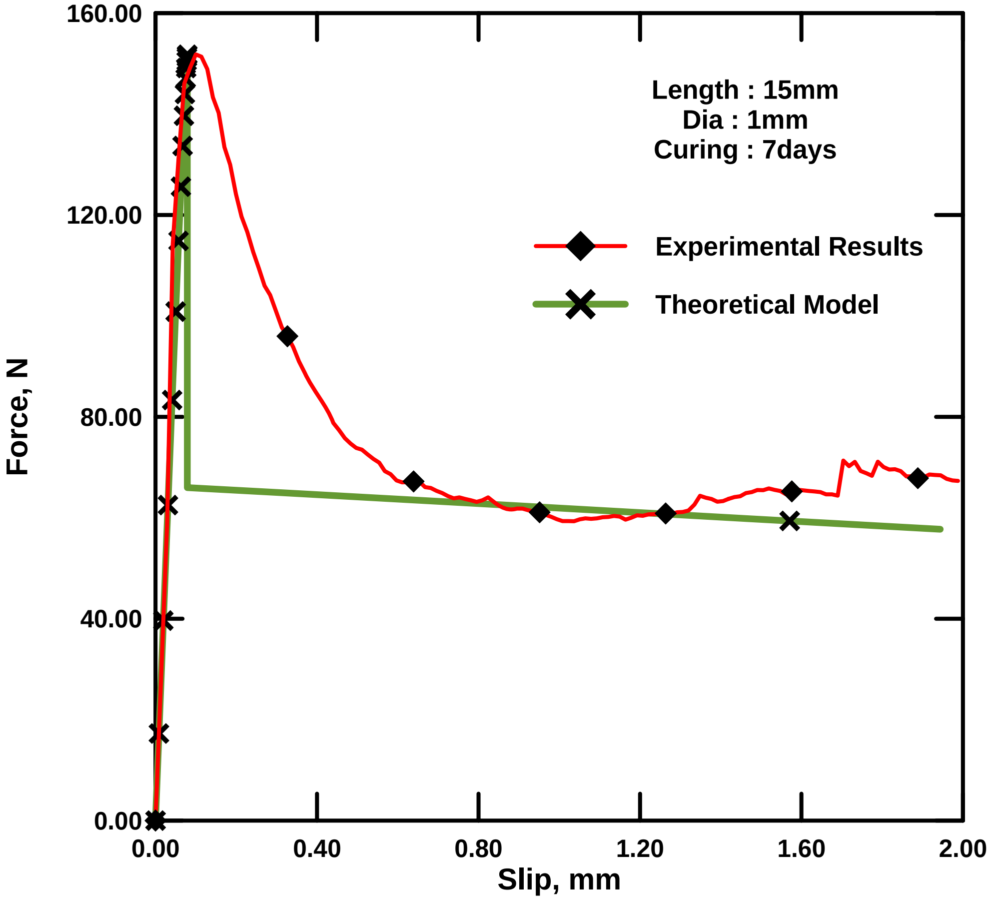

Figure 4.12 Theoretical model predicted by GA, matched with specimen 1D15cLS20 response

In this case, although the peak load is matched accurately, the stiffness does not match very well. Therefore, weights are to be increased on the first part of the objective function in Eqn. (4.6a) to decrease the error in stiffness.

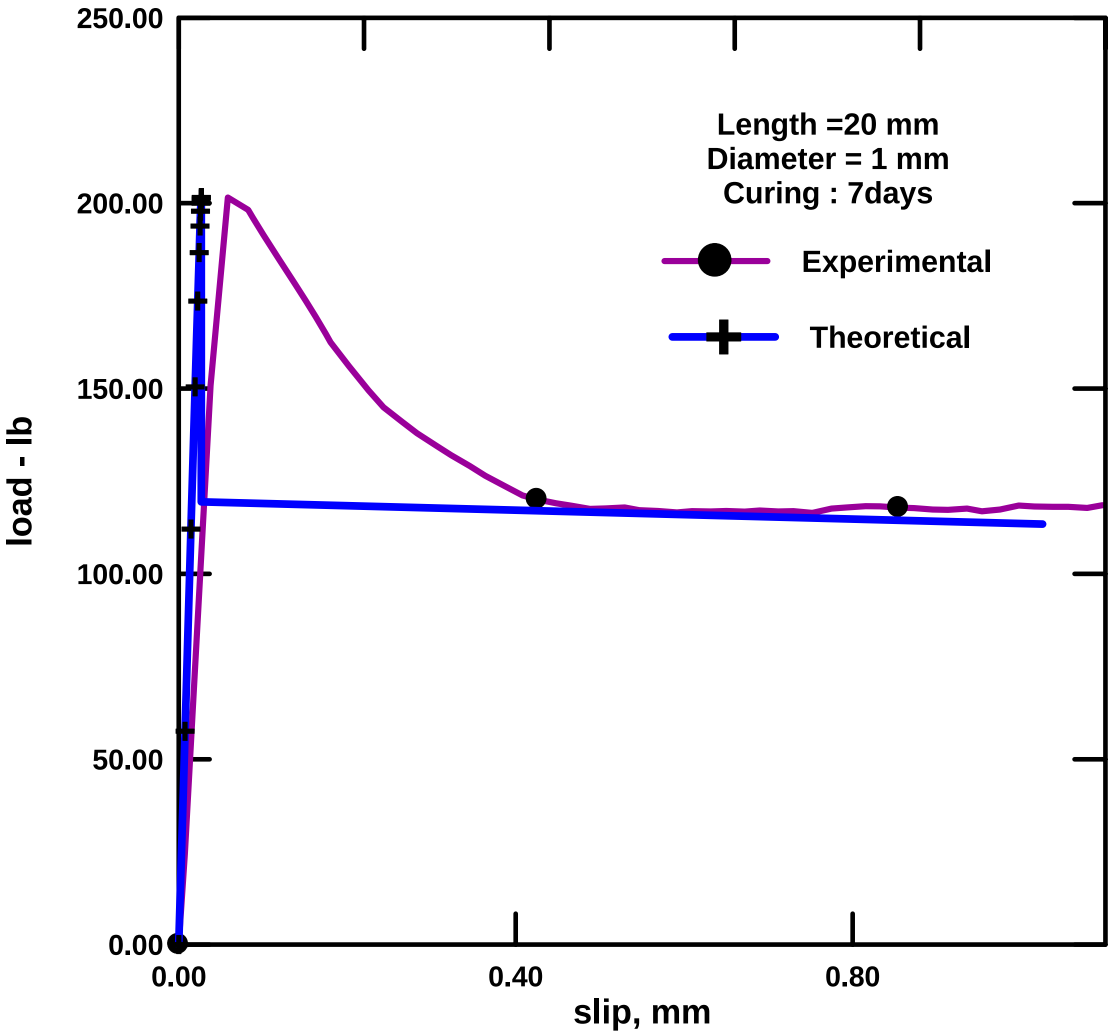

Figure 4.13 Theoretical model matched with specimen 1D2cLS26 response

As in the case of the previous specimen, in this case the weights have to be increased to match the stiffness more accurately. The peak load and the post peak region shows fairly good matching.

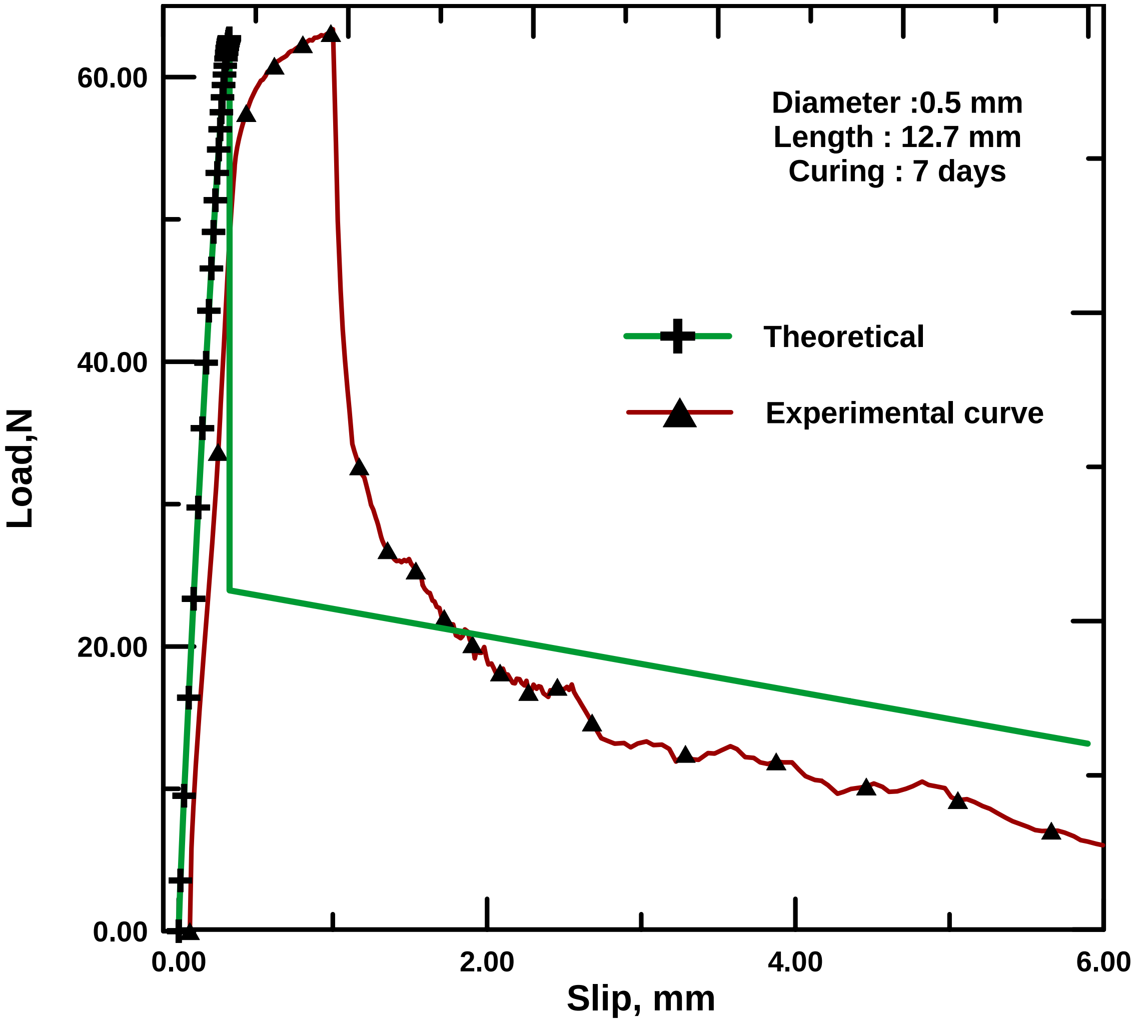

Figure 4.14 Theoretical model matched with specimen 1D05iLS29 response

The stiffness is to be weighted more in this case (Figure 4.15) in order to minimize the error. A fairly good estimate of the peak and the post peak response is made.

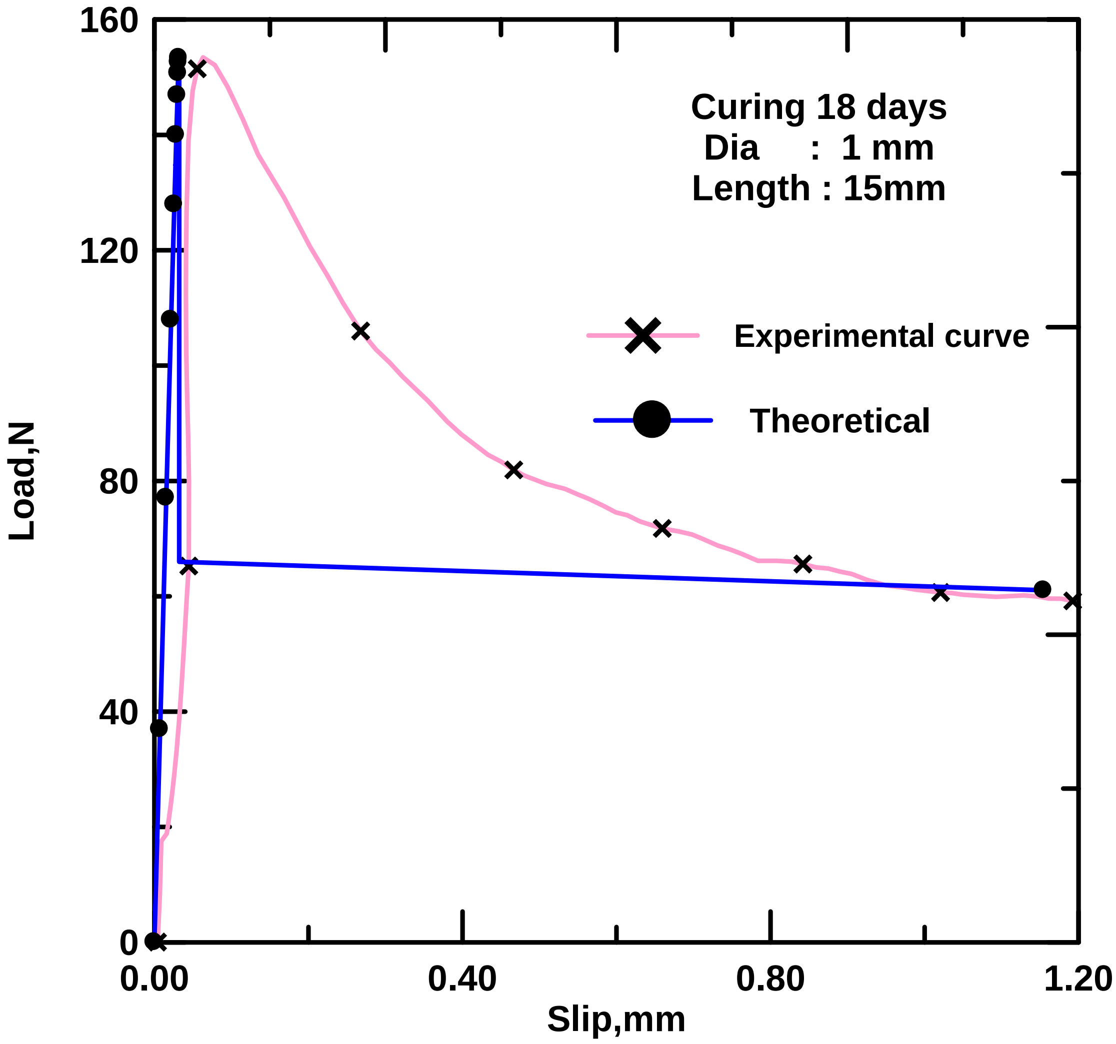

Figure 4.15 Theoretical model matched with specimen 4B1D15cLS16 response

In this case (Figure 4.16), the stiffness and the peak load predicted by the theoretical model are very close to the experimental response. But the immediate post peak region is not predicted accurately.

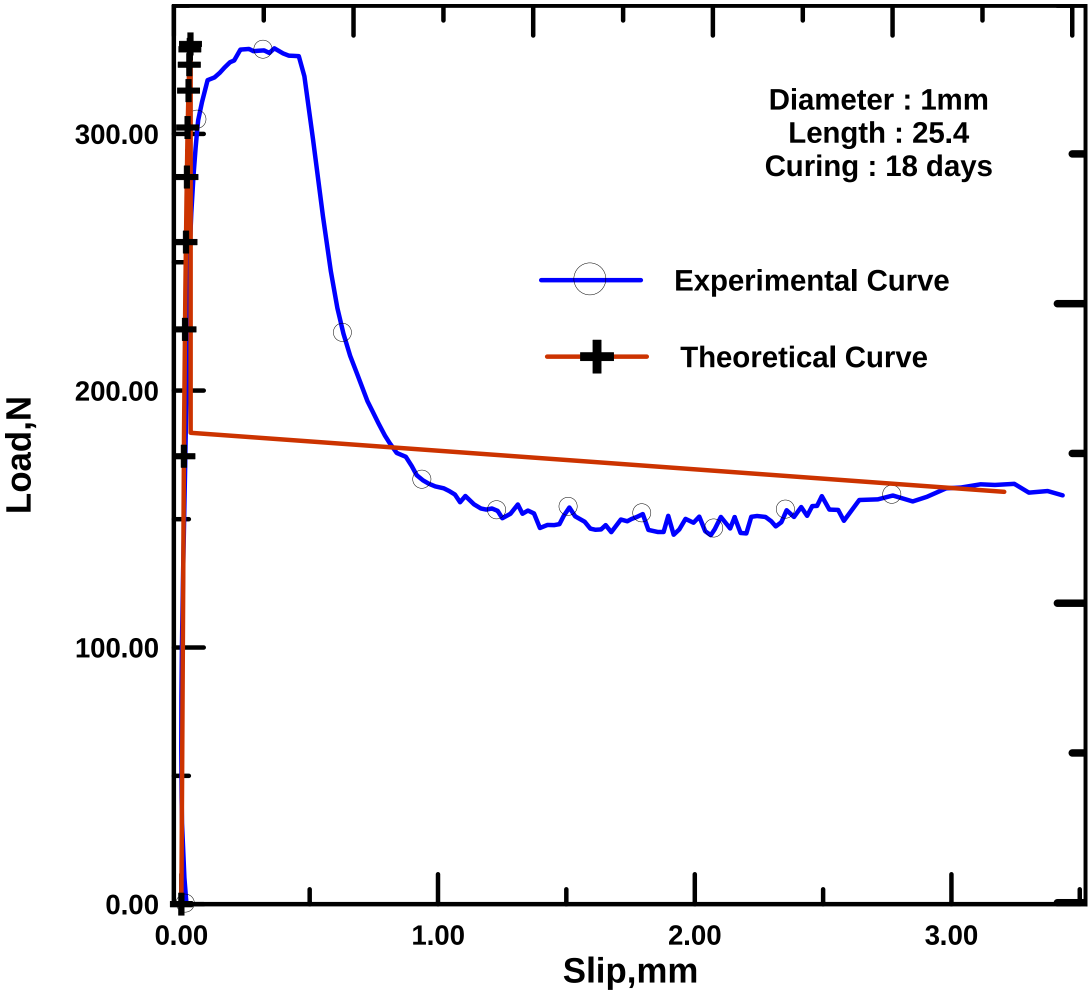

Figure 4.16 Theoretical model matched with specimen 4B1D1iLS14 response

In the following Figure, an almost perfect matching of the stiffness and the peak load is obtained. The post peak region shows an estimate.

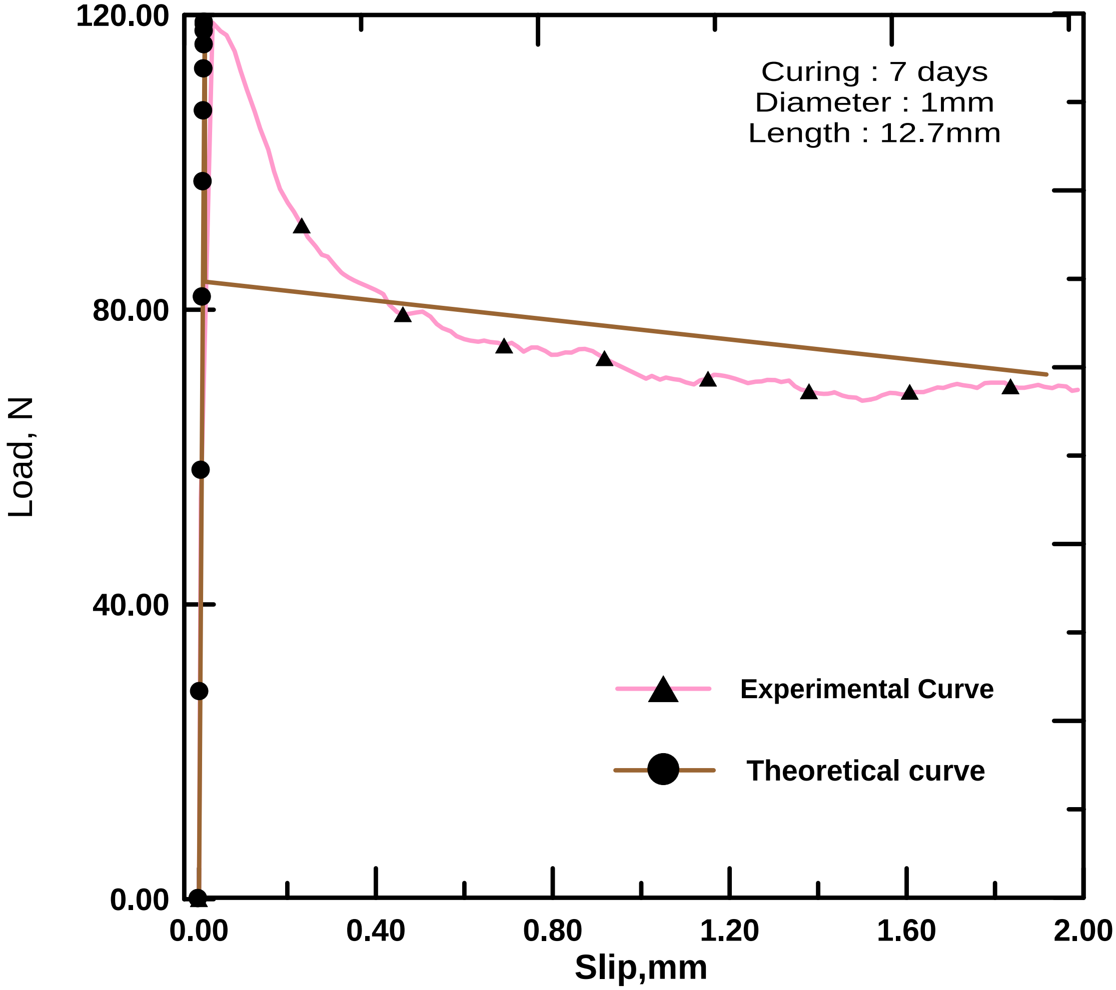

Figure 4.17 Theoretical model matched with 1D05iLS25 specimen data

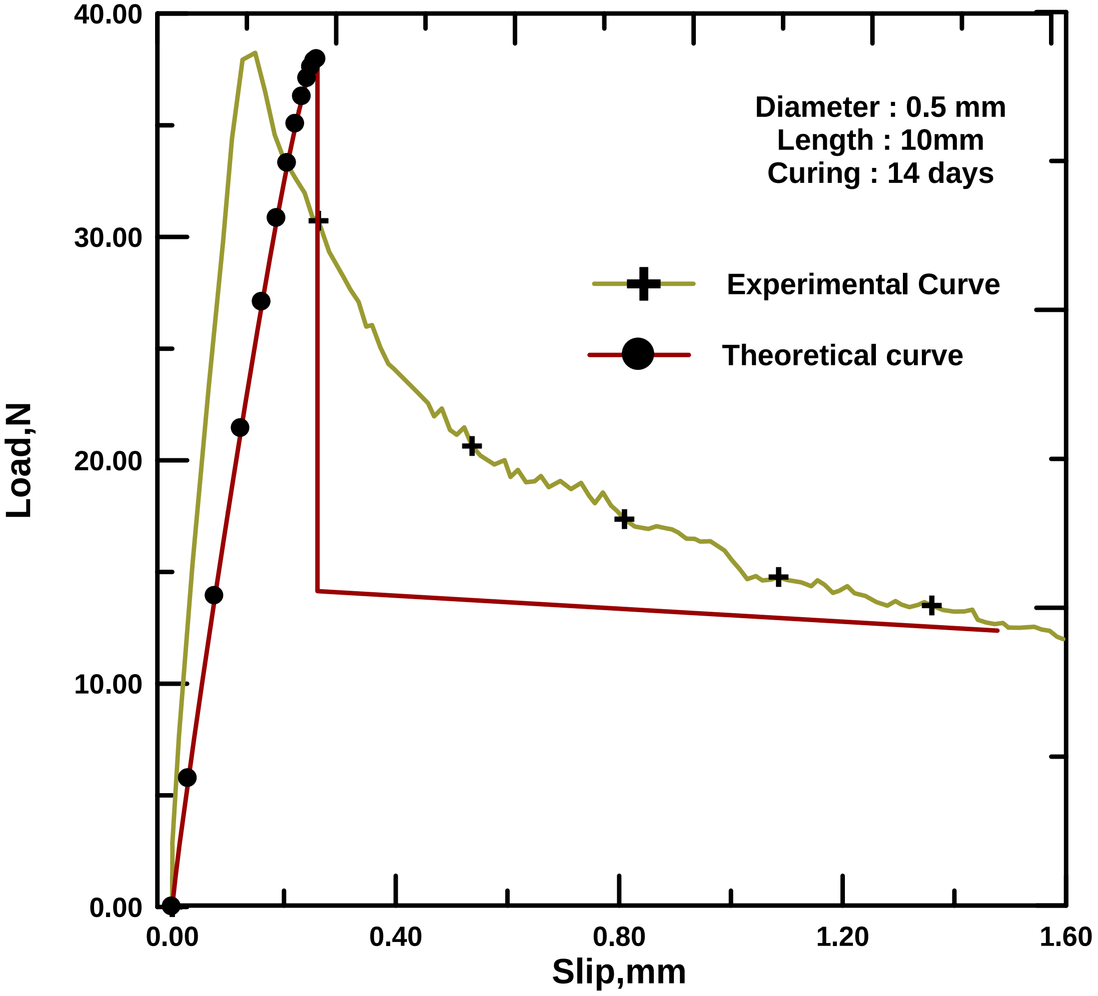

Figure 4.18 Theoretical model matched with the specimen 4B05D1cL3 response

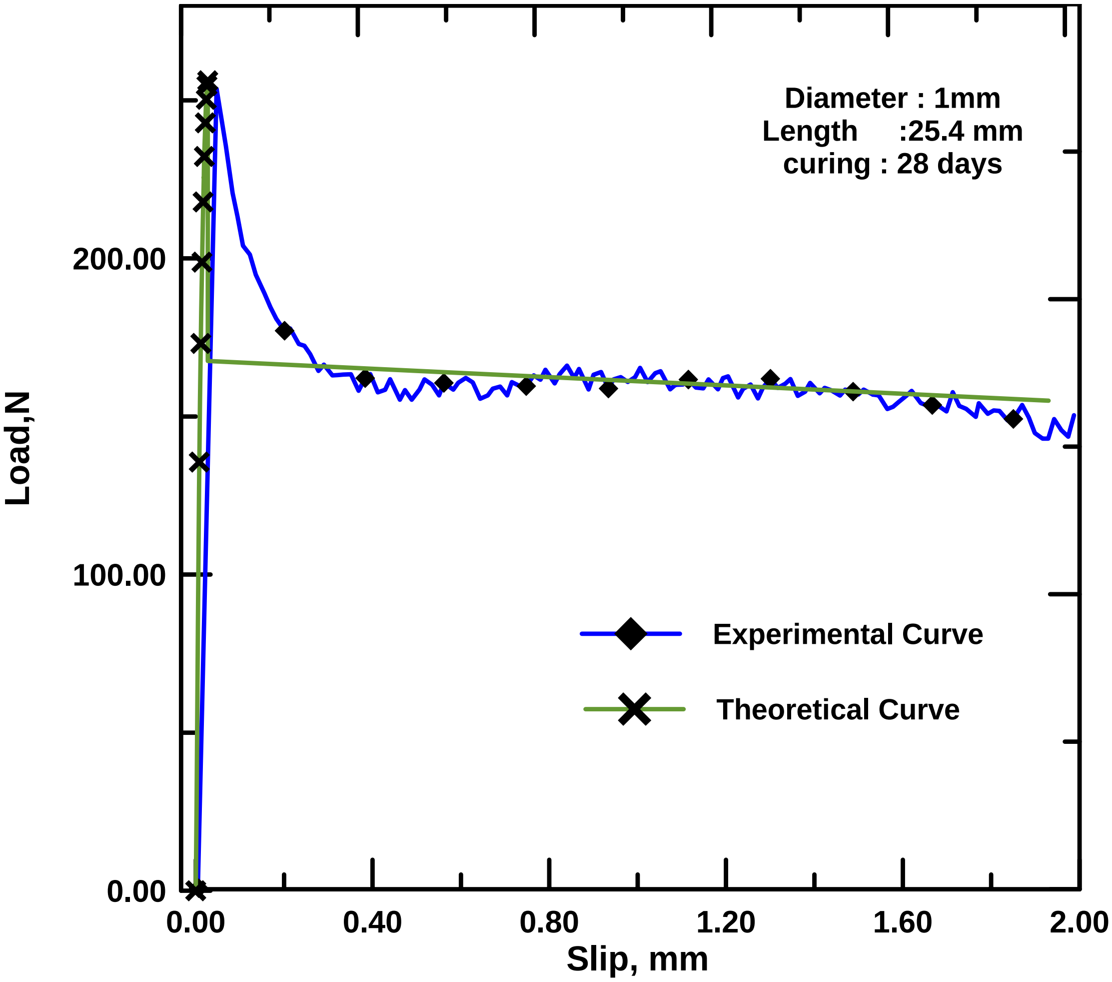

Figure 4.19 Theoretical model matched with the experimental response of specimen 1D05LS3

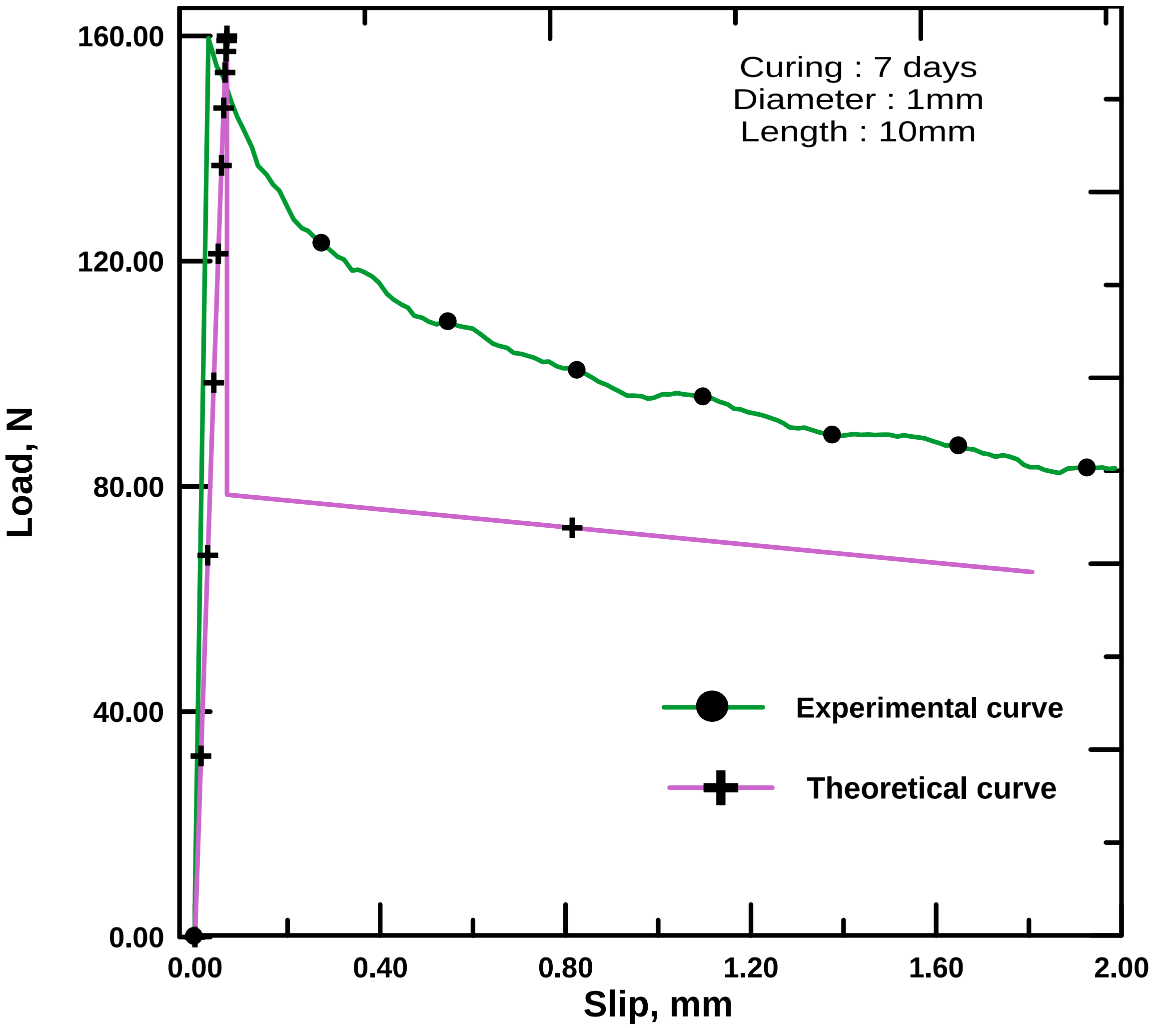

Figure 4.20 Theoretical model matched with specimen 1D1cS23 response

As seen in the following Figure, the peak load and the slip at the peak load is estimated accurately. But, the stiffness is slightly away from that of the experimental response.

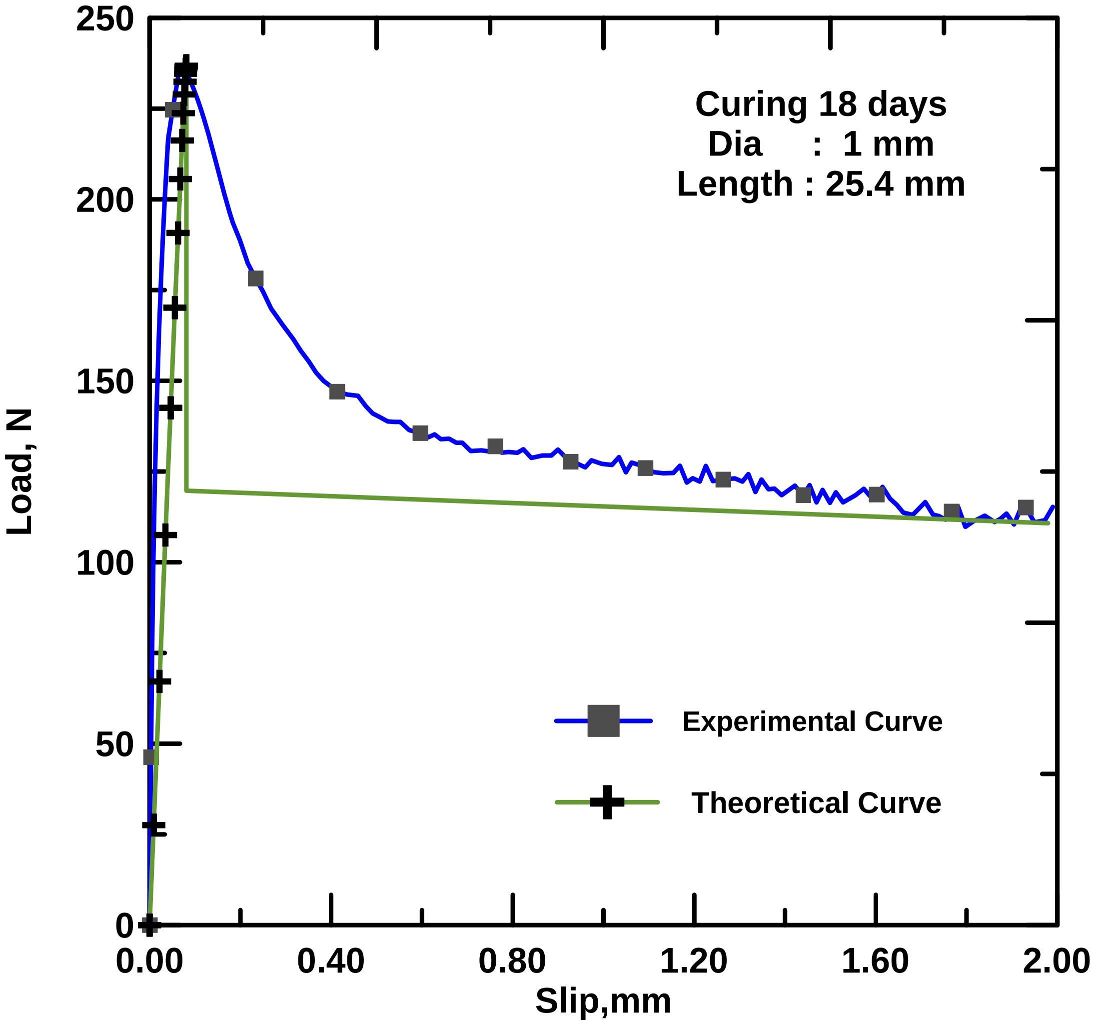

Figure 4.21 Theoretical model matched with specimen 4B1D1iLS13a response

In the following case (Figure 4.21) the theoretical model is slightly altered, to predict a nonlinear response in the post peak region. But the objective function for optimization being the same, the results are expected to be the same as above. But the post peak response of the theoretical model shows a similar behavior as the experimental response, hence a better fit.

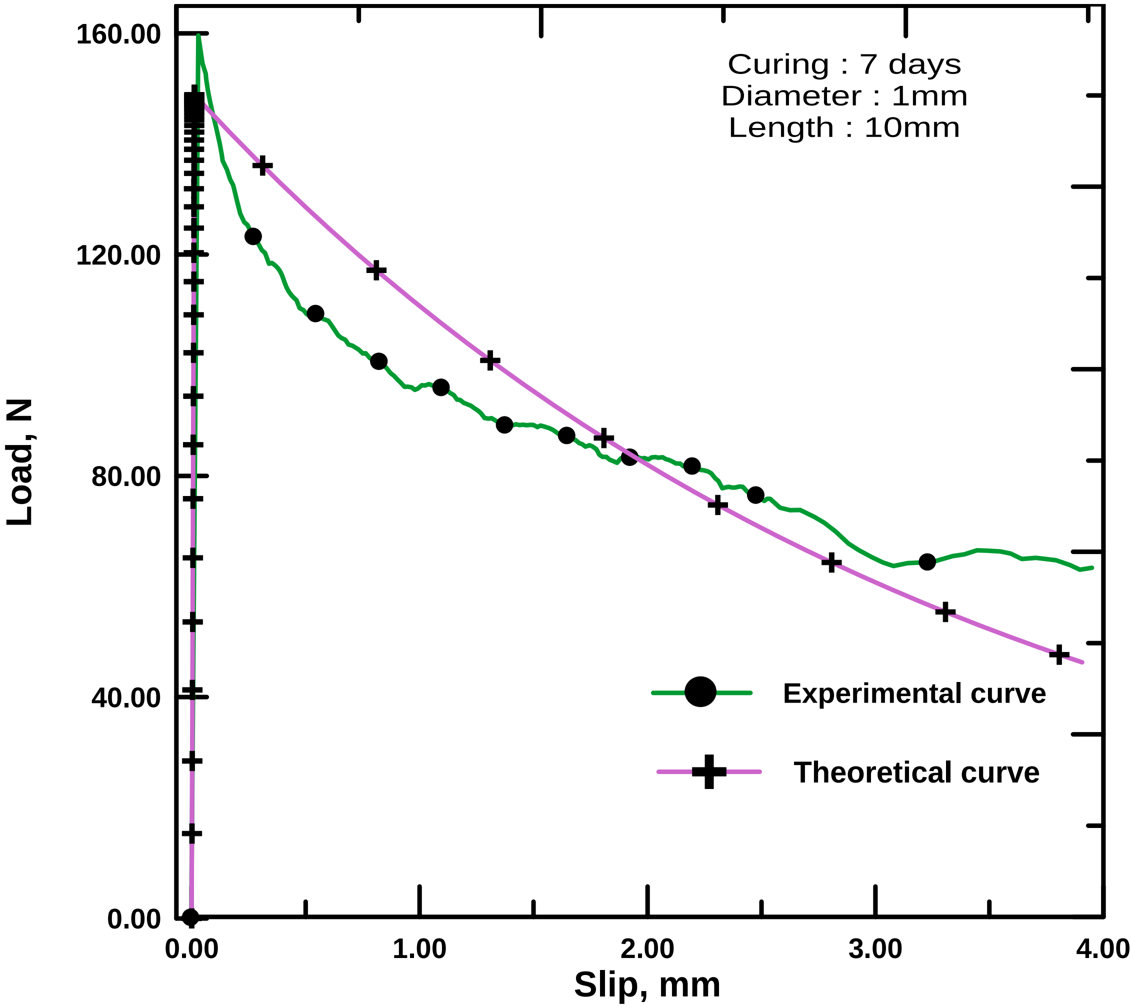

Figure 4.22 Theoretical model matched with specimen 1D1cS23 response

The stiffness and the peak load are matched in Figure 4.23 though not quite accurately. But considering the fact that the weights are not used, the fit is very close. This is because as opposed to previous cases, the objective function is normalized. Weights can be used if higher accuracy is desired. The same trend is seen in all the following figures, except that the peak pullout force is not matched closely. Therefore, weights should be used on the matching of peak force.

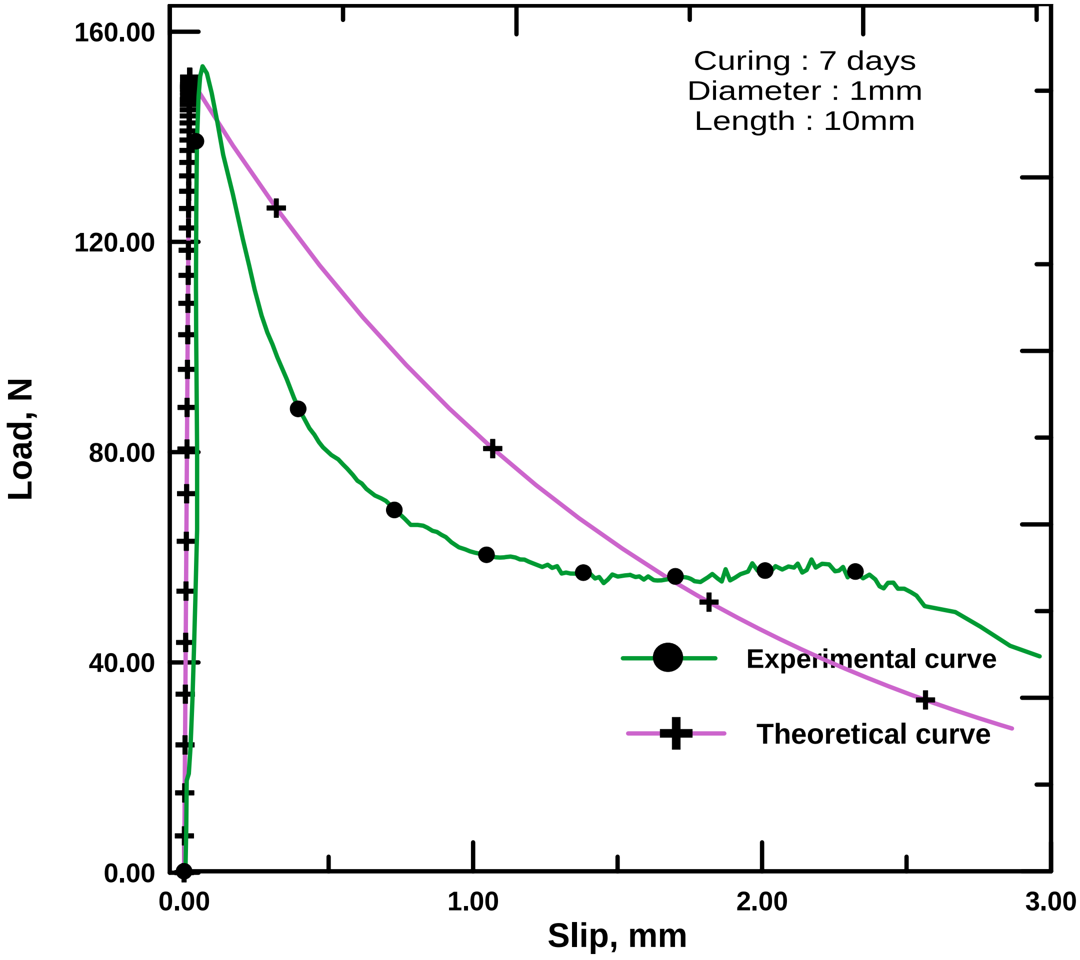

Figure 4.23 Theoretical model matched with specimen 4B1D15Cls16 response

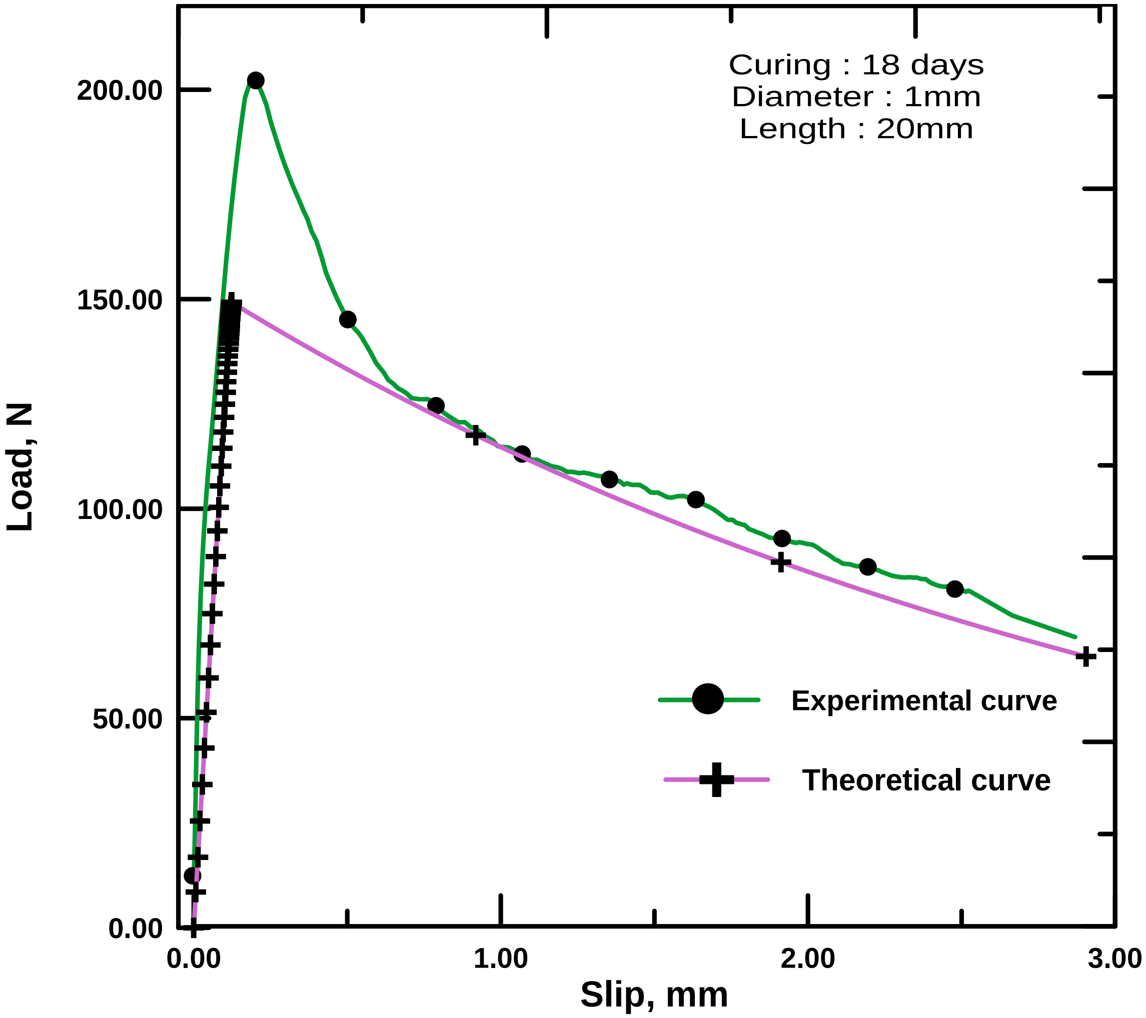

Figure 4.24 Theoretical model matched with specimen 4B1D2cLS18 response

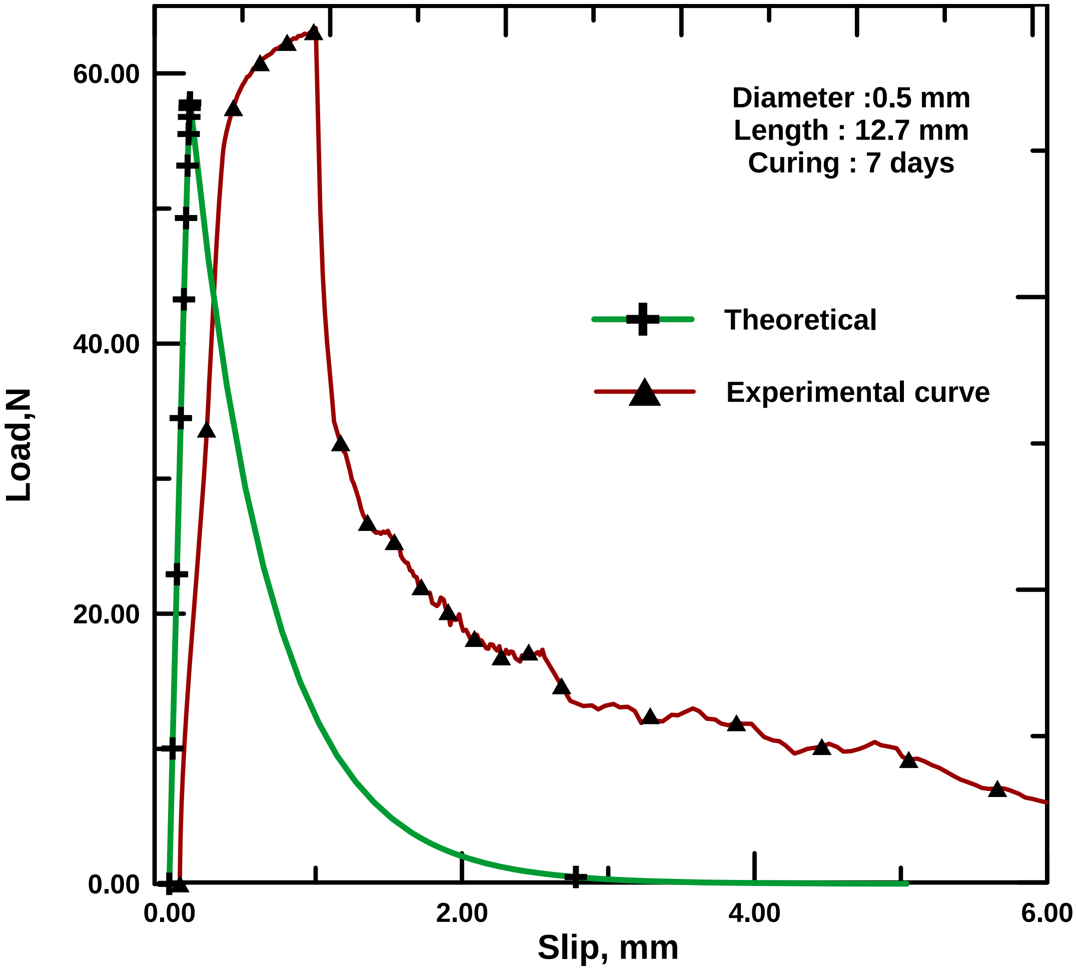

Figure 4.25 Theoretical model matched with specimen 1D05iLS29 response

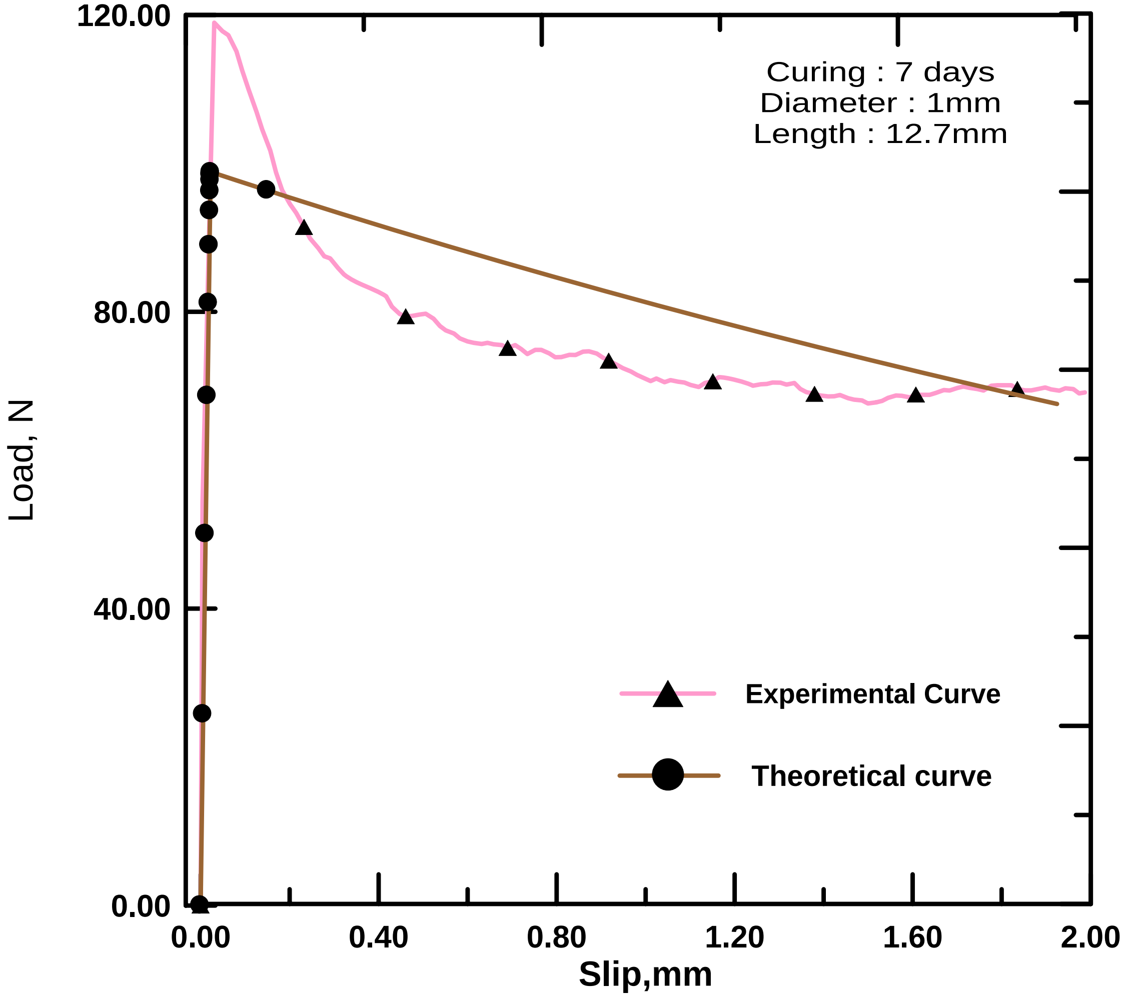

Figure 4.26 Theoretical model matched with specimen 1D05iLS25 response

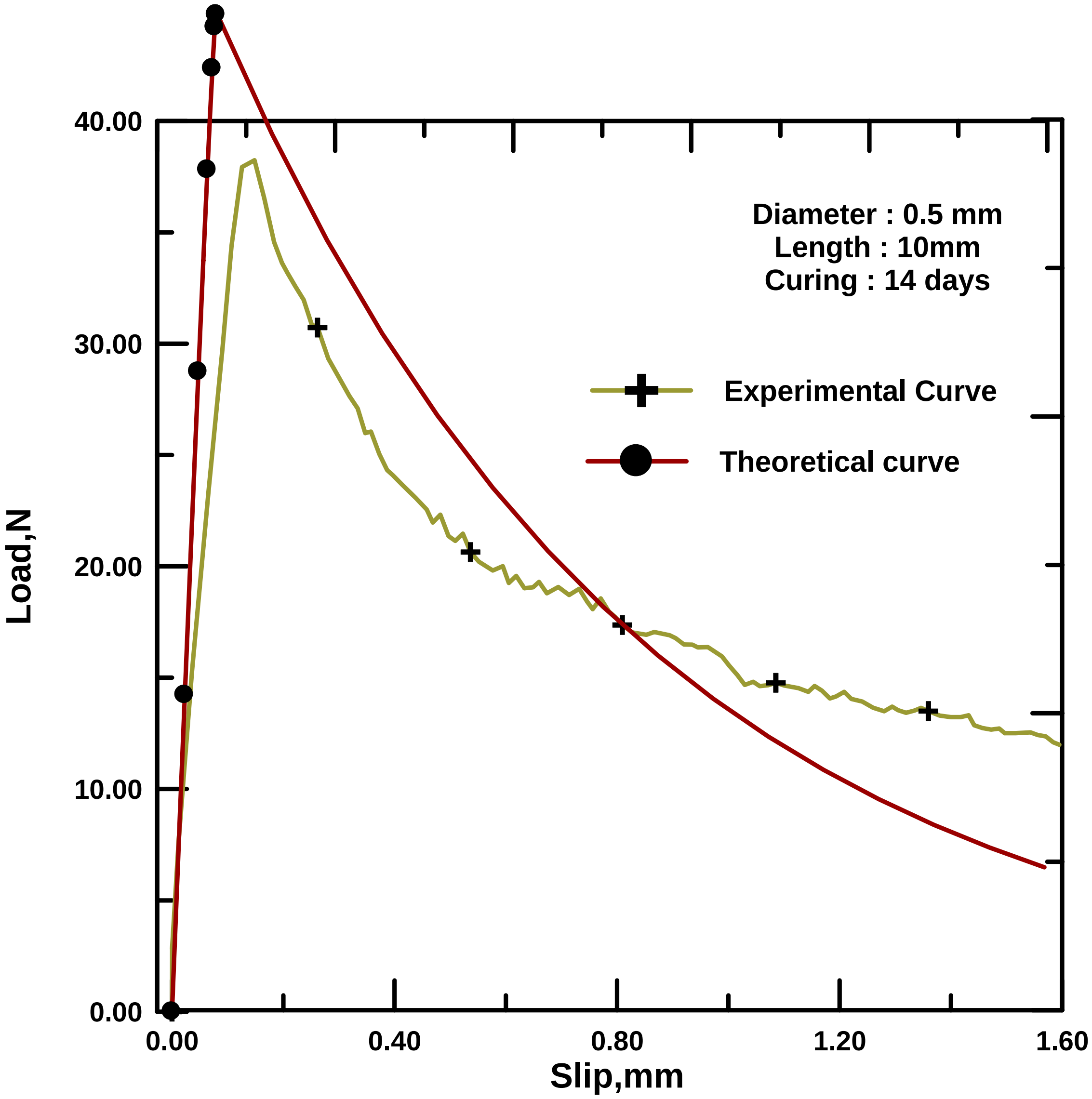

Figure 4.27 Theoretical model matched with specimen 4B05D1cL3 response

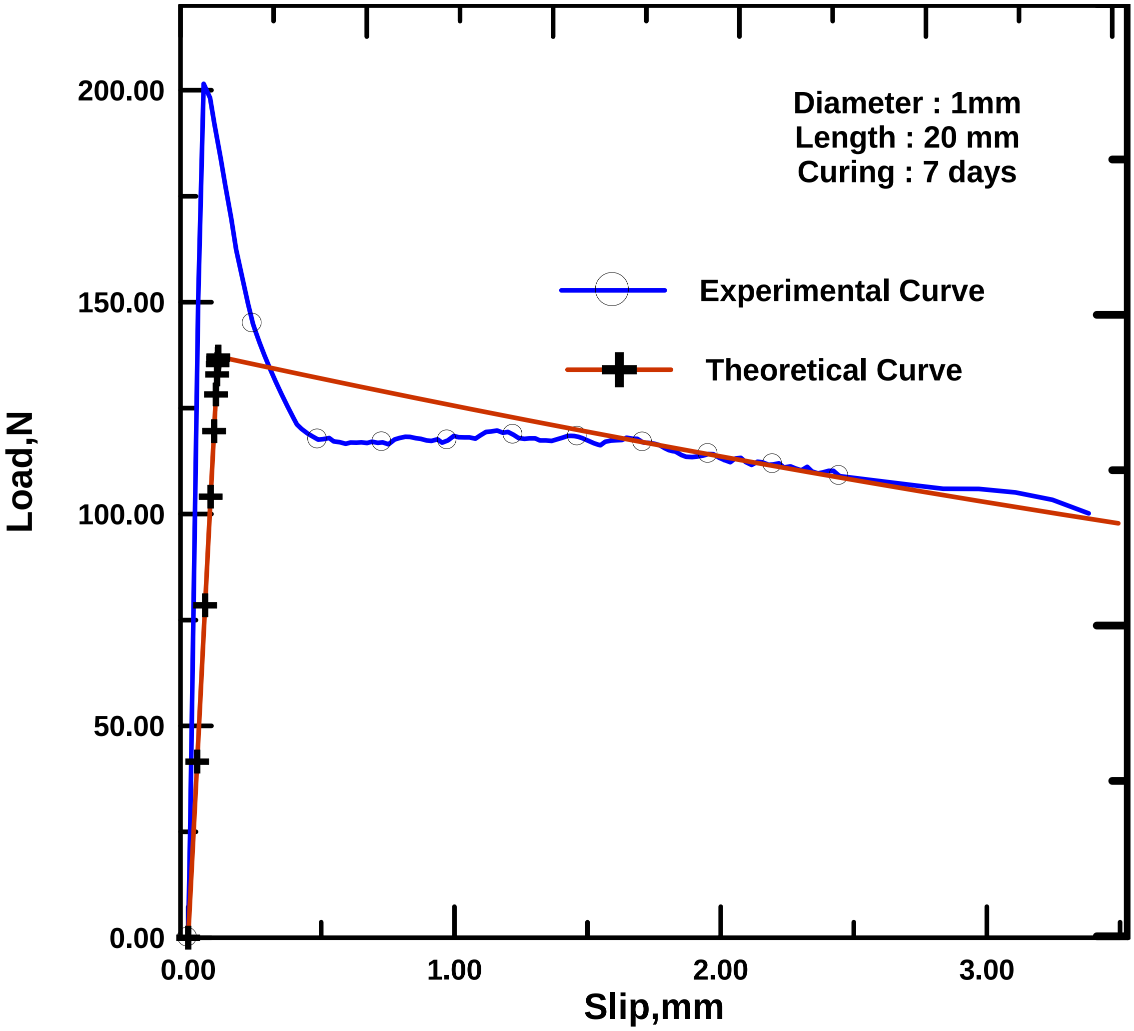

Figure 4.28 Theoretical model matched with specimen 1D2cLS26 response

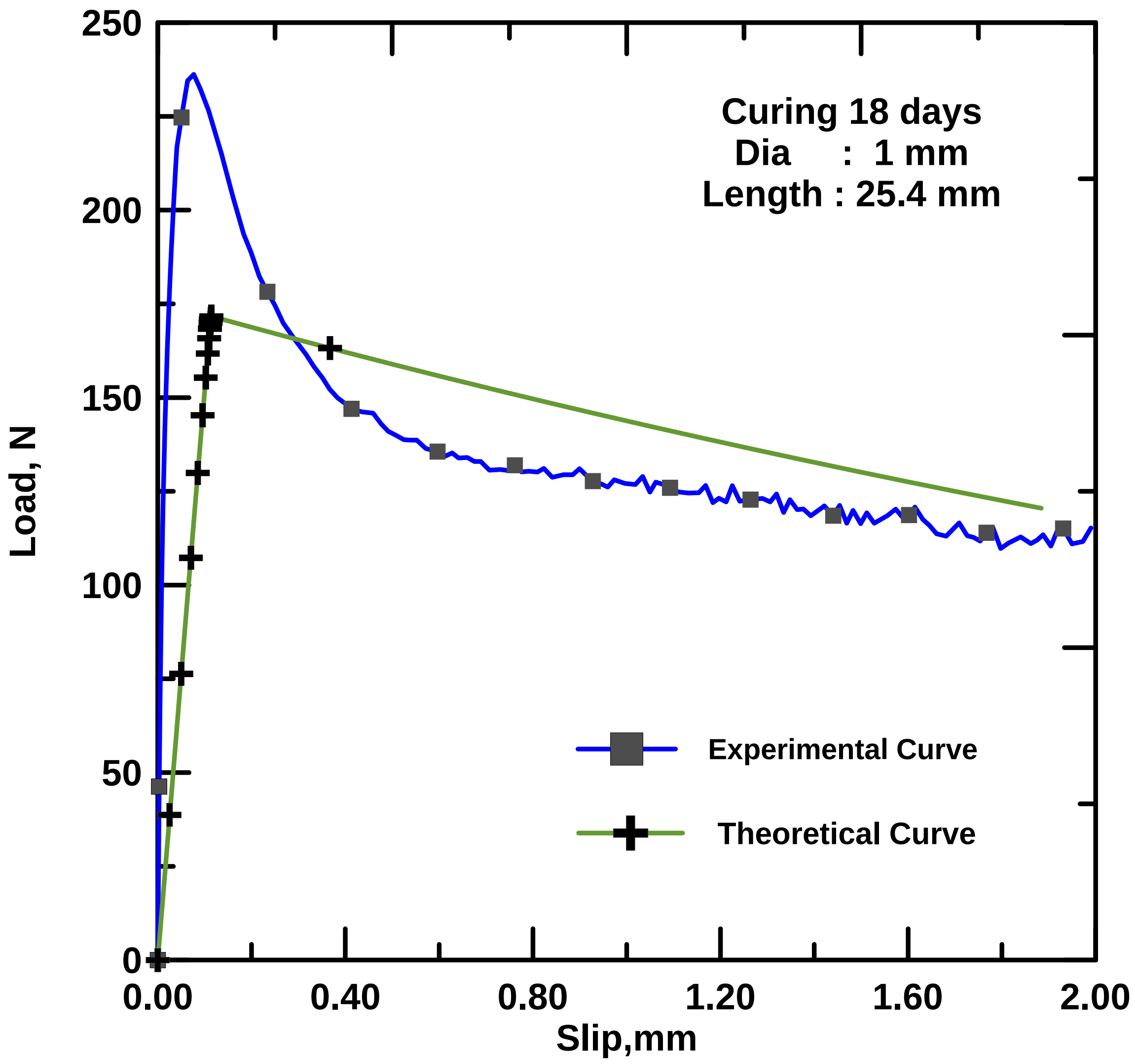

Figure 4.29 Theoretical model matched with specimen 4B1D1iLS13a response

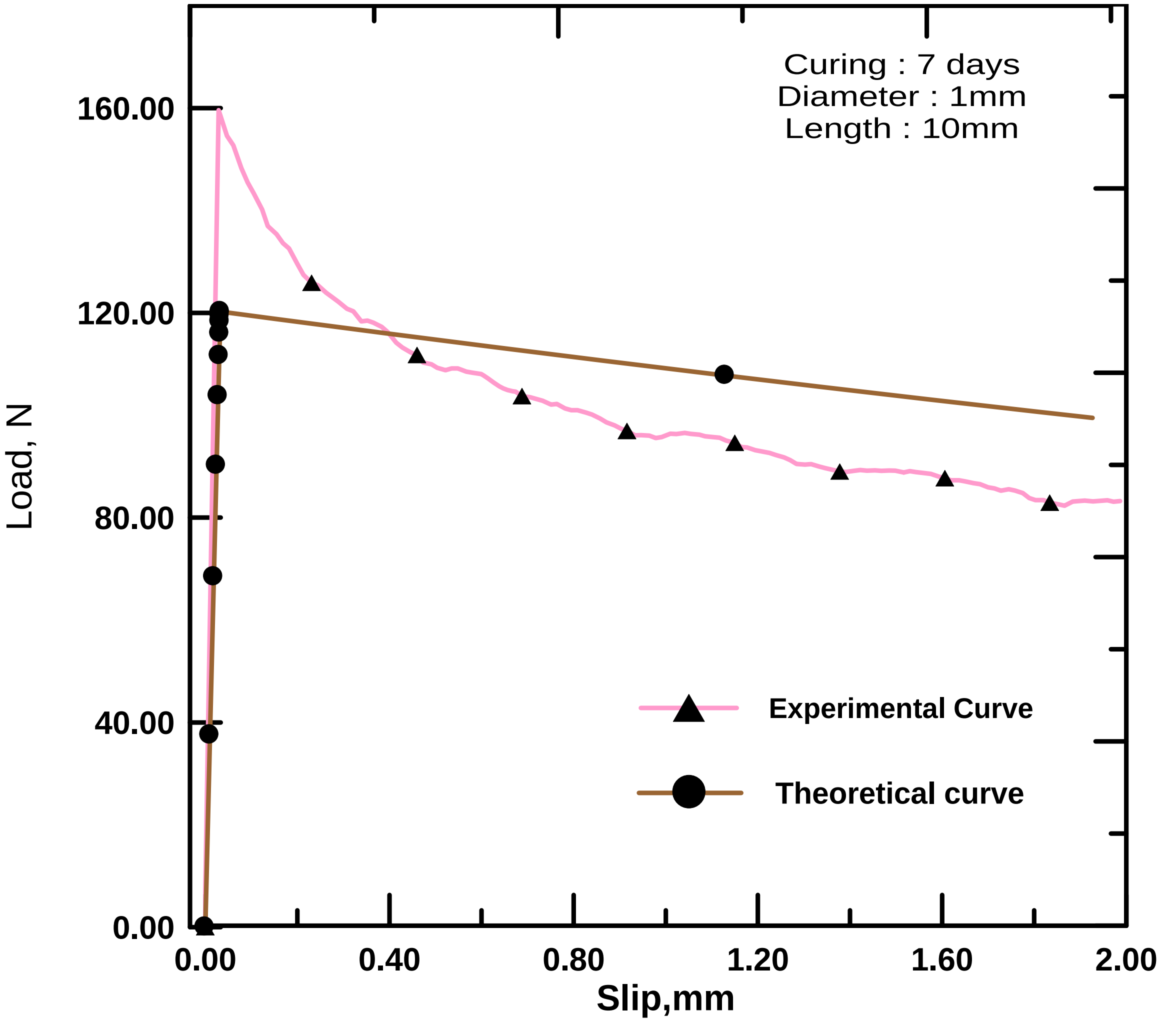

Figure 4.30 Theoretical model with specimen 1D1cS23 using normalization

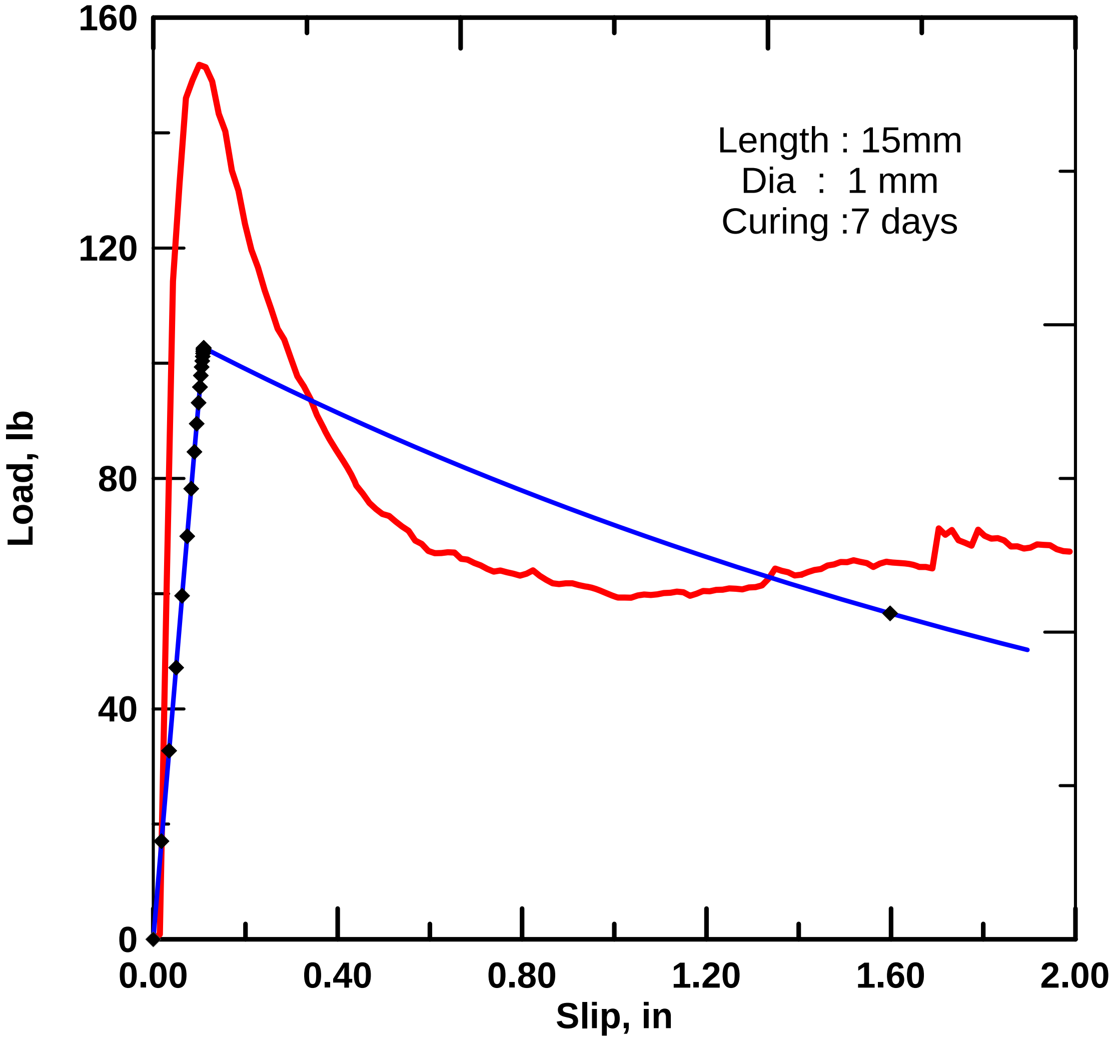

Figure 4.31 Theoretical model with specimen 1D15Cls20 using normalization

The results of all the above cases are briefly summarized in this section. For case 1, the curve fitting is very close and accurate. But there was no rational way of obtaining the weights. The weights were chosen arbitrarily and modified to obtain a close fit. Moreover, the theoretical model itself had a drawback because it did not simulate the experimental response accurately in the post peak region. This was rectified in Cases 2 and 3 by modifying the model, to predict a nonlinear post-peak response. So case 2 ensured a better fit in the post peak region. But the results from the optimization were similar in Case 1 and Case 2 because the objective function was not altered. The problem of choosing the weights arbitrarily persisted in Case 2 as well. Hence in Case 3 the objective function was normalized. This ensures a very close overall fit. If accuracy is desired in certain modes like the peak, pre-peak etc., weights can be used.

CHAPTER 5

SUMMARY AND CONCLUSIONS

5.1 SUMMARY AND CONCLUSIONS

A simple and reliable experimental test setup was developed to conduct fiber-pullout tests, and necessary fixtures were designed for this purpose. Single-fiber reinforced cement specimens were cast and cured in different trials, by varying the fiber geometry, embedded length and the curing period. Pullout tests were performed on these specimens to obtain the pullout slip response. An existing theoretical model was studied. The results predicted by the theoretical model were fitted with the experimental data, using Genetic Algorithm. Subsequently the parameters governing the interface were obtained from the theoretical model.

The estimation of the interfacial zone parameters leads to manufacturing of better fiber reinforced composites. The study of the energy absorption capabilities allows optimization of the fiber geometry for best results. Obtaining the results from the theoretical model based on the fracture mechanics approach, ensures better understanding and utilization of materials. Also, use of a scientific curve fitting technique instead of mathematical fit, yields superior results. Moreover, the proposed parameter modeling technique is scientific and general enough to be applied in various areas.

5.2 FUTURE RECOMMENDATIONS

The mechanical properties of the interface, obtained from the pullout-slip response of a single fiber, could be extended. For example extending the above results tension test of a fiber-reinforced-cement specimen with randomly oriented fibers can be simulated. From the load-slip response obtained from the above tests, the response of structural systems, for example an FRC pipe, could be studied.

The experimental test setup can be used to perform pullout-slip experiments in the future, and variations to the tests can be easily accommodated. The parameter modeling technique developed, could be applied in different areas viz. system analysis, 3-point bend tests, rebar, earthquake analysis etc. Moreover, modifications can be made to the objective function to maximize efficiency.

REFERENCES

Alberto, C., and Roberta, M., (1996). “Bridged versus cohesive crack in the flexural behavior of brittle-matrix composites,” *International Journal of Fracture,* No 81, July, pp 125-145.

Dattaguru, B., Venkatesha, K.S., Ramamurthy, T.S., and Buchjolz, F.G., (1994). “Finite Element Estimates of Strain Energy Release Rate Components at the Tip of an Interface Crack under Mode I Loading,” *Engineering Fracture Mechanics*, Vol. 49, No. 3, pp. 451-463.

Dubey, A., and Banthia, N., (1999). “High-Performance Fiber Reinforced Concrete: Optimizing Interfacial Properties for High Modulus and Low Modulus Fibers,” *UBC Civil Engineering,* paper in review.

Gopalratnam, V.S., and Shah, S.P.(1987). “Tensile Failure of Steel Fiber Reinforced Concrete,” *Journal of Engineering Mechanics*, ASCE, Vol. 113, No. 5, May, pp.635-652.

Hutchinson, J.W., and Jensen, H.M. (1990). “Models of Fiber Debonding and Pullout in Brittle Composites with Friction,” *Mechanics of Materials*, 9, pp. 139–163.

Jenq Y.S., and Shah S.P. (1986). “ Application of two parameter fracture model to concrete and fiber reinforced concrete,” *Fracture toughness and fracture energy of concrete*, pp. 499-512.

Karr, C.L. Stanley, D.A., and Scheiner, B.J. (1991). “Genetic algorithm applied to least squares curve fitting,” *U.S. Dept. of the Interior, Bureau of Mines*.

Li, Z., Mobasher, B., and Shah, S.P. (1991). “Characterization of Interfacial Properties of Fiber Reinforced Cementitious Composites,” *Journal of American Ceramic Society,* 74(9), pp.2156-64.

Li, C., (1995). “Mechanical Behavior of Cementitious Composites Reinforced with High Volume Content of Fibers,” Doctoral Dissertation, Arizona State University, May.

Li, Z., Mobasher, B., and Shah, S.P. (1990). “Effect of Aging on The Interfacial Properties of GFRC,” Proceedings, MRS, Sym. O, MRS Fall Meeting, Boston, MA.

Marshall, D.B., Cox, B.N., and Evans, A.G. (1985). “The Mechanics of Matrix Cracking in Brittle Matrix Fiber Composites,” *Acta Metall. Mater.*, V. 33, No. 11, pp. 2013-2021.

Mobasher, B., and Li, C., (1996). "Effect of Interfacial Properties on the Crack Propagation in Cementitious Composites," *Advanced Cement Based Materials*., 4, pp. 93-105.

Mobasher, B., and Shah, S.P. (1989). " Test parameters in Toughness Evaluation of Glass Fiber Reinforced Concrete Panels," *ACI Materials Journal*, Sept-Oct., pp. 448-458.

Naaman, A.E., Namur, G.G., Alwan, J.M., and Najm, H.S.(1991). "Fiber Pullout and Bond Slip, I: Analytical Study," *Journal of Structural Engineering,* Vol. 117, No. 9, pp.2769-800.

Naaman, A.E., and Shah, S.P. (1976). "Pull-out Mechanism in Steel Fiber Reinforced Concrete," ASCE, *Journal of Structural Division*, Vol. 102, No. 8, pp. 1537-1548.

Nahta, R., and Moran, B., (1996). "Film Cracking and Debonding in a Coated Fiber," *International Journal of Fracture*, 79, pp. 351-372.

Noggle, J.H., "Practical Curve Fitting and Data Analysis: Software and Self Instruction for Scientists and Engineers," 1993.

Ouyang, C., Mobasher, B., and Shah, S.P. (1990). "An R-Curve Approach for Fracture of Quasi-Brittle Materials," *Engineering Fracture Mechanics*, Vol. 37, pp. 901-913.

Paris, F., Cano, J.C., and Varna, J., (1996). "The Fiber-matrix Interface Crack – A Numerical Analysis using Boundary Elements," *International Journal of Fracture*, 82, pp 11-29.

Rajan, S.D., (1999). "Structural Analysis and Design," Text book in review.

Renjie, M., and Sun, G., "A Study of the Interaction Between Matrix Crack and Matrix – Fiber Interface," *Engineering Fracture Mechanics,* Vol. 51, No.3, pp.469-477, 1995.

Stang, H., Li, Z., and Shah, S.P. (1990). "Pull-Out Problem: Stress versus Fracture Mechanical Approach," ASCE, *Journal of Engineering Mechanics* , Vol. 116, No. 10, pp. 2136-2150.

Yin, S.W., (1993). " A Fiber Bridging Model for the Fracture of Brittle Matrix Composites," *Engineering Fracture Mechanics,* Vol. 46, No. 5, pp. 895-900.

APPENDIX A

PULLOUT TEST SETUP

Figure A1 Pullout Test Setup

APPENDIX B

FIBER PULLOUT-SLIP RESPONSE OF SPECIMENS

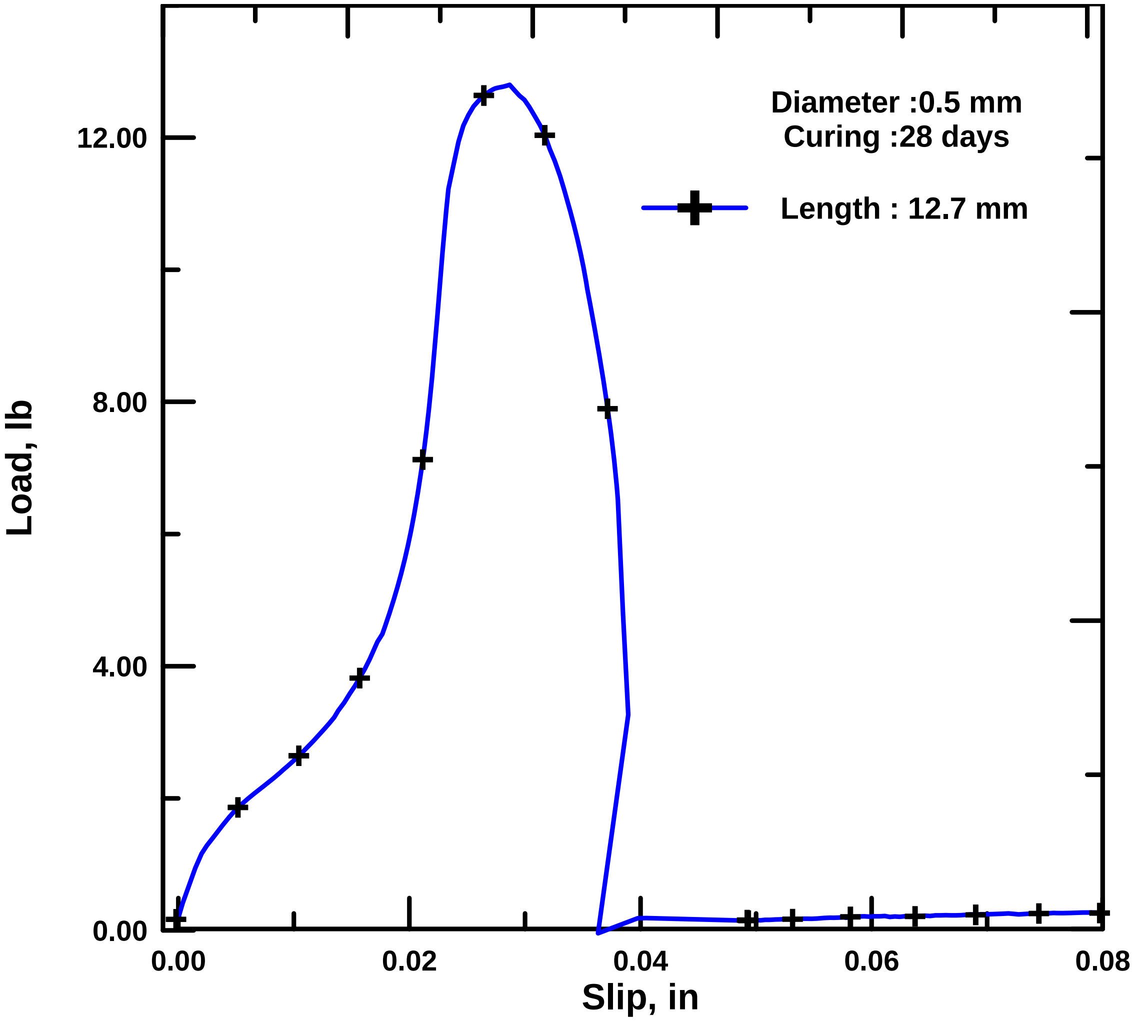

Figure B1 Specimen 05D05LS6

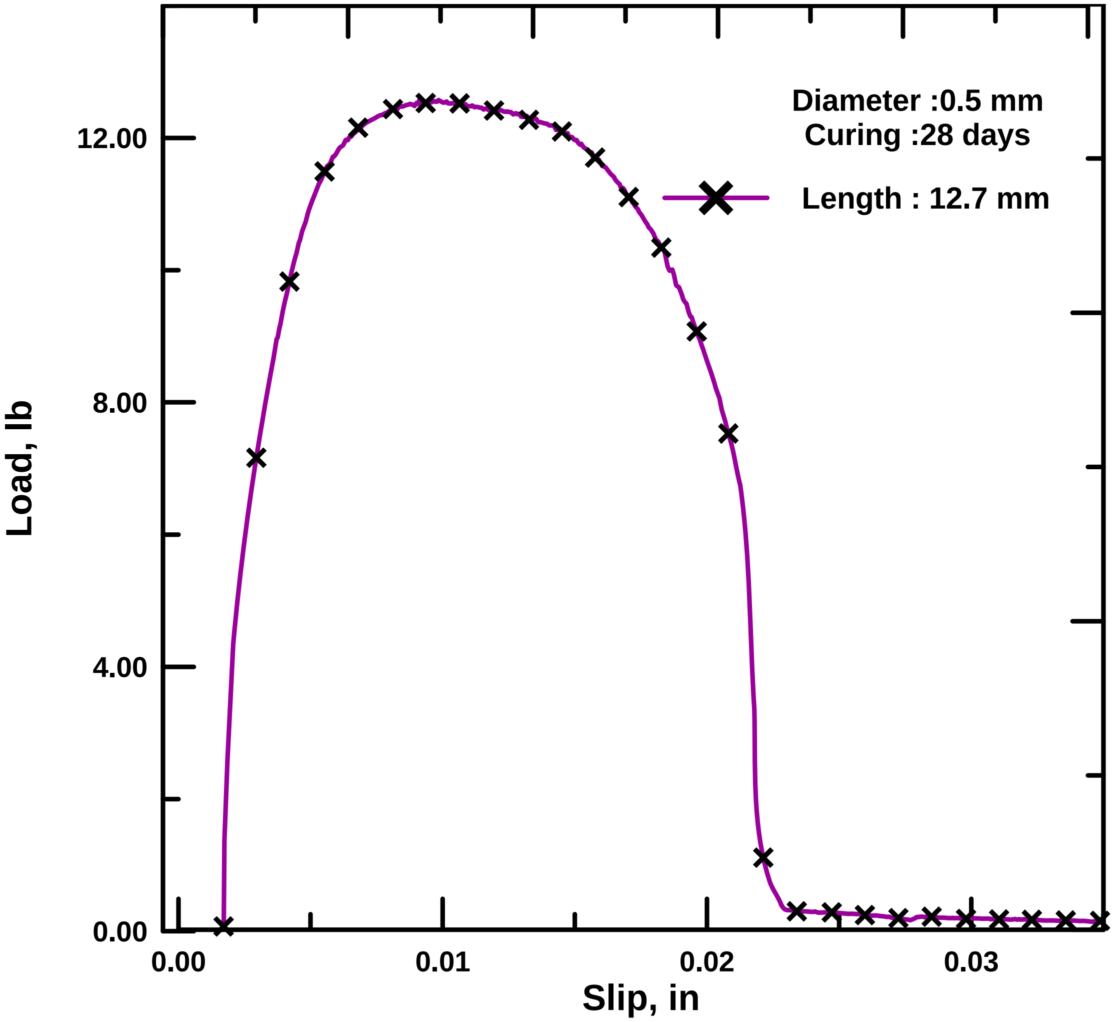

Figure B2 Specimen 05D05LS7

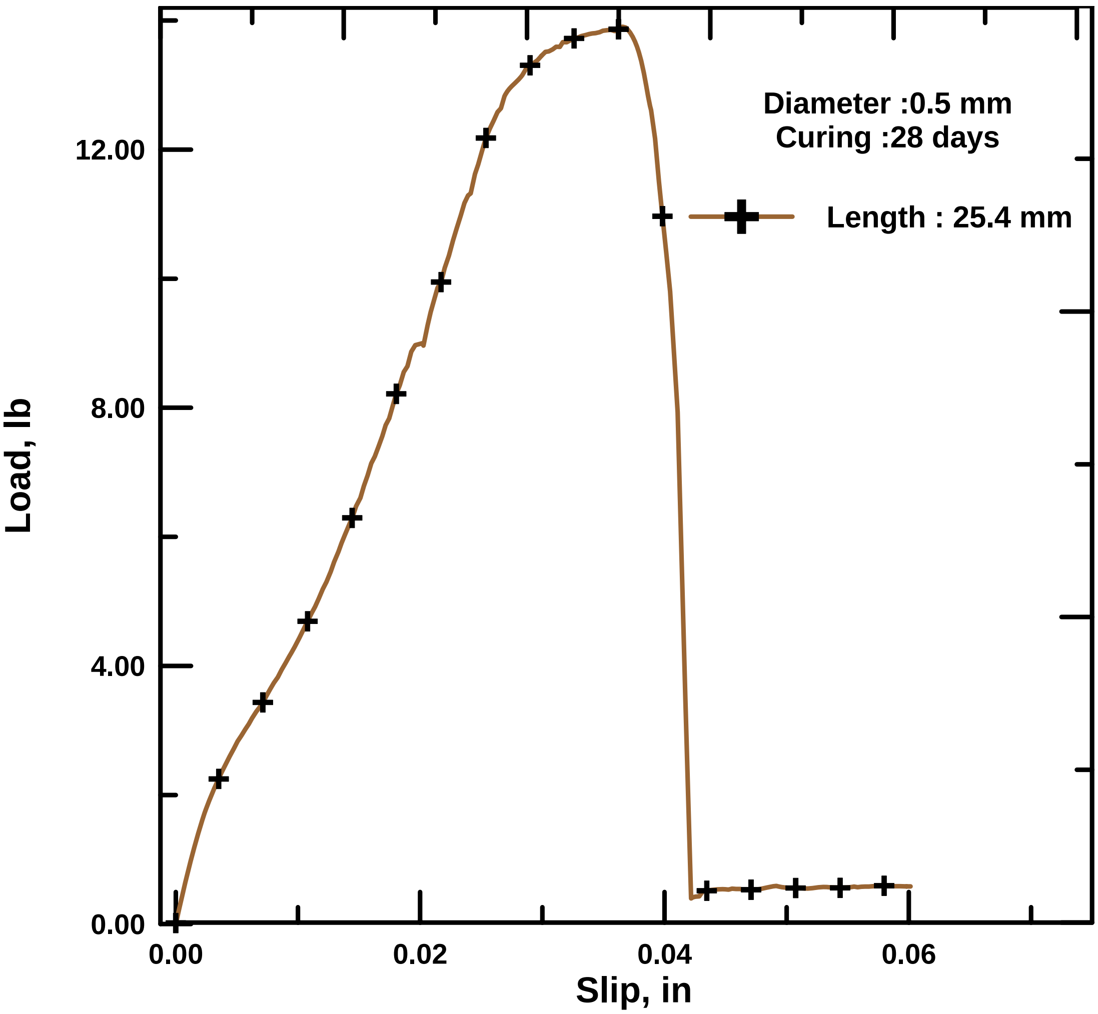

Figure B3 Specimen 05D1LS12

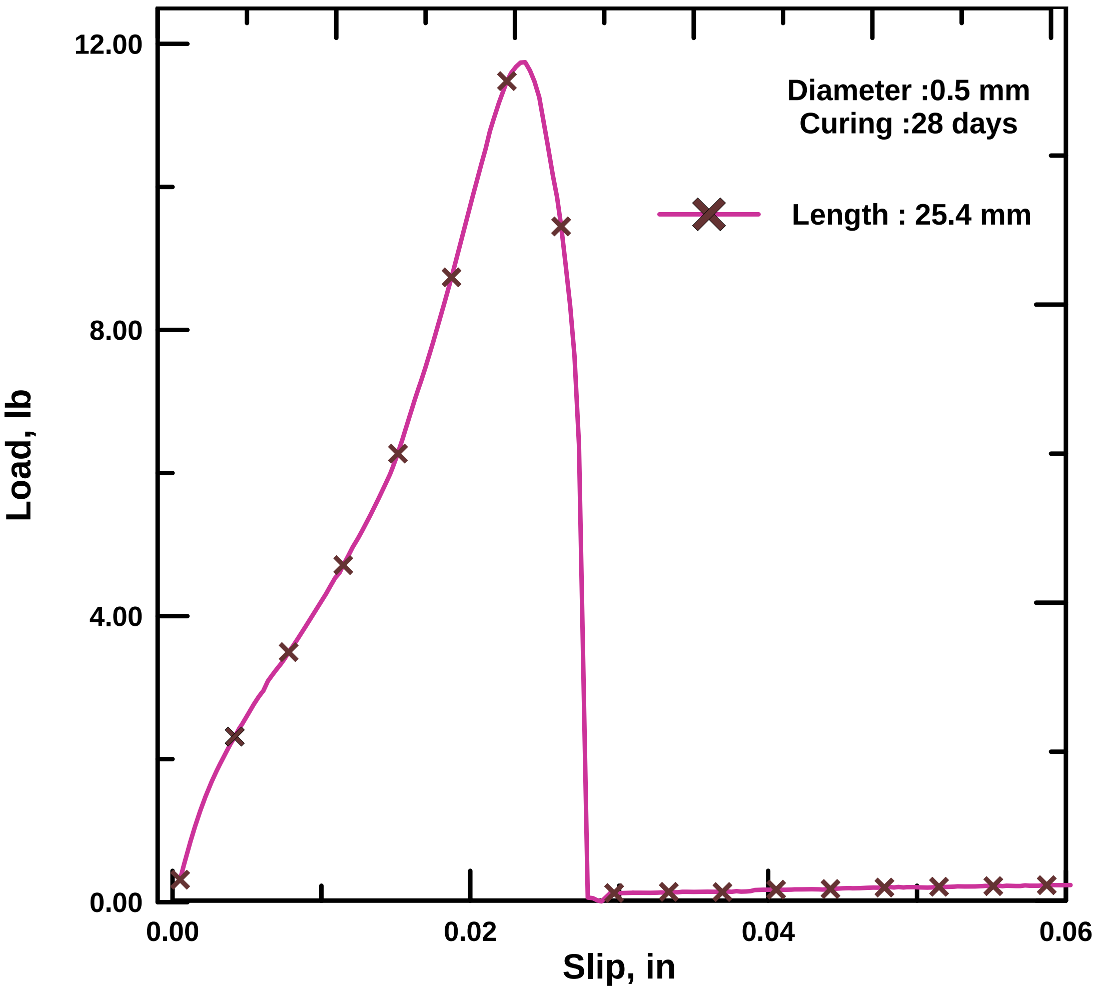

Figure B4 Specimen 05D1LS13

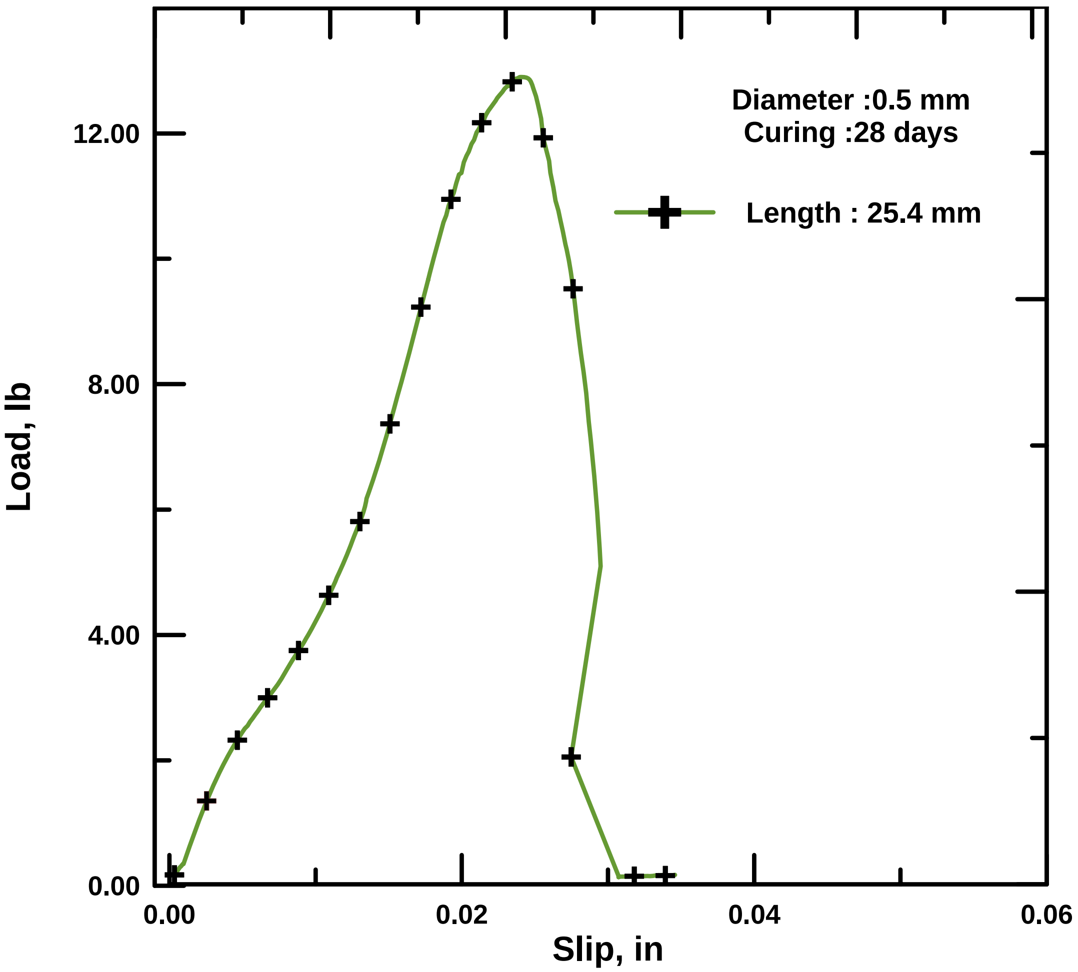

Figure B5 Specimen 05D1LS14

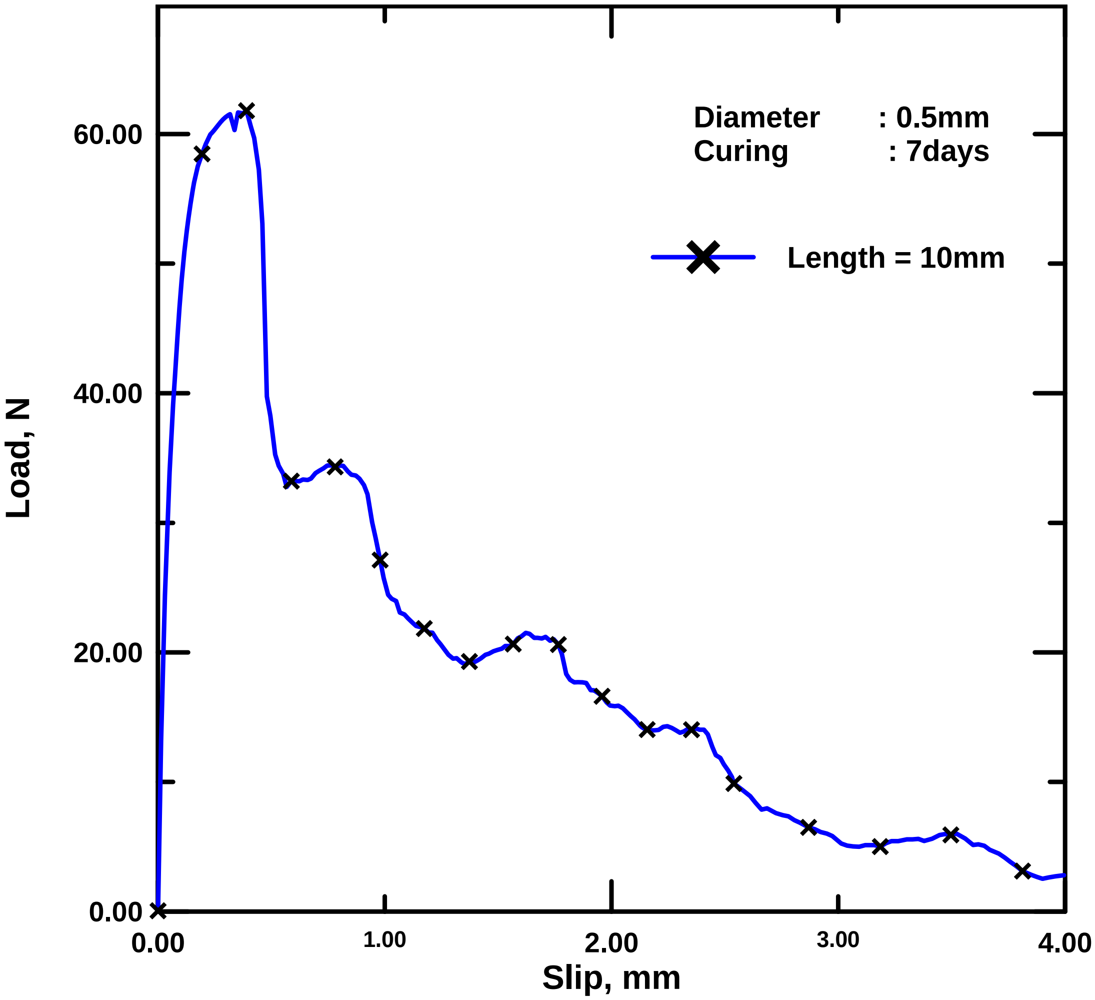

Figure B6 Specimen 05D1cLS17

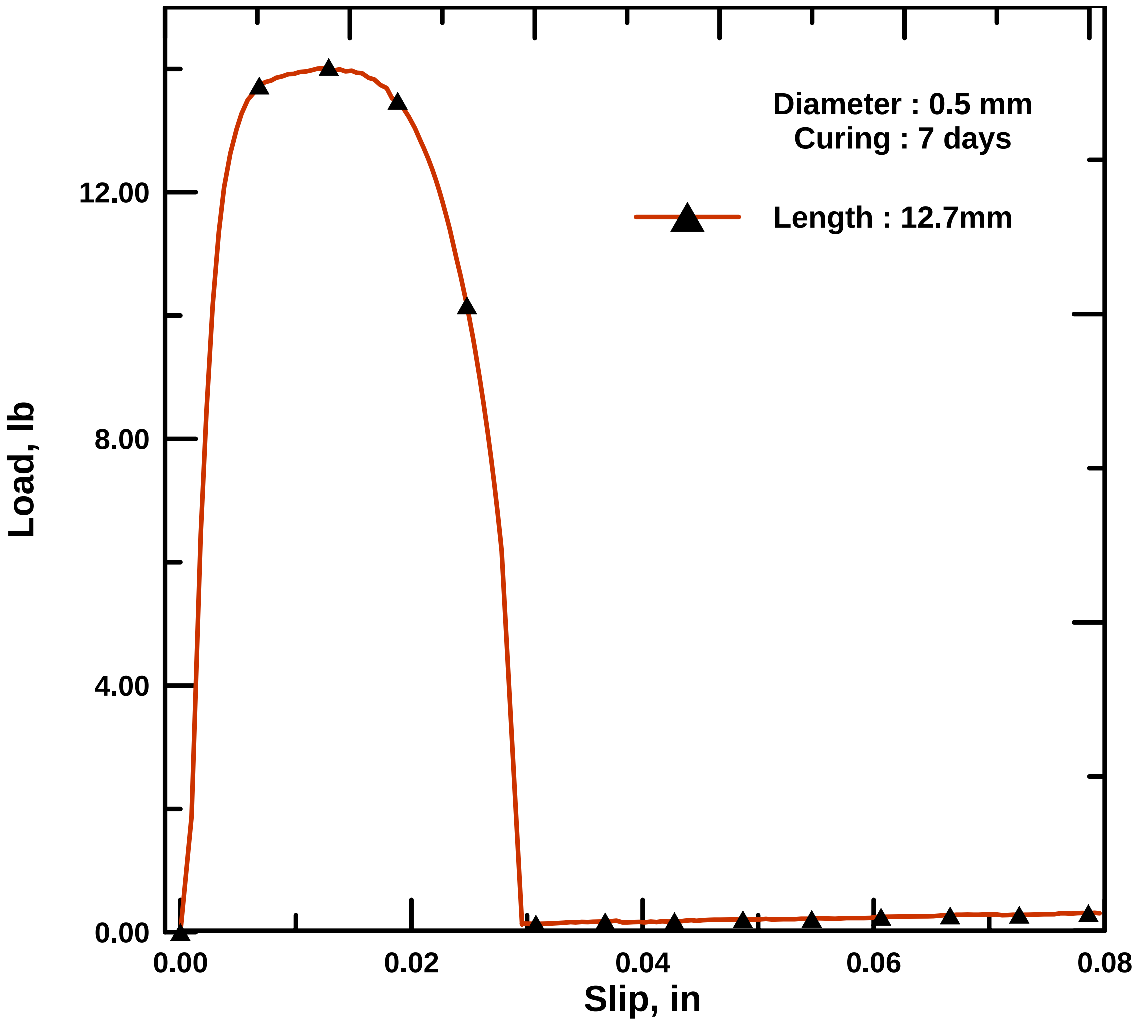

Figure B7 Specimen 1D15cLS20

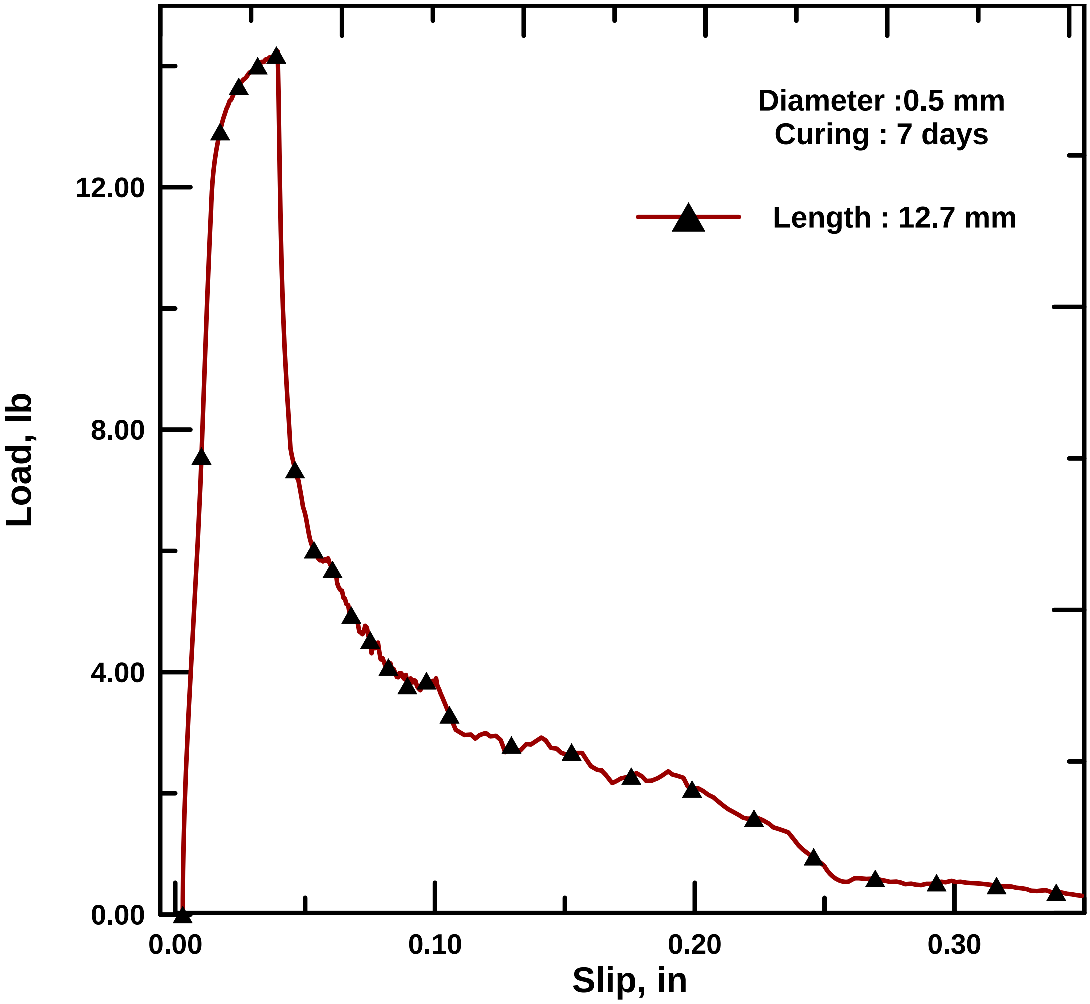

Figure B8 Specimen 1D05iLS29

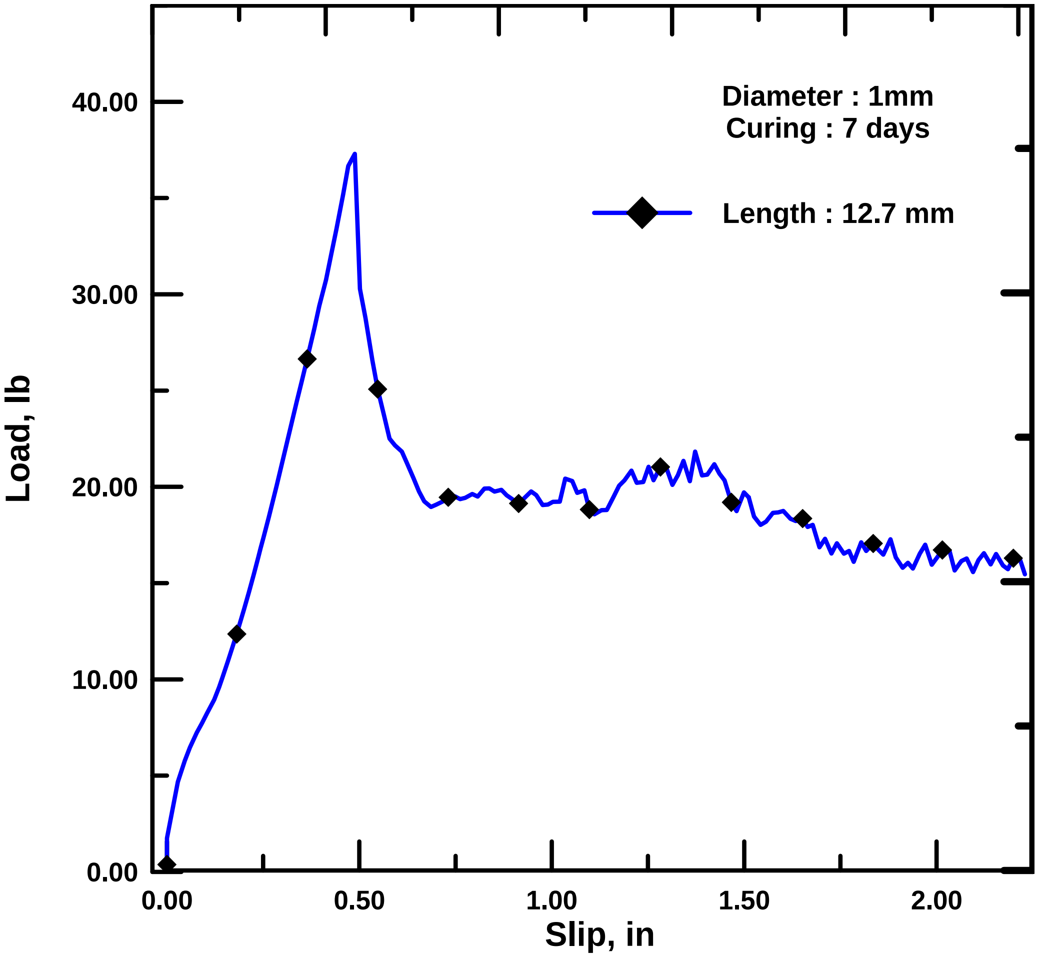

Figure B9 Specimen 1D05iLS30

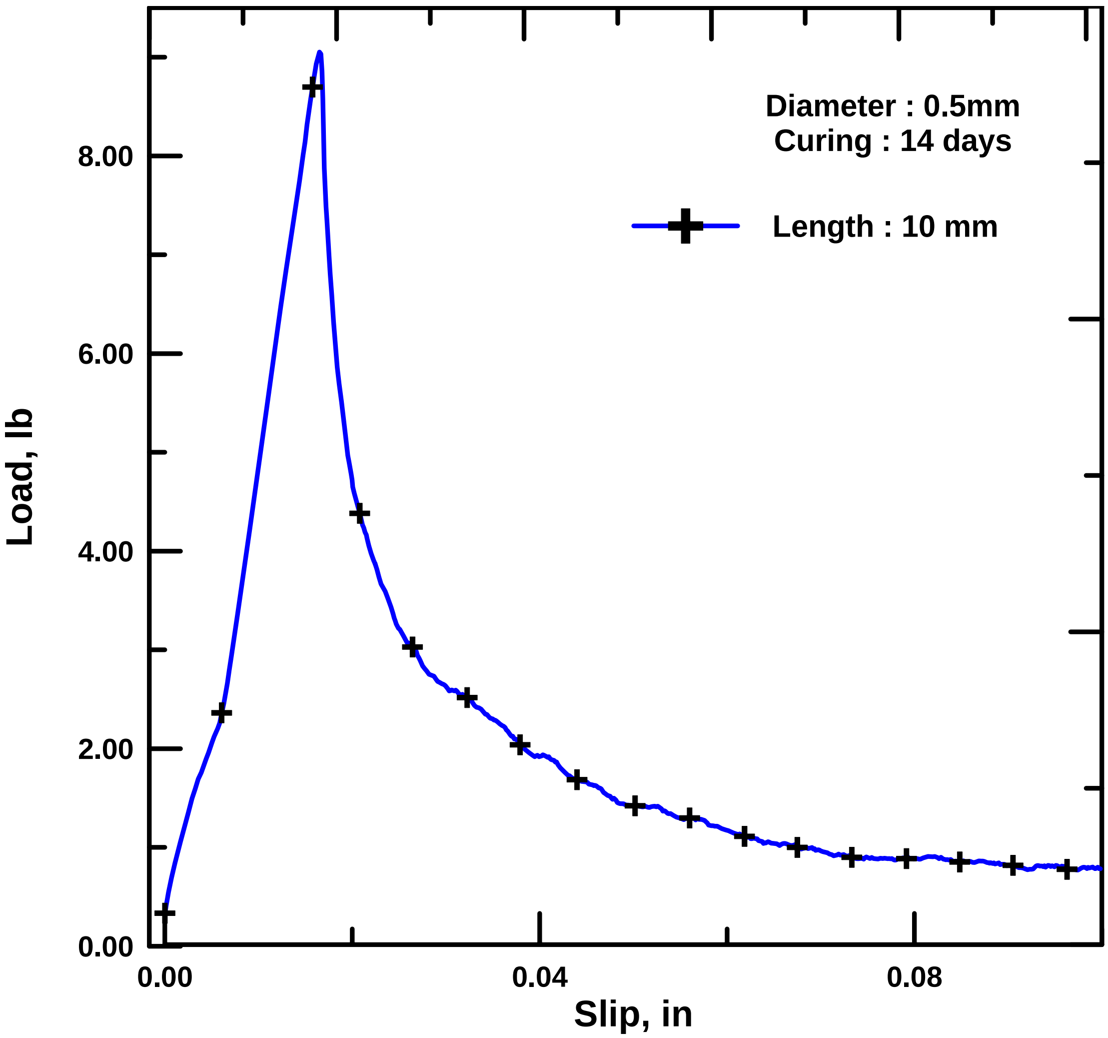

Figure B10 Specimen 4B05D1cL

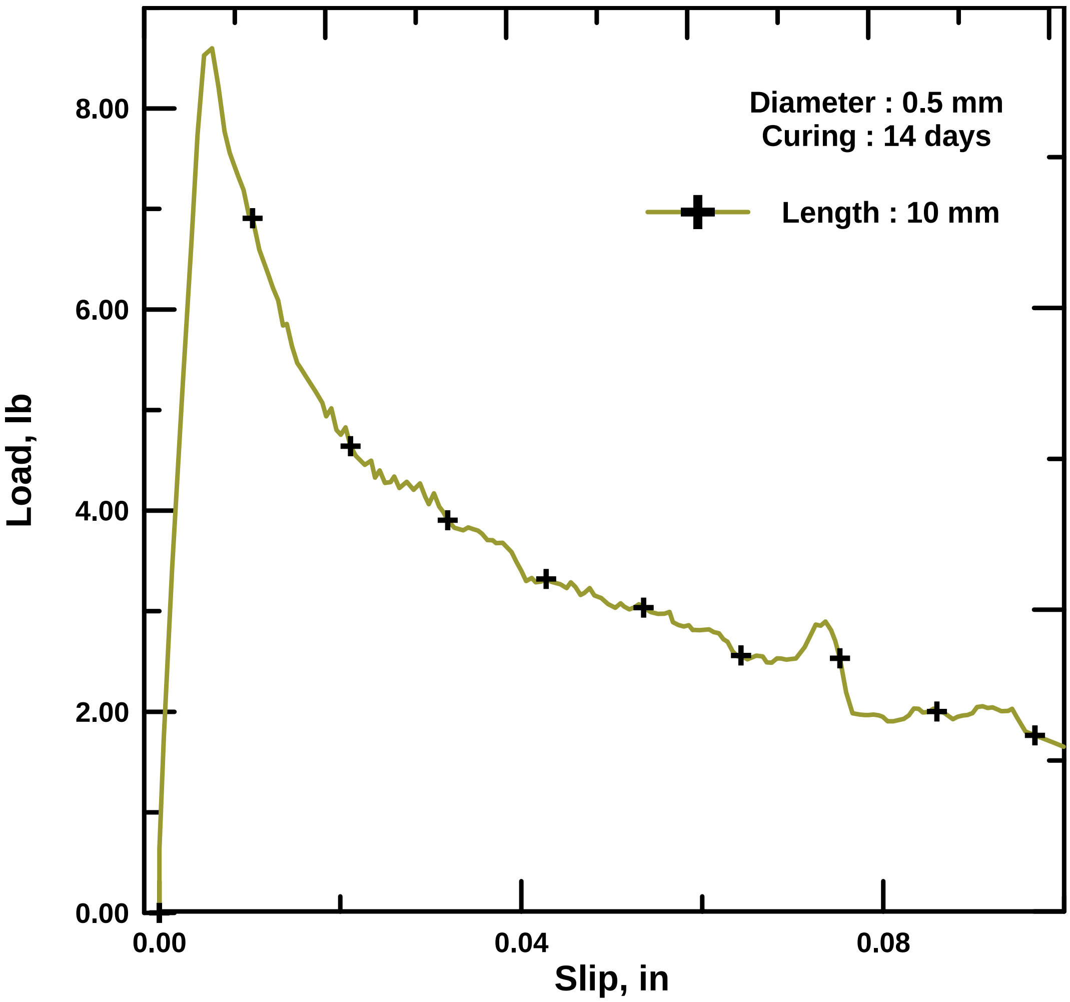

Figure B12 Specimen 4B05D1cL3

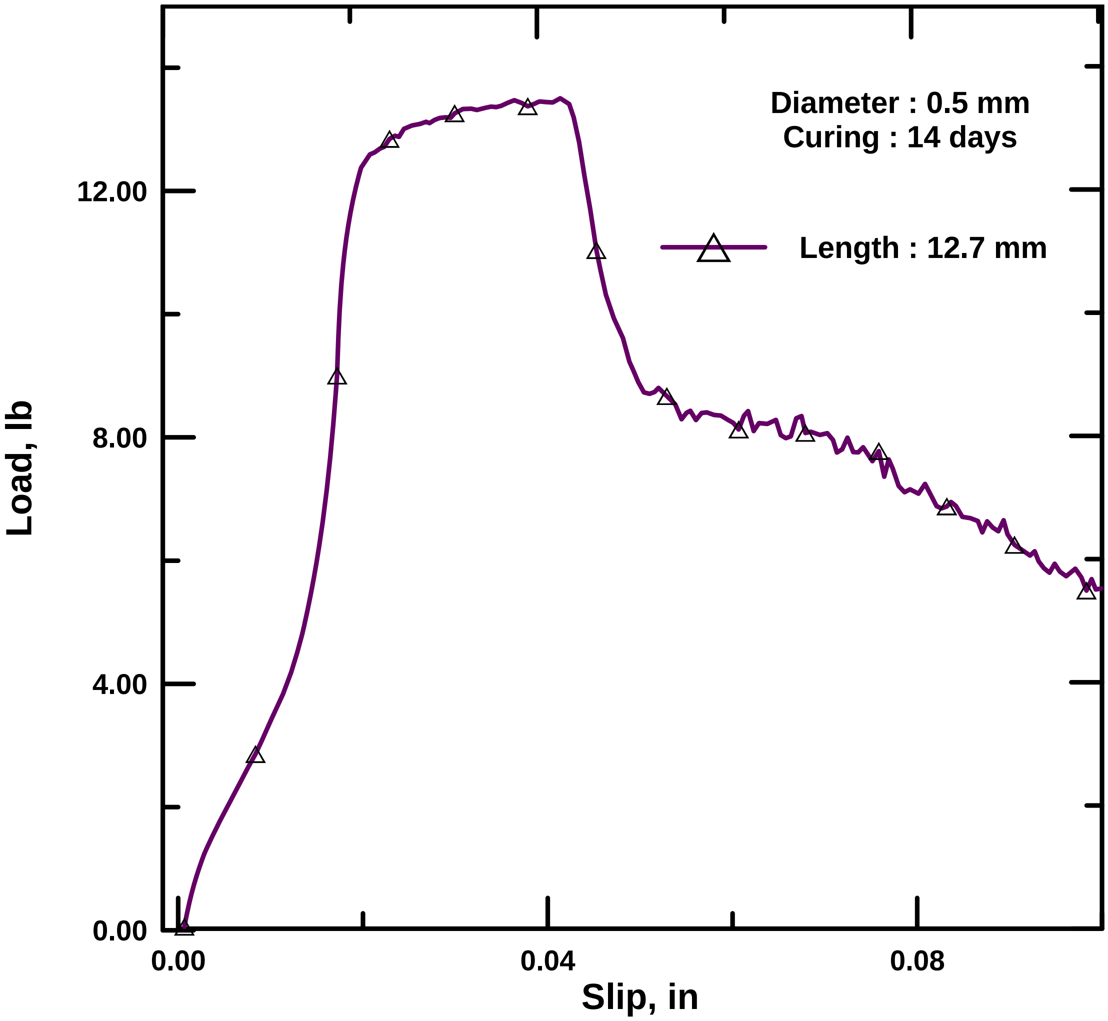

Figure B13 Specimen 4B05D05iLS4

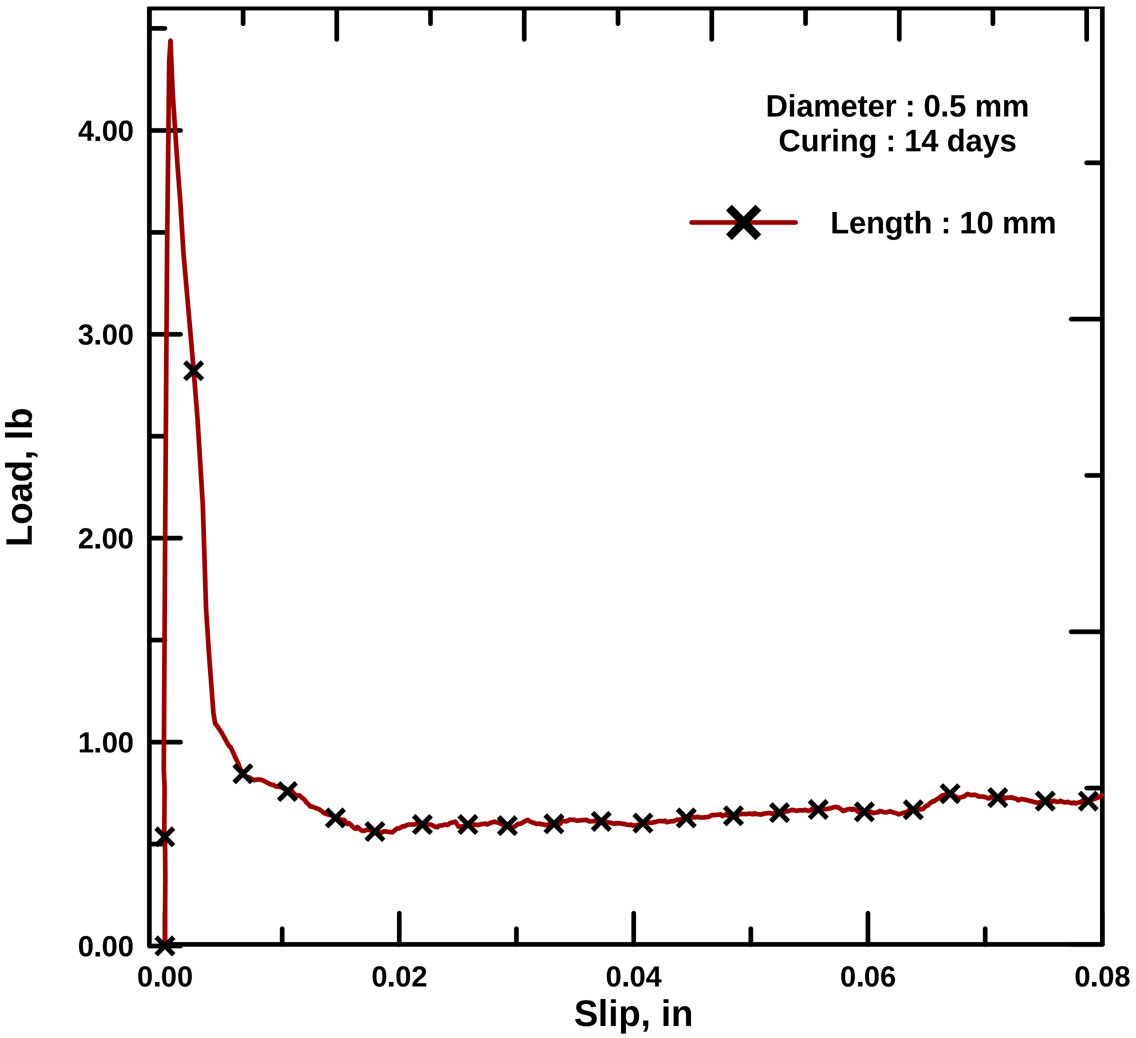

Figure B14 Specimen 4B05D1Cls5

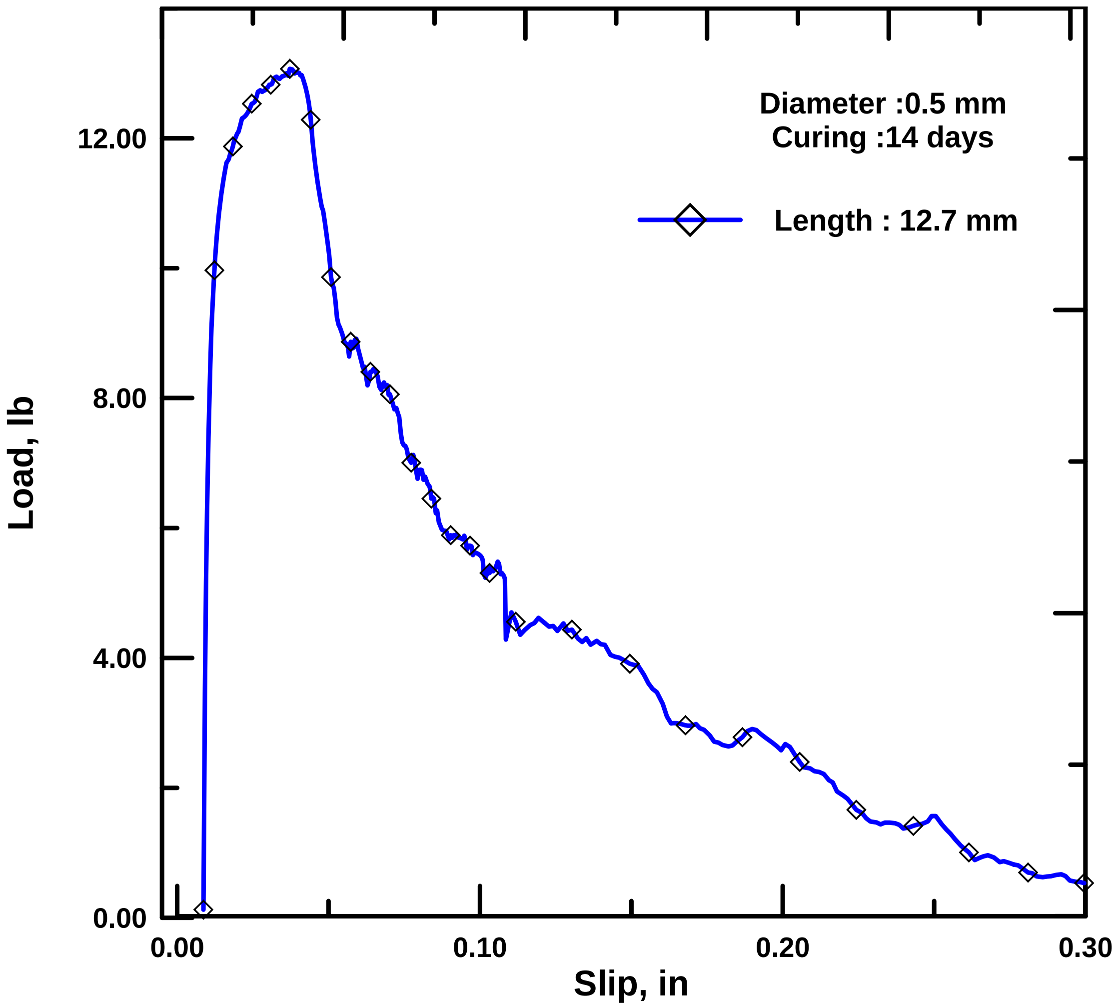

Figure B15 Specimen 4B05D05iLS6

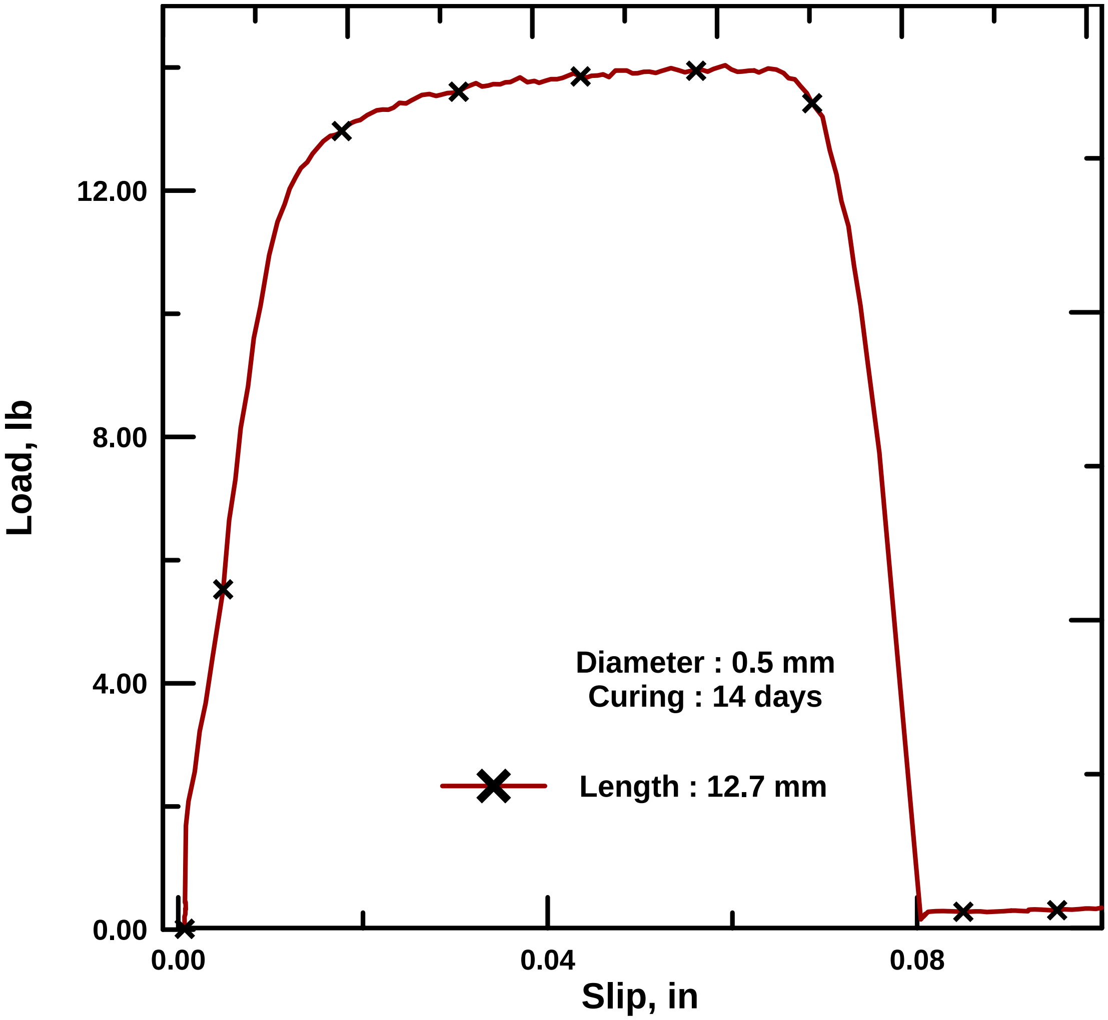

Figure B16 Specimen 4B05D05iLS7

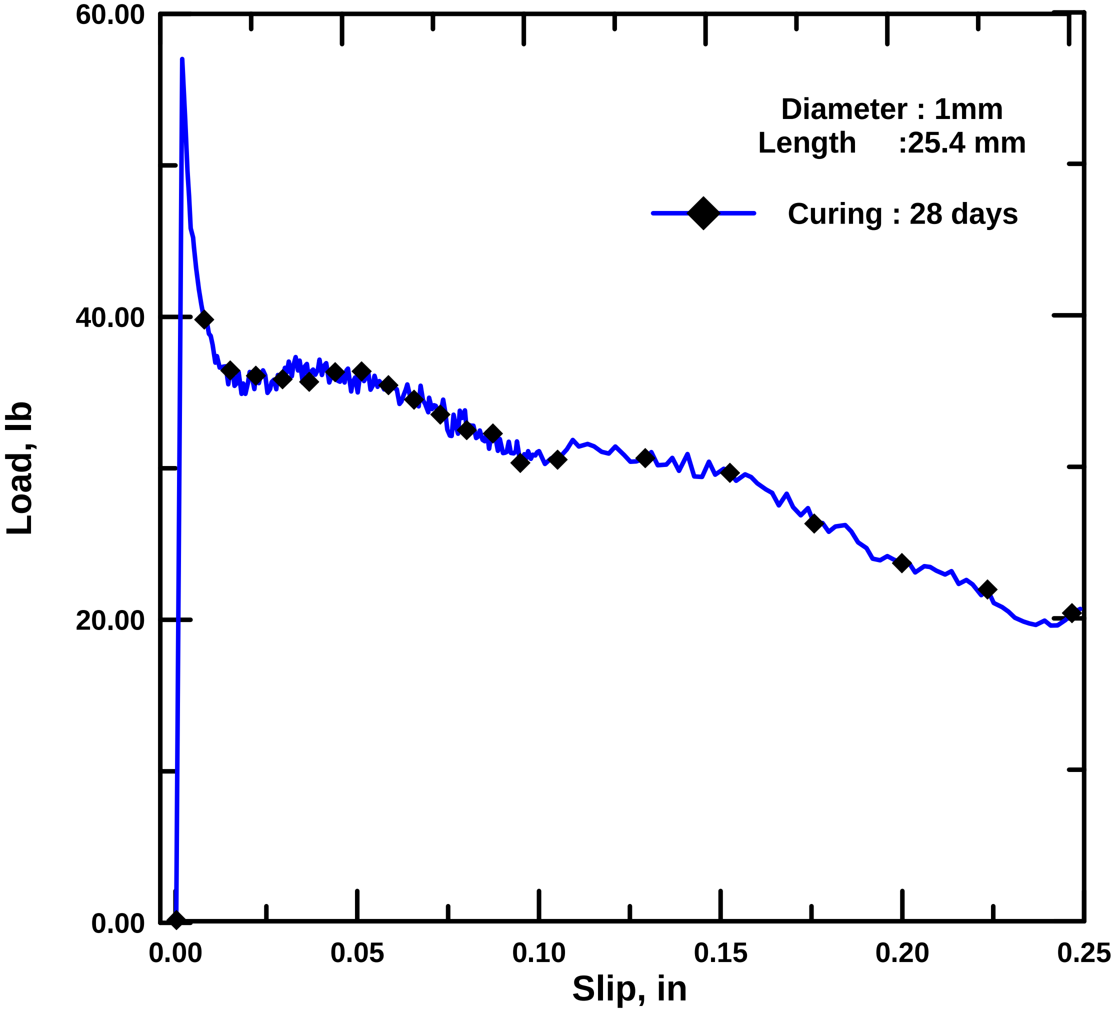

Figure B17 Specimen 1D05LS3

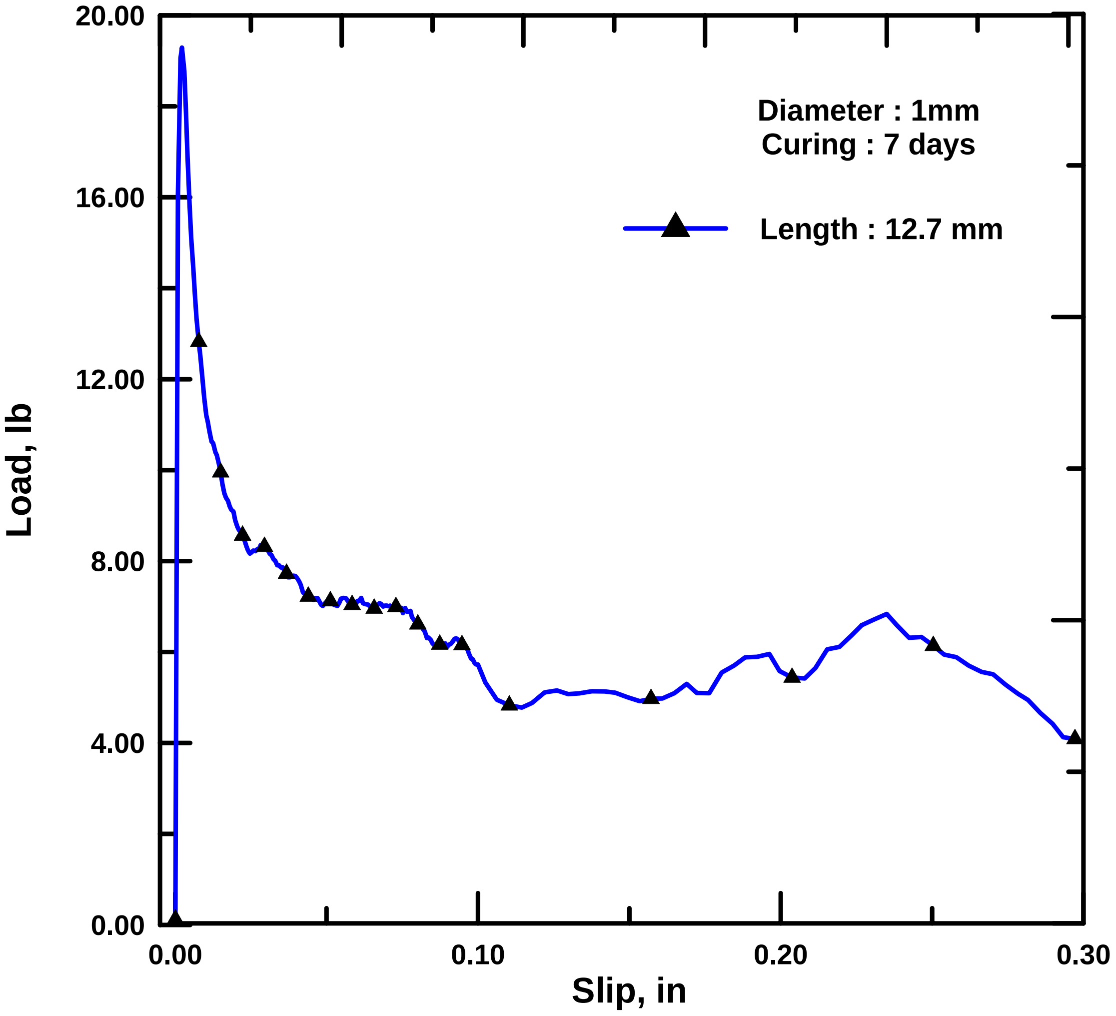

Figure B18 Specimen 1D05iLS24

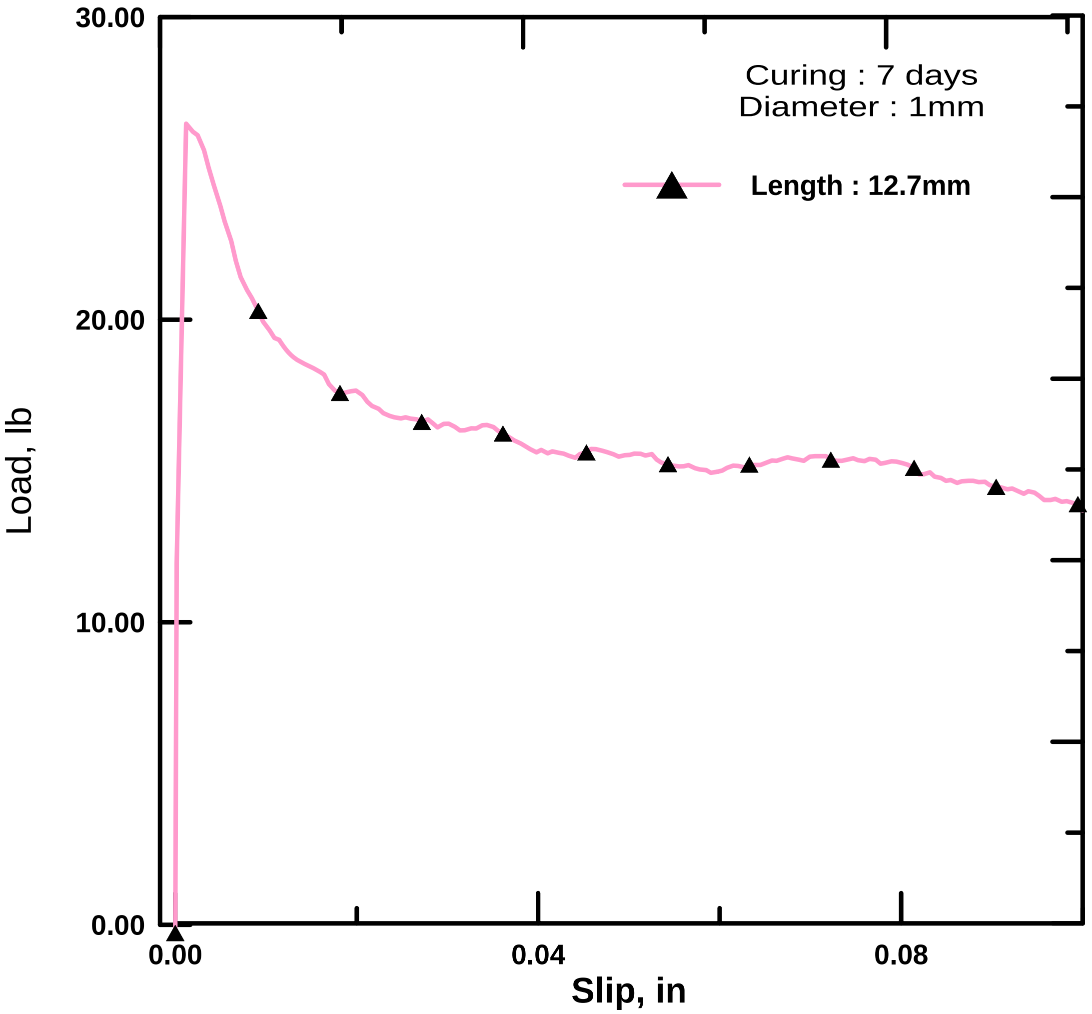

Figure B19 Specimen 1D05iLS25

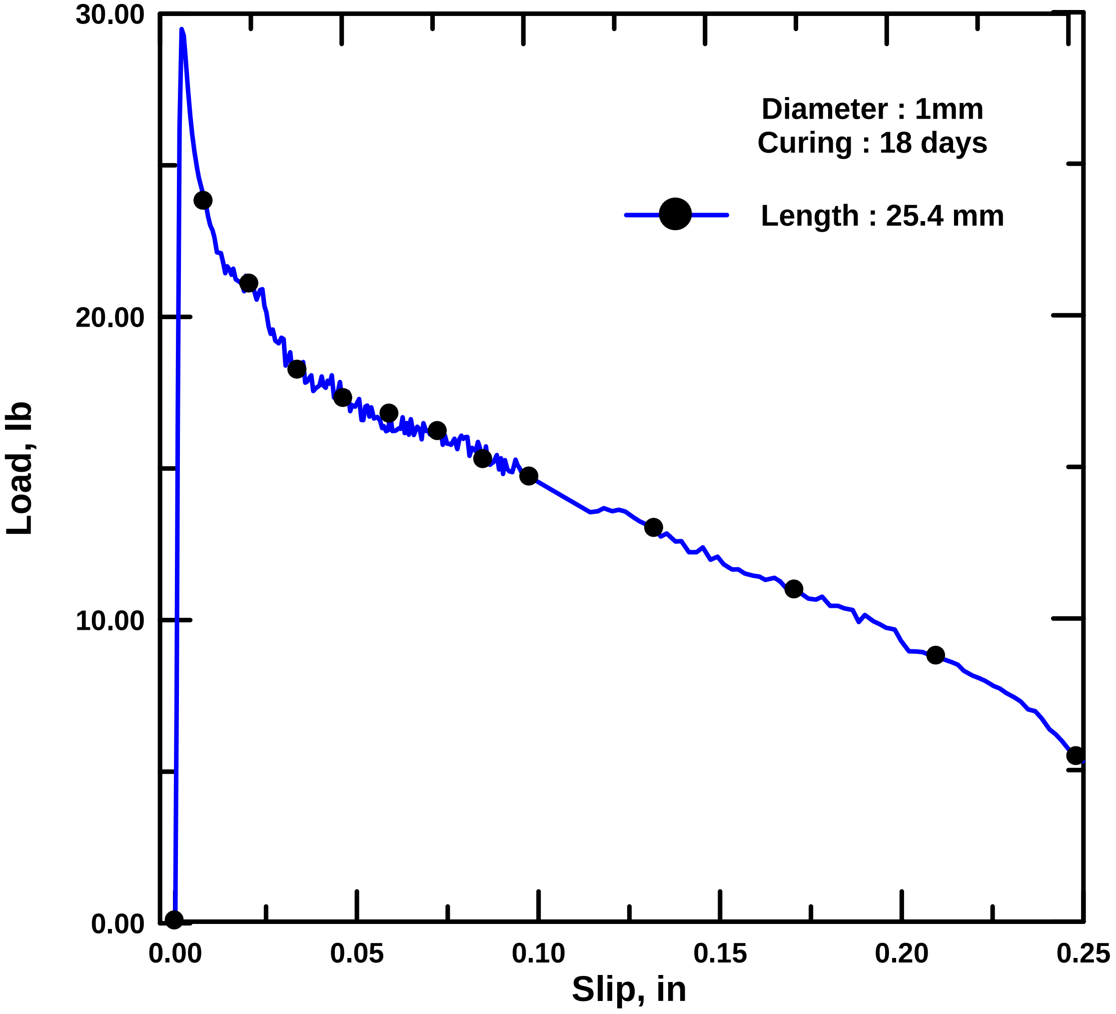

Figure B20 Specimen 4B1D1iLS12

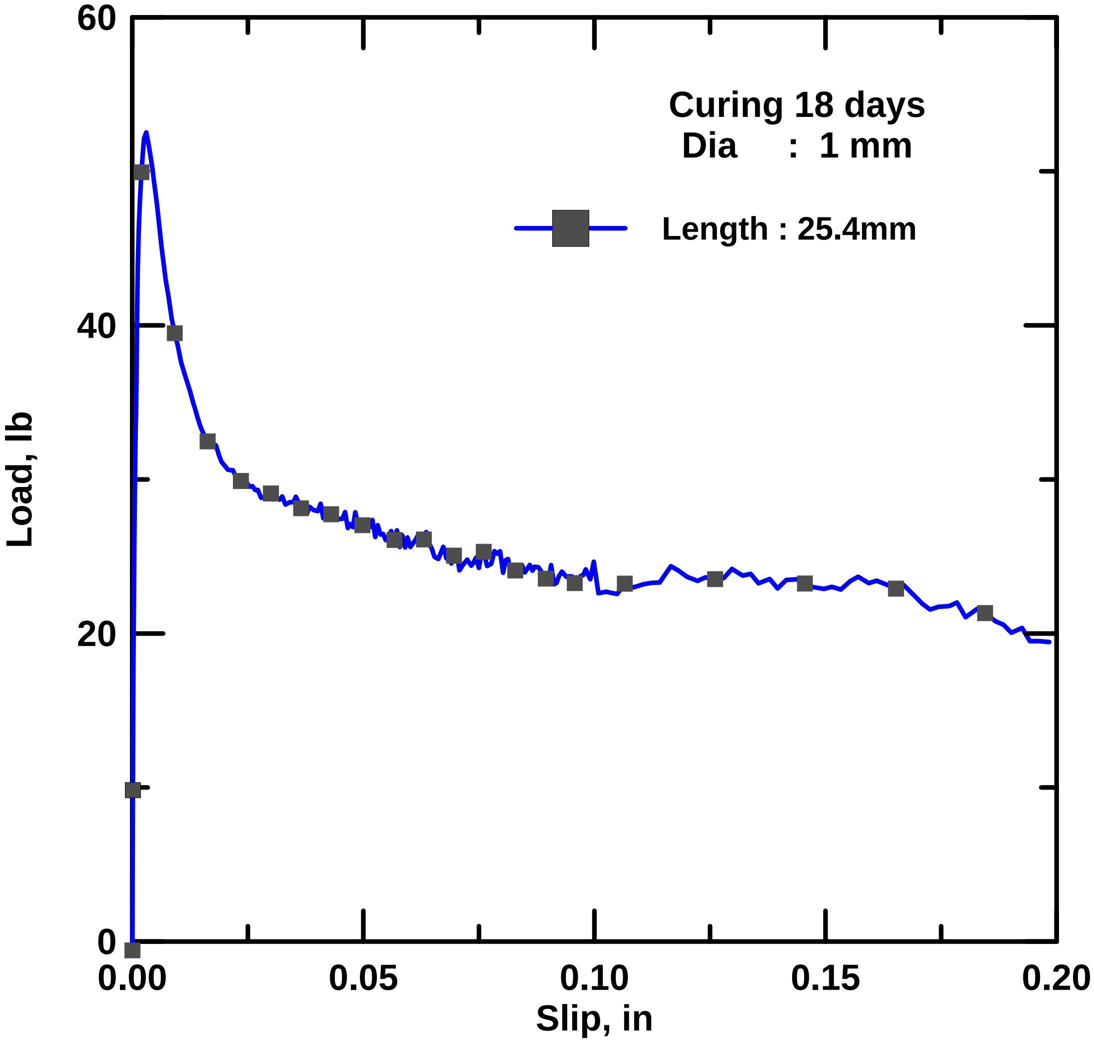

Figure B21 Specimen 4B1D1iLS13a

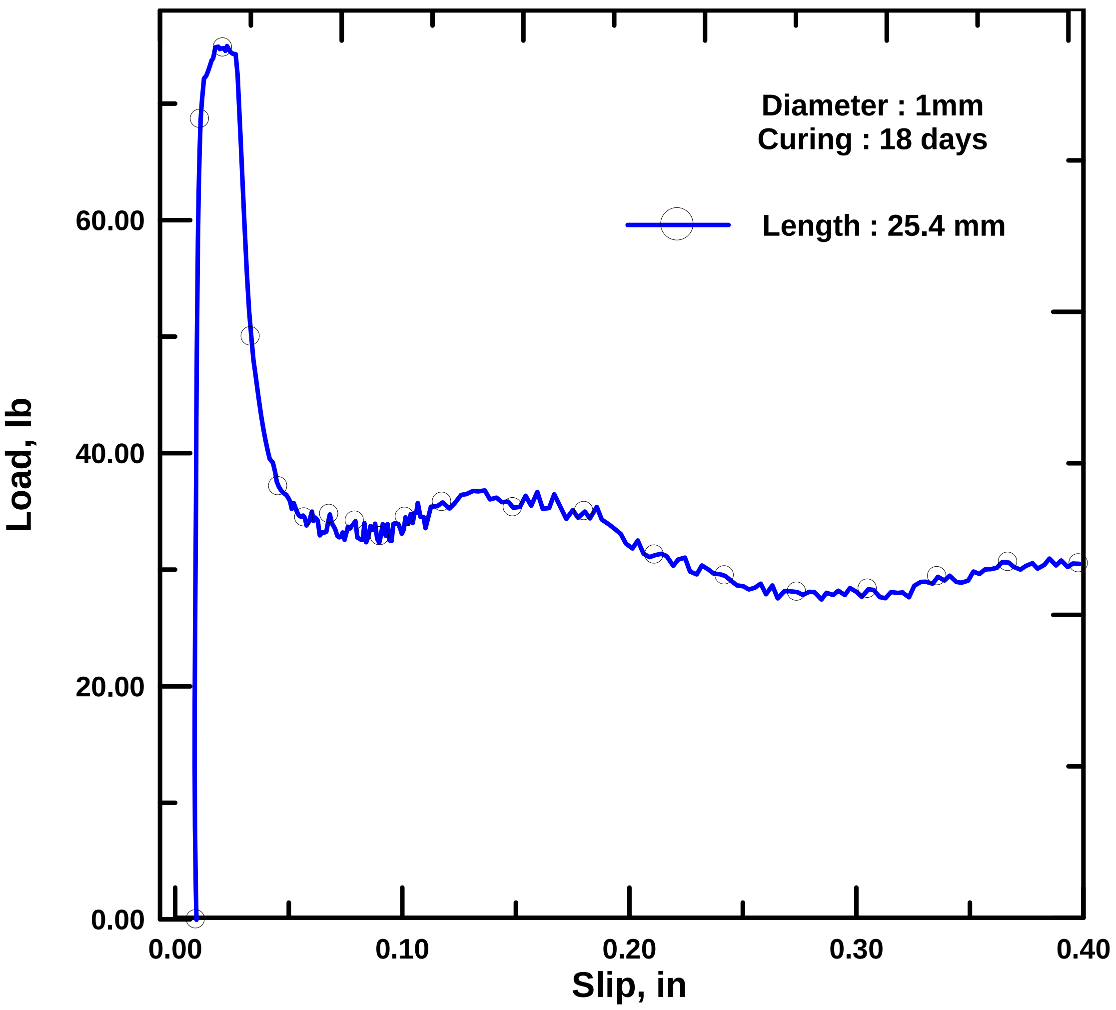

Figure B22 Specimen 4B1D1iLS14

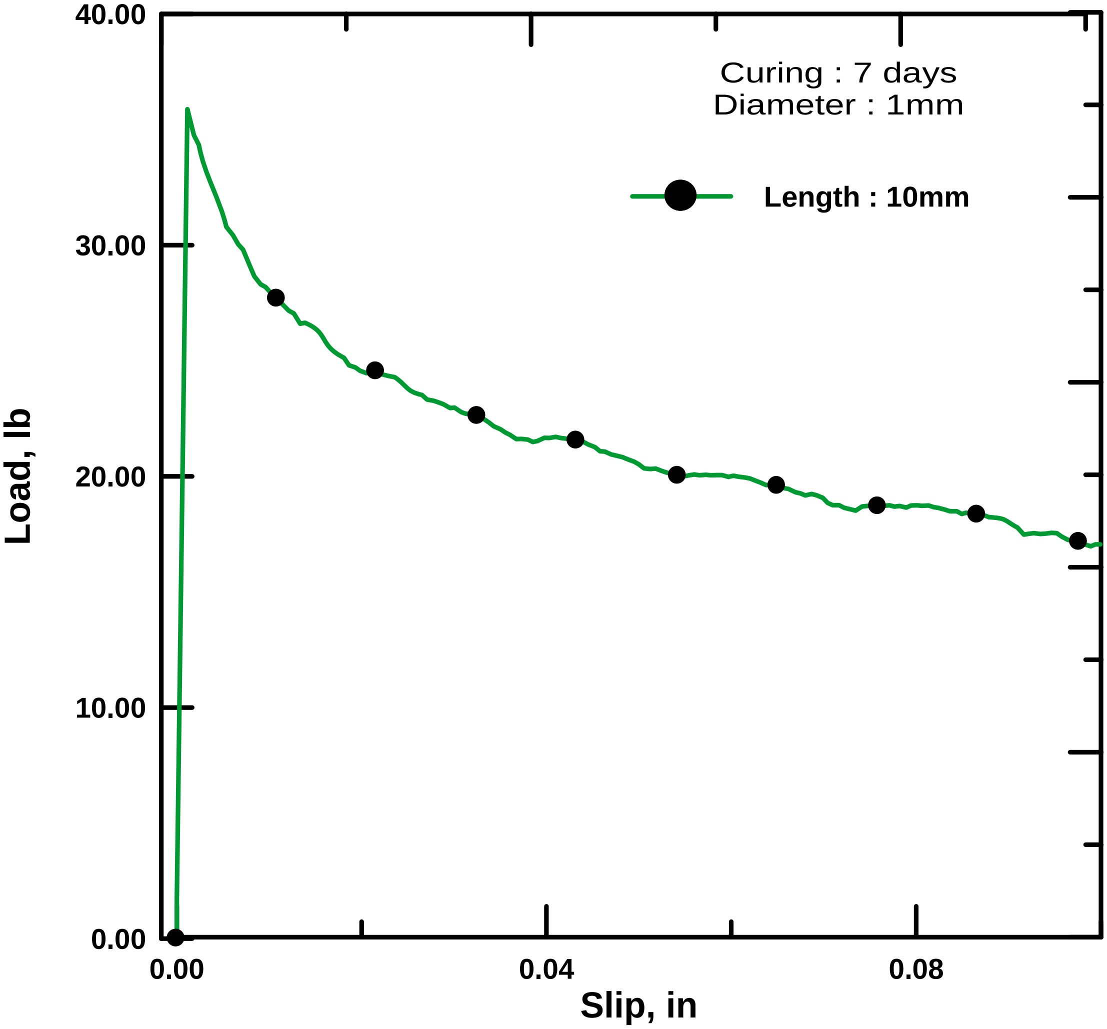

Figure B23 Specimen 1D1cS23

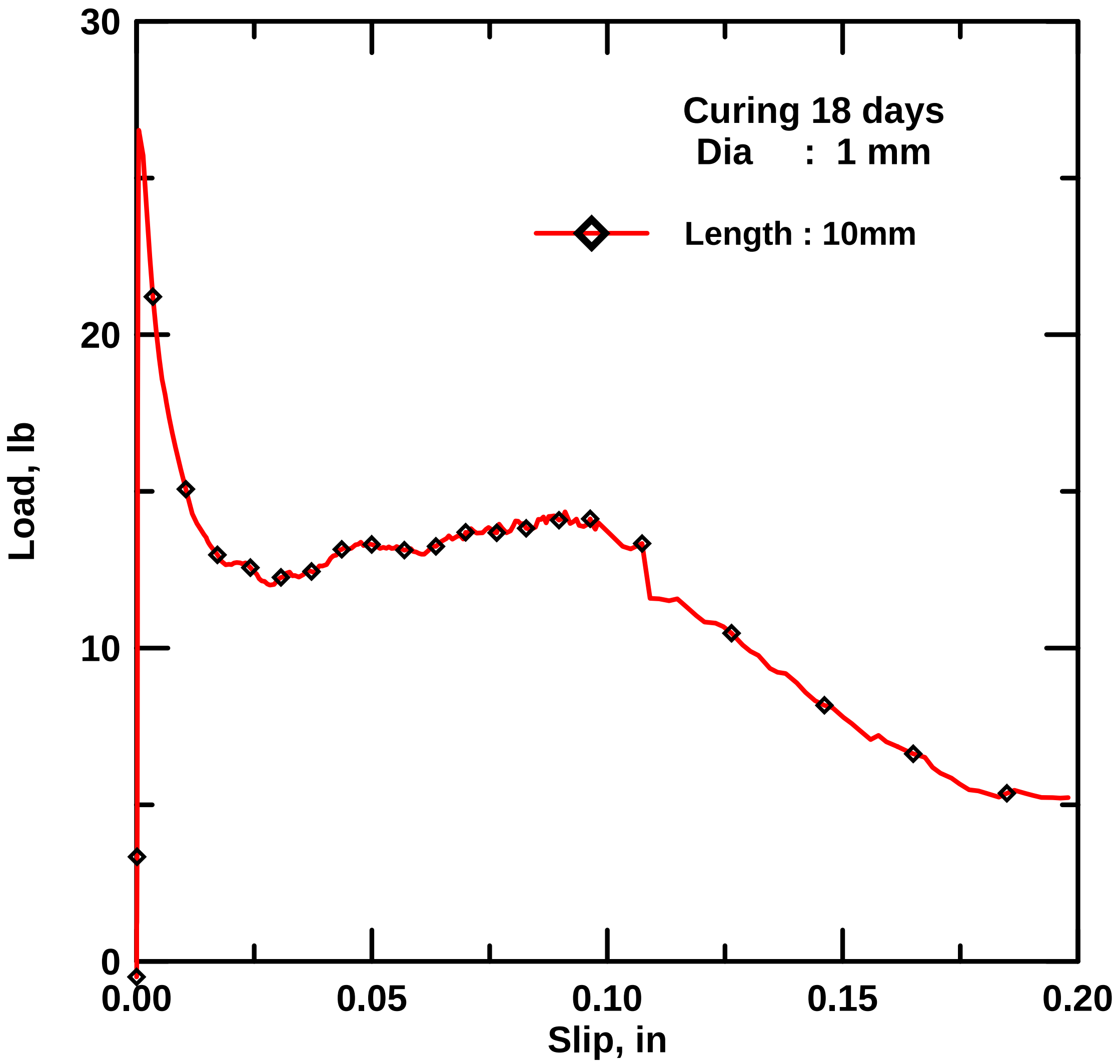

Figure B24 Specimen 4B1D1cLS10

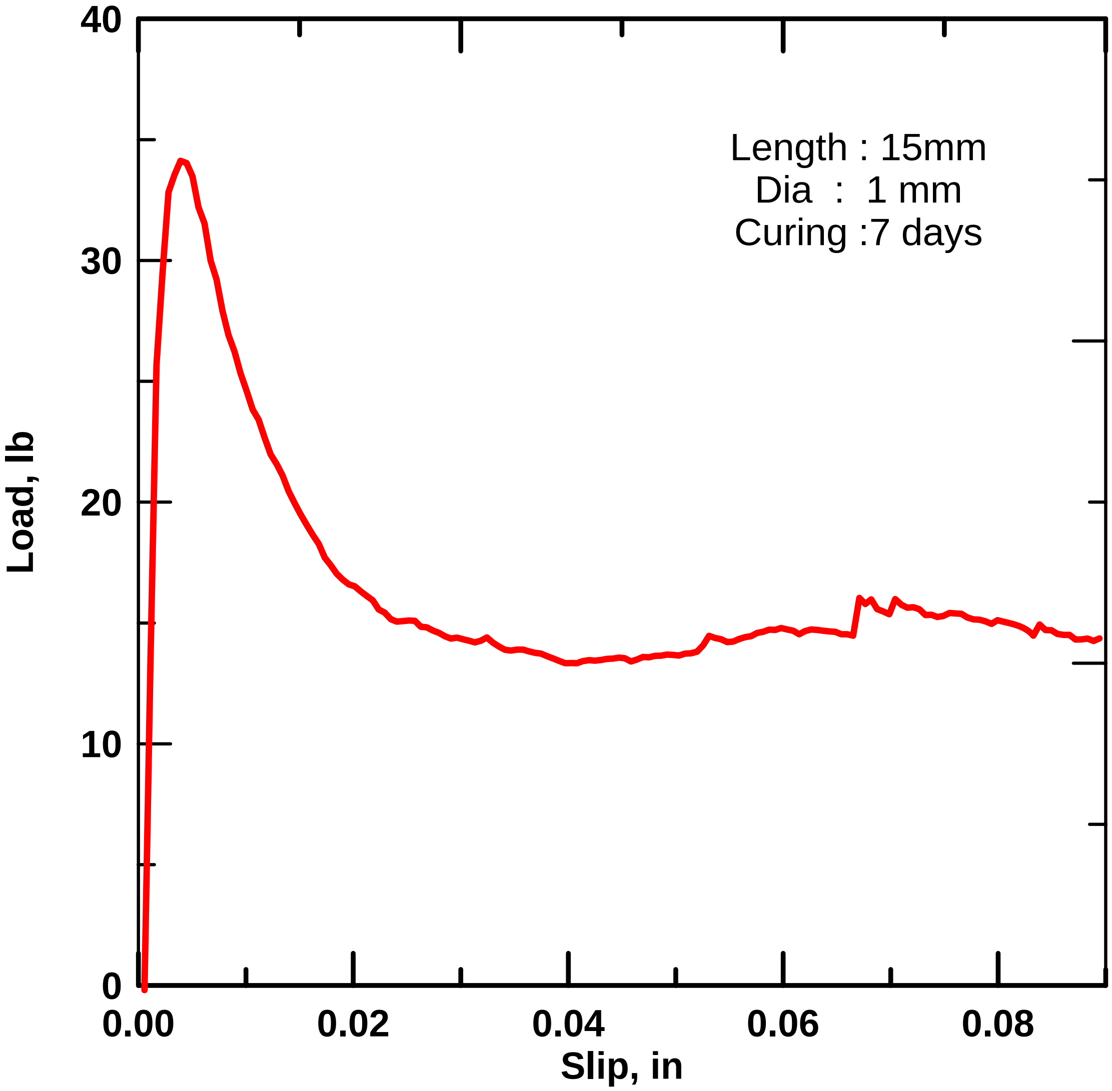

Figure B25 Specimen 1D15cLS20

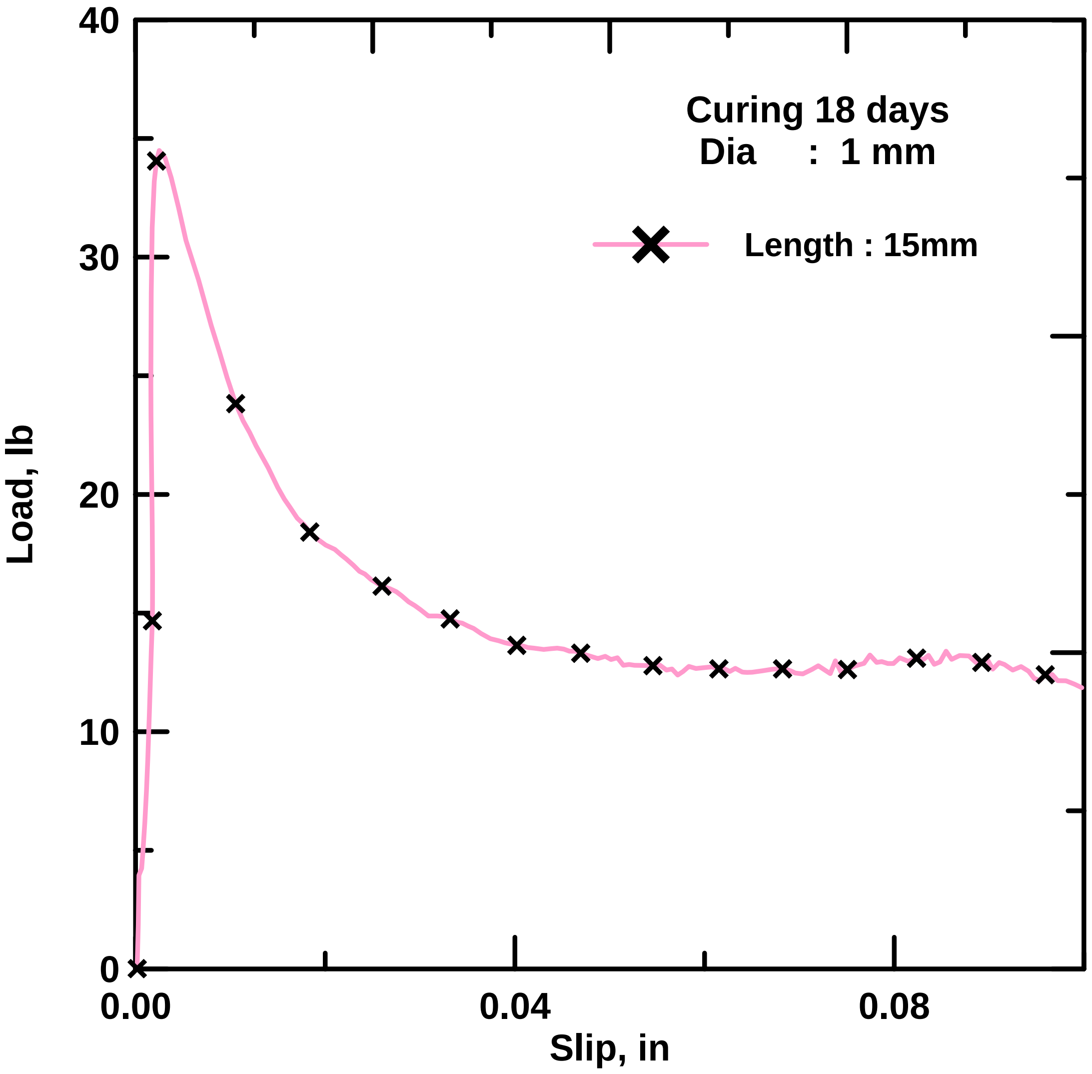

Figure B26 Specimen 4B1D15cLS16

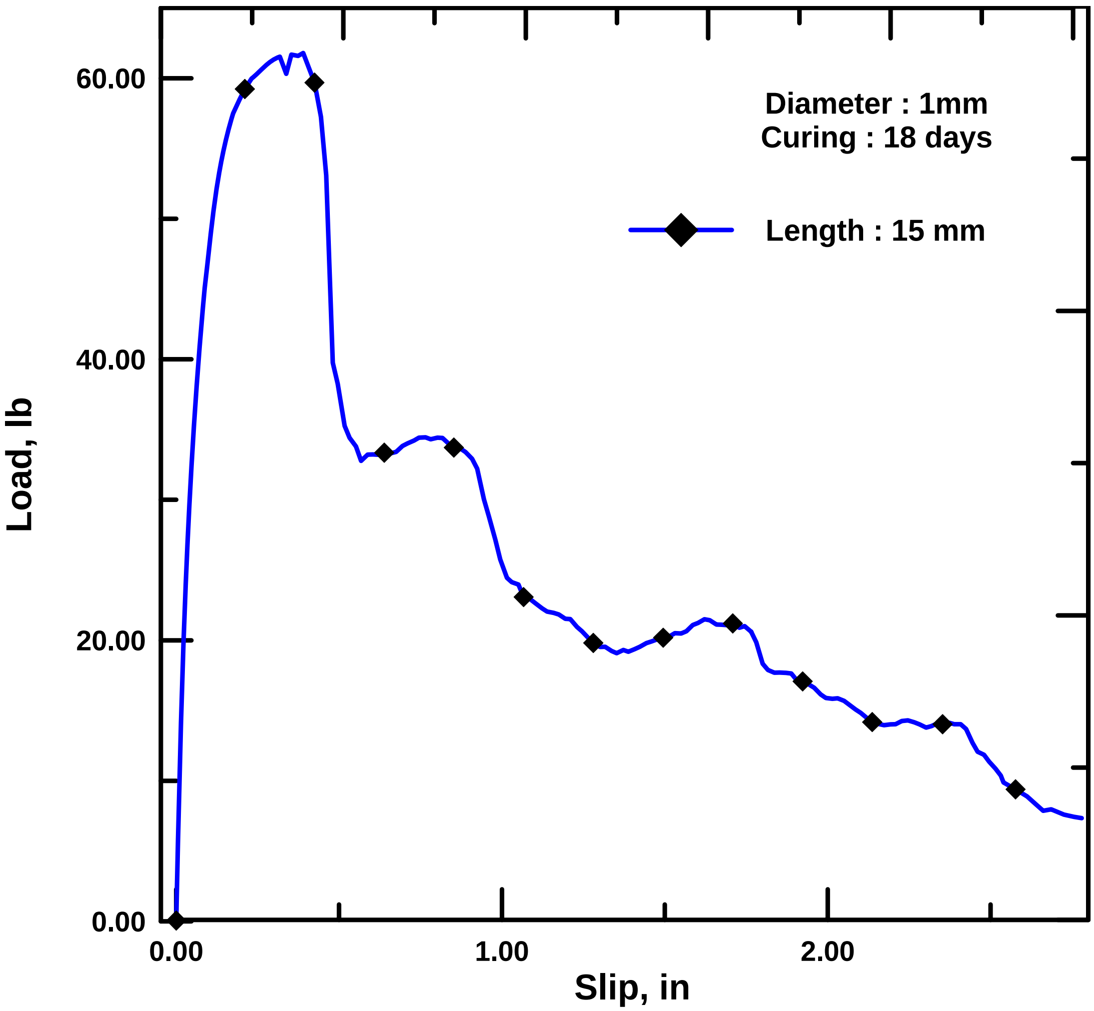

Figure B27 Specimen 4B1D2cLS17

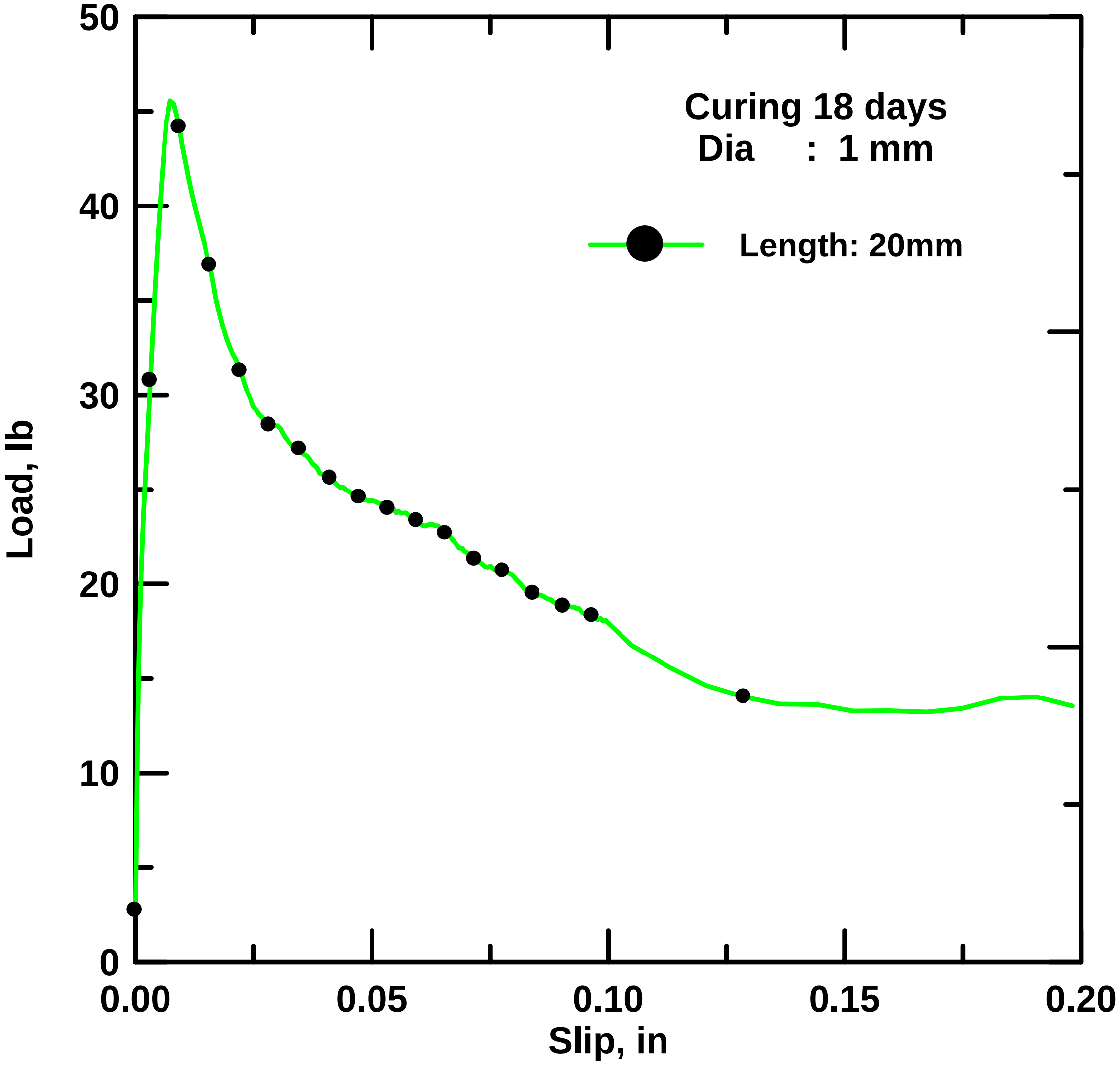

Figure B28 Specimen 4B1D2cLS18

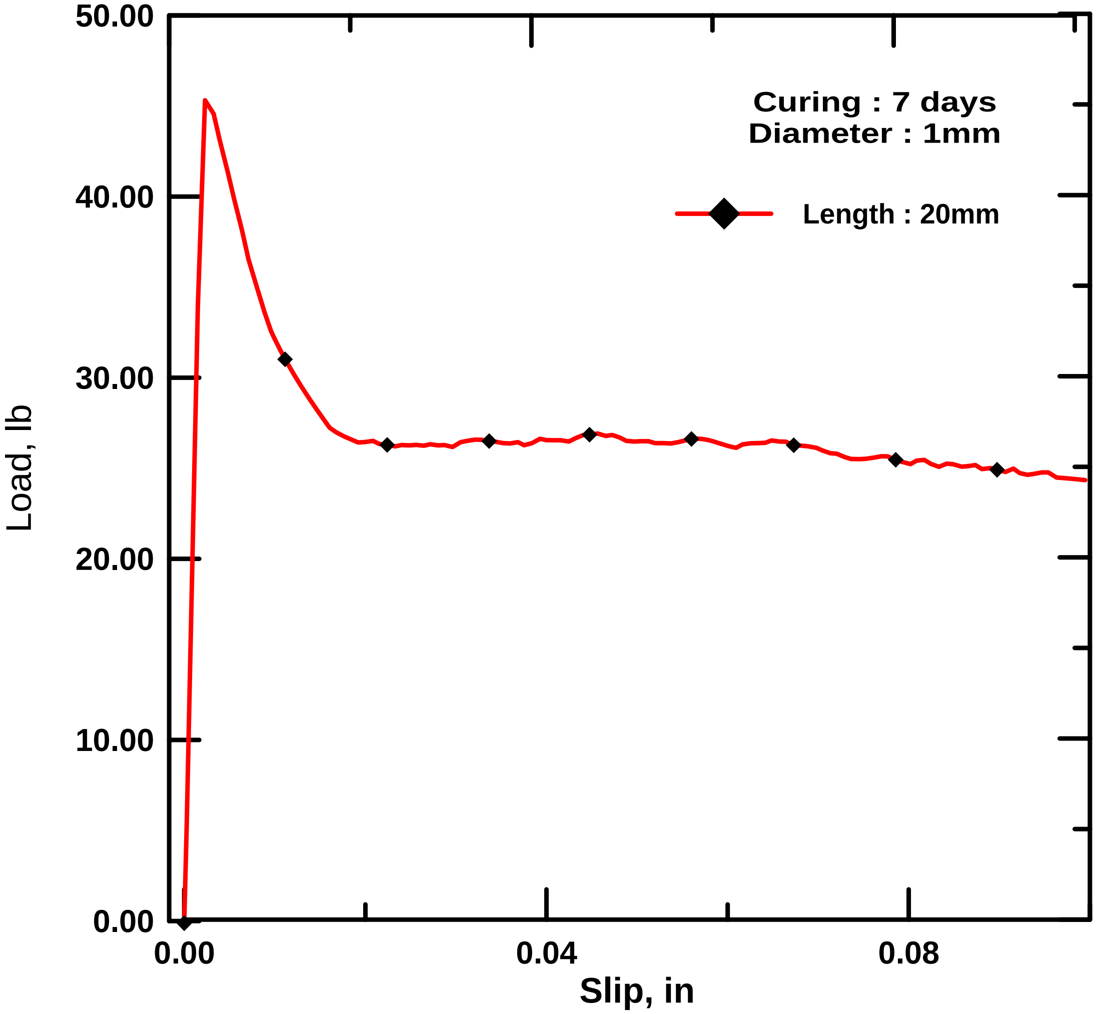

Figure B29 Specimen 1D2cLS26